USGS
science for a changing world

Prepared in cooperation with the Greater Cincinnati Water Works and the American Water Works Association Research Foundation

An Initial Investigation of Multidimensional Flow and Transverse Mixing Characteristics of the Ohio River near Cincinnati, Ohio

Scientific Investigations Report 2009–5107

U.S. Department of the Interior
U.S. Geological Survey

Cover: Meldahl Dam on the Ohio River near Neville, Ohio. (Photograph by U.S. Army Corps of Engineers (*http://www.lrh.usace.army.mil/_storage/Photos/1951.jpg*, accessed March 2, 2006). Used with permission.)

An Initial Investigation of Multidimensional Flow and Transverse Mixing Characteristics of the Ohio River near Cincinnati, Ohio

By David J. Holtschlag

Prepared in cooperation with the Greater Cincinnati Water Works and the American Water Works Association Research Foundation

Scientific Investigations Report 2009–5107

U.S. Department of the Interior
U.S. Geological Survey

U.S. Department of the Interior
KEN SALAZAR, Secretary

U.S. Geological Survey
Suzette M. Kimball, Acting Director

U.S. Geological Survey, Reston, Virginia: 2009

Suggested citation:
Holtschlag, D.J., 2009, An initial investigation of multidimensional flow and transverse mixing characteristics of the Ohio River near Cincinnati, Ohio: U.S. Geological Survey Scientific Investigations Report 2009–5107, 56 p.

Contents

Figures

Tables

Conversion Factors

Multiply	By	To obtain
	Length	
inch (in.)	2.54	centimeter (cm)
inch (in.)	25.4	millimeter (mm)
foot (ft)	0.3048	meter (m)
mile (mi)	1.609	kilometer (km)
yard (yd)	0.9144	meter (m)
	Area	
square foot (ft^2)	0.09290	square meter (m^2)
square inch (in^2)	6.452	square centimeter (cm^2)
square mile (mi^2)	259.0	hectare (ha)
square mile (mi^2)	2.590	square kilometer (km^2)
	Volume	
gallon (gal)	3.785	liter (L)
gallon (gal)	0.003785	cubic meter (m^3)
million gallons (Mgal)	3,785	cubic meter (m^3)
cubic foot (ft^3)	0.02832	cubic meter (m^3)
	Flow rate	
foot per second (ft/s)	0.3048	meter per second (m/s)
cubic foot per second (ft^3/s)	0.02832	cubic meter per second (m^3/s)
gallon per minute (gal/min)	0.06309	liter per second (L/s)
gallon per day (gal/d)	0.003785	cubic meter per day (m^3/d)
million gallons per day (Mgal/d)	0.04381	cubic meter per second (m^3/s)
million gallons per day per square mile [(Mgal/d)/mi^2]	1,461	cubic meter per day per square kilometer [(m^3/d)/km^2]
mile per hour (mi/h)	1.609	kilometer per hour (km/h)
	Mass	
ounce, avoirdupois (oz)	28.35	gram (g)
pound, avoirdupois (lb)	0.4536	kilogram (kg)

Temperature in degrees Celsius (°C) may be converted to degrees Fahrenheit (°F) as follows:

°F=(1.8×°C)+32

Temperature in degrees Fahrenheit (°F) may be converted to degrees Celsius (°C) as follows:

°C=(°F-32)/1.8

Vertical coordinate information is referenced to North American Vertical Datum of 1988 (NAVD 88) in feet.

Horizontal coordinate information is referenced to the Ohio South (zone 3402) State Plane Coordinate System of 1983 (Ohio South SPCS 83) in U.S. Survey Feet. A U.S. Survey Foot is 1200/3937 of a meter.

Altitude, as used in this report, refers to distance above the vertical datum.

Abbreviations

2D	Two Dimensional
ADCP	acoustic Doppler current profiler
AwwaRF	American Water Works Association Research Foundation
BIC	Big Indian Creek
EST	Eastern Standard Time
FORTRAN	Formula Translation (computer language)
GCWW	Greater Cincinnati Water Works
GPS	Global Positioning System
NAD 83	North American Datum of 1983
NAVD 88	North American Vertical Datum of 1988
NGVD 29	National Geodetic Vertical Datum of 1929
OHRFC	Ohio River Forecast Center
ORD	Ohio River Datum
RM	River Mile
RMA2	Resource Management Association 2D hydrodynamic model
RMA4	Resource Management Association 2D transport model
SMS	Surface Water Modeling System by Environmental Modeling Systems, Inc.
SPCS	State Plane Coordinate System
TMC	Twelvemile Creek
UCODE	universal parameter estimation code
USACE	U.S. Army Corps of Engineers
USGS	U.S. Geological Survey

An Initial Investigation of Multidimensional Flow and Transverse Mixing Characteristics of the Ohio River near Cincinnati, Ohio

By David J. Holtschlag

Abstract

Two-dimensional hydrodynamic and transport models were applied to a 34-mile reach of the Ohio River from Cincinnati, Ohio, upstream to Meldahl Dam near Neville, Ohio. The hydrodynamic model was based on the generalized finite-element hydrodynamic code RMA2 to simulate depth-averaged velocities and flow depths. The generalized water-quality transport code RMA4 was applied to simulate the transport of vertically mixed, water-soluble constituents that have a density similar to that of water. Boundary conditions for hydrodynamic simulations included water levels at the U.S. Geological Survey water-level gaging station near Cincinnati, Ohio, and flow estimates based on a gate rating at Meldahl Dam. Flows estimated on the basis of the gate rating were adjusted with limited flow-measurement data to more nearly reflect current conditions. An initial calibration of the hydrodynamic model was based on data from acoustic Doppler current profiler surveys and water-level information. These data provided flows, horizontal water velocities, water levels, and flow depths needed to estimate hydrodynamic parameters related to channel resistance to flow and eddy viscosity. Similarly, dye concentration measurements from two dye-injection sites on each side of the river were used to develop initial estimates of transport parameters describing mixing and dye-decay characteristics needed for the transport model.

A nonlinear regression-based approach was used to estimate parameters in the hydrodynamic and transport models. Parameters describing channel resistance to flow (Manning's "*n*") were estimated in areas of deep and shallow flows as 0.0234, and 0.0275, respectively. The estimated RMA2 Peclet number, which is used to dynamically compute eddy-viscosity coefficients, was 38.3, which is in the range of 15 to 40 that is typically considered appropriate. Resulting hydrodynamic simulations explained 98.8 percent of the variability in depth-averaged flows, 90.0 percent of the variability in water levels, 93.5 percent of the variability in flow depths, and 92.5 percent of the variability in velocities.

Estimates of the water-quality-transport-model parameters describing turbulent mixing characteristics converged to different values for the two dye-injection reaches. For the Big Indian Creek dye-injection study, an RMA4 Peclet number of 37.2 was estimated, which was within the recommended range of 15 to 40, and similar to the RMA2 Peclet number. The estimated dye-decay coefficient was 0.323. Simulated dye concentrations explained 90.2 percent of the variations in measured dye concentrations for the Big Indian Creek injection study. For the dye-injection reach starting downstream from Twelvemile Creek, however, an RMA4 Peclet number of 173 was estimated, which is far outside the recommended range. Simulated dye concentrations were similar to measured concentration distributions at the first four transects downstream from the dye-injection site that were considered vertically mixed. Farther downstream, however, simulated concentrations did not match the attenuation of maximum concentrations or cross-channel transport of dye that were measured. The difficulty of determining a consistent RMA4 Peclet was related to the two-dimension model assumption that velocity distributions are closely approximated by their depth-averaged values. Analysis of velocity data showed significant variations in velocity direction with depth in channel reaches with curvature. Channel irregularities (including curvatures, depth irregularities, and shoreline variations) apparently produce transverse currents that affect the distribution of constituents, but are not fully accounted for in a two-dimensional model. The two-dimensional flow model, using channel resistance to flow parameters of 0.0234 and 0.0275 for deep and shallow areas, respectively, and an RMA2 Peclet number of 38.3, and the RMA4 transport model with a Peclet number of 37.2, may have utility for emergency-planning purposes. Emergency-response efforts would be enhanced by continuous streamgaging records downstream from Meldahl Dam, real-time water-quality monitoring, and three-dimensional modeling. Decay coefficients are constituent specific.

Introduction

The Ohio River is formed by the confluence of the Allegheny and Monongahela Rivers in Pittsburgh, Pa. (fig. 1). It flows 891 mi westward to the Mississippi River near Cairo, Ill. The U.S. Army Corps of Engineers (USACE) operates a series of 20 locks and dams along the Ohio River to maintain a minimum 9-ft depth of flow to support commercial navigation and recreational activities. The Ohio River is a source of drinking water for more than 3 million people (more than 25 million people live in the Ohio River Basin). The total drainage area of the Ohio River is 203,940 mi^2 (Ohio River Valley Water Sanitation Commission, 2006).

Water-related problems in the Ohio River Basin include spills and accidental discharges, effluent from municipal wastewater-treatment plants, combined-sewage and stormwater overflows, urban stormwater, mine drainage, runoff from agricultural and forest lands, sedimentation, brines associated with oil and gas recovery, reservoir sedimentation, drinking-water contamination, and invasive aquatic species.

The U.S. Geological Survey (USGS), in cooperation with the Greater Cincinnati Water Works (GCWW) and the American Water Works Association Research Foundation, made an initial investigation of flow and mixing characteristics of the Ohio River near Cincinnati, Ohio, to facilitate the protection of drinking-water supplies from contamination.

Purpose and Scope

This report documents an initial investigation of flow and mixing characteristics along a 34-mi reach of the Ohio River from a water-level gaging station at Cincinnati, Ohio, upstream to the Meldahl Dam. Acoustic Doppler current profiler (ADCP) surveys and ancillary data provided flow, velocity, flow-depth, and water-level information needed to estimate channel roughness and eddy-viscosity parameters associated with a two-dimensional (2D) hydrodynamic model, and two dye-injection studies provided concentration data needed to estimate turbulent mixing and dye-decay parameters in a 2D water-quality transport model. Boundary conditions for model simulations included water-level data from the USGS gaging station at Cincinnati, Ohio, and available flow information at Meldahl Dam.

Model Area

The model area extends about 34 mi along the Ohio River from Cincinnati, Ohio, upstream to Meldahl Dam, near Neville, Ohio (fig. 2). The downstream limit of the model is at the USGS water-level gaging station Ohio River at Cincinnati, Ohio (station number 03255000), which is near river mile (RM) 471 on the Roebling suspension bridge that crosses the Ohio River. The drainage area of the Ohio River at the Cincinnati gaging station is 76,580 mi^2. The upstream model limit is near the Meldahl Dam, operated by the Huntington District of the USACE near RM 436. River miles (RM), as shown on navigational charts of the Ohio River (U.S. Army Corps of Engineers, 2008), reference distances downstream from zero at the confluence of the Allegheny and Monongahela Rivers to 891 mi at the mouth at the Mississippi River near Cairo, Ill.

Summary of Hydrologic, Bathymetric, and Hydraulic Data Used in Models

Water Levels and Flows within the Model Area

Operations at Markland Dam, downstream from Cincinnati at RM 531.3, exert primary control over normal water levels in the 95.3-mi reach that extends upstream to Meldahl Dam (fig. 2). Water levels at Cincinnati, however, also respond to storms, typically causing an annual 25-ft excursion over the project-pool elevation of 455 ft above the Ohio River Datum for Markland Dam (fig. 3). Of the 123 annual peak flows recorded on the Ohio River at the Cincinnati water-level gaging station, 1773–1975, the maximum flow of 894,000 ft^3/s was recorded on January 26, 1937, with a gage height of 80 ft. Water levels referenced to the National Geodetic Vertical Datum of 1929 (NGVD 29) are obtained by adding 428.88 ft to the gage heights; water levels referenced to the North American Vertical Datum of 1988 (NAVD 88) are obtained by adding 428.227 ft to the gate heights.

Prior to its conversion to a water-level-only gaging station, the USGS Cincinnati gaging station also provided flow information. Based on USGS flow data from 1940 to 1975, the average flow of about 91,900 ft^3/s varies monthly from about 25,000 ft^3/s in October to about 215,000 ft^3/s in March (fig. 4). These historical flows at the USGS Cincinnati gaging station were computed from an empirically derived relation between water level and flow, which is commonly referred to as a stage-discharge relation, similar to the historical one shown in figure 5. When the gaging station was operated as a streamgage from 1940 to 1975, this relation was maintained and updated on a near-monthly basis, but when the streamgage was converted to a water-level gaging station, these updates ended, thus, the reliability of this historical relation is uncertain. Within the study area, major tributaries to the Ohio River include Licking River and the Little Miami River; minor tributaries include Twelvemile Creek, Big Indian Creek, Little Indian Creek, and Fourmile Creek.

The GCWW provides about 136 Mgal/d of water to the Cincinnati Metropolitan Area and to nearby communities in northern Kentucky. Intakes on the Ohio River and wells within the Great Miami Aquifer are used for public-water supply.

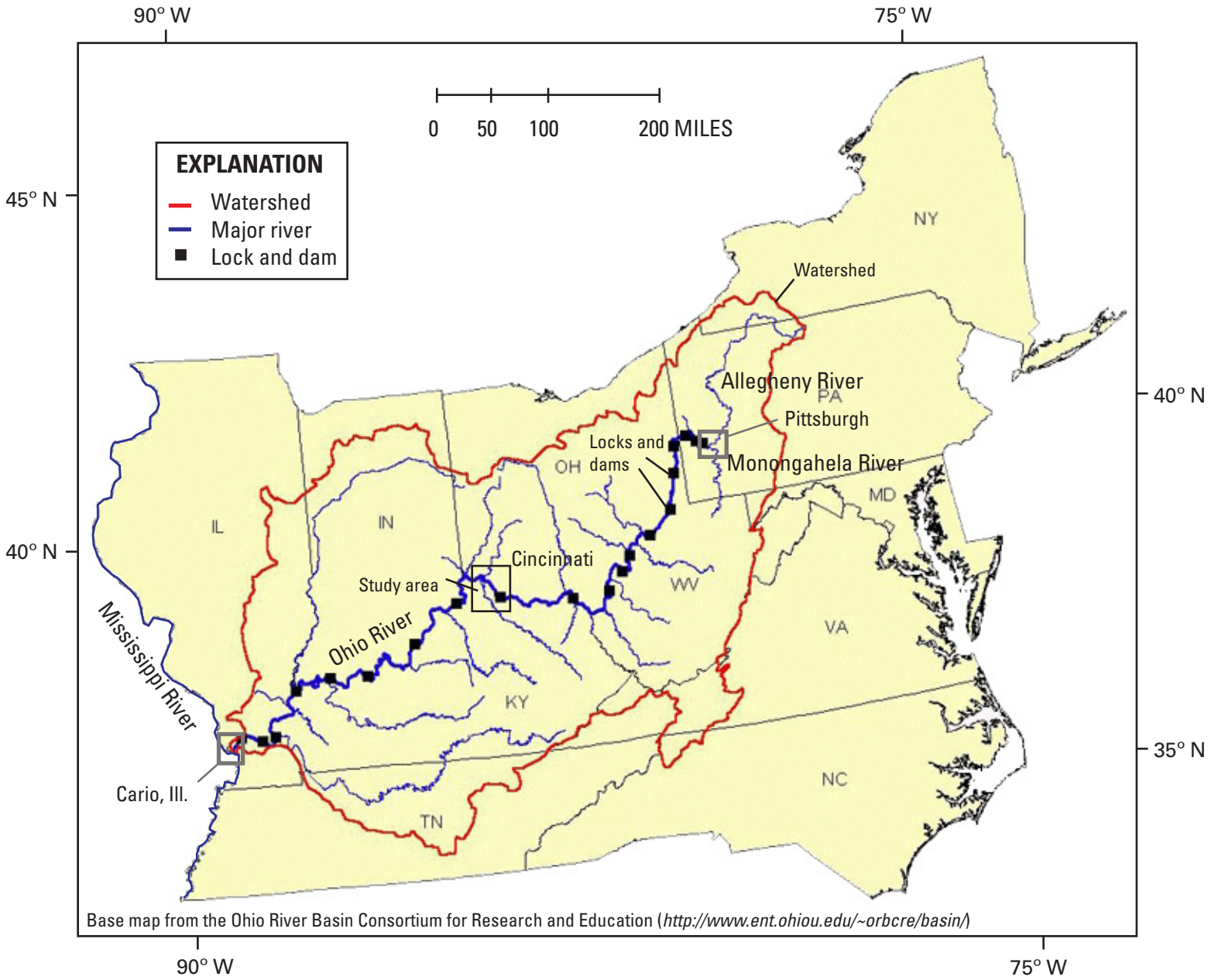

Figure 1. The Ohio River Basin, excluding the Tennessee River, in northeastern United States.

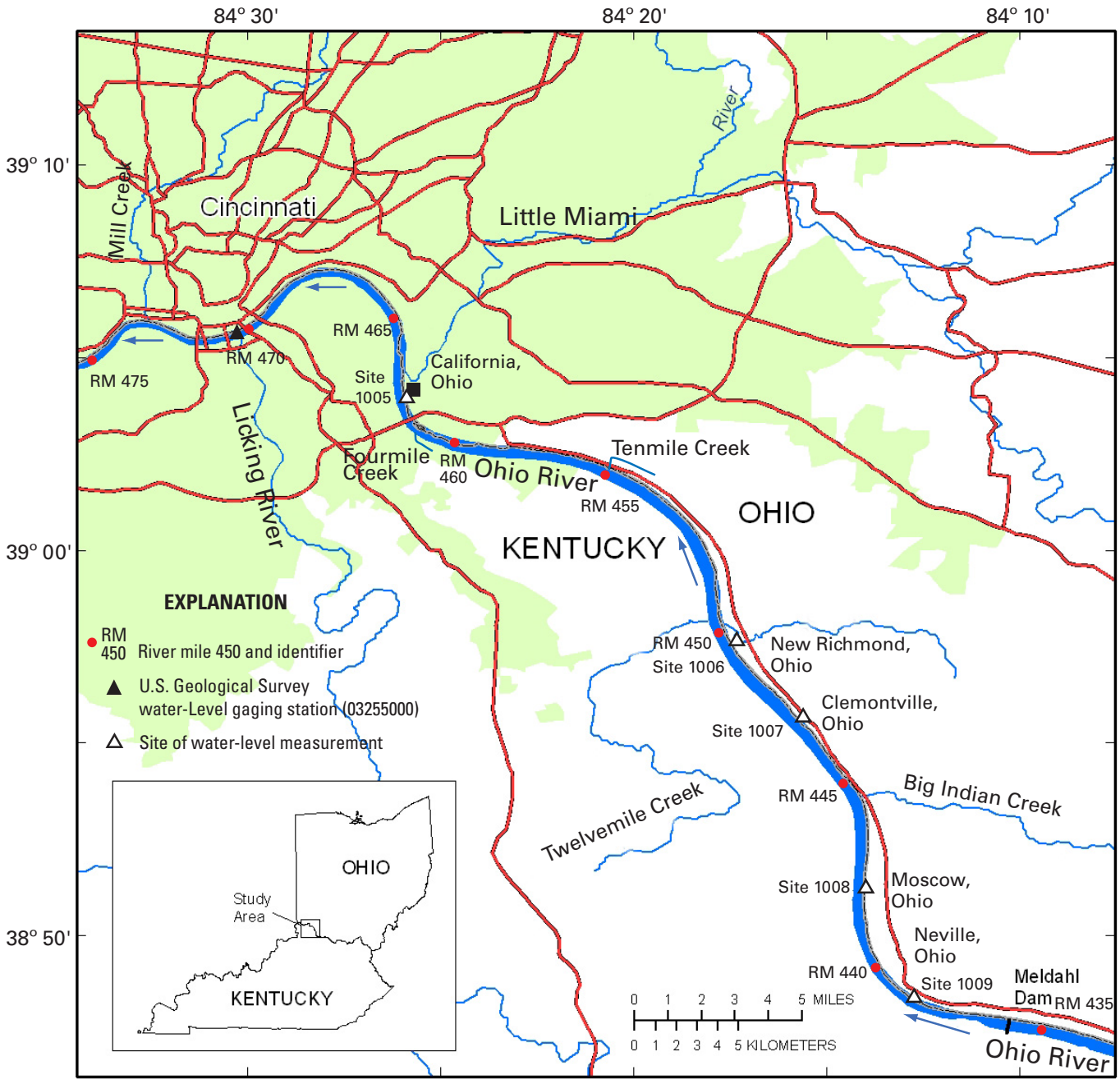

Figure 2. Study area of the Ohio River from Meldahl Dam to Cincinnati, Ohio.

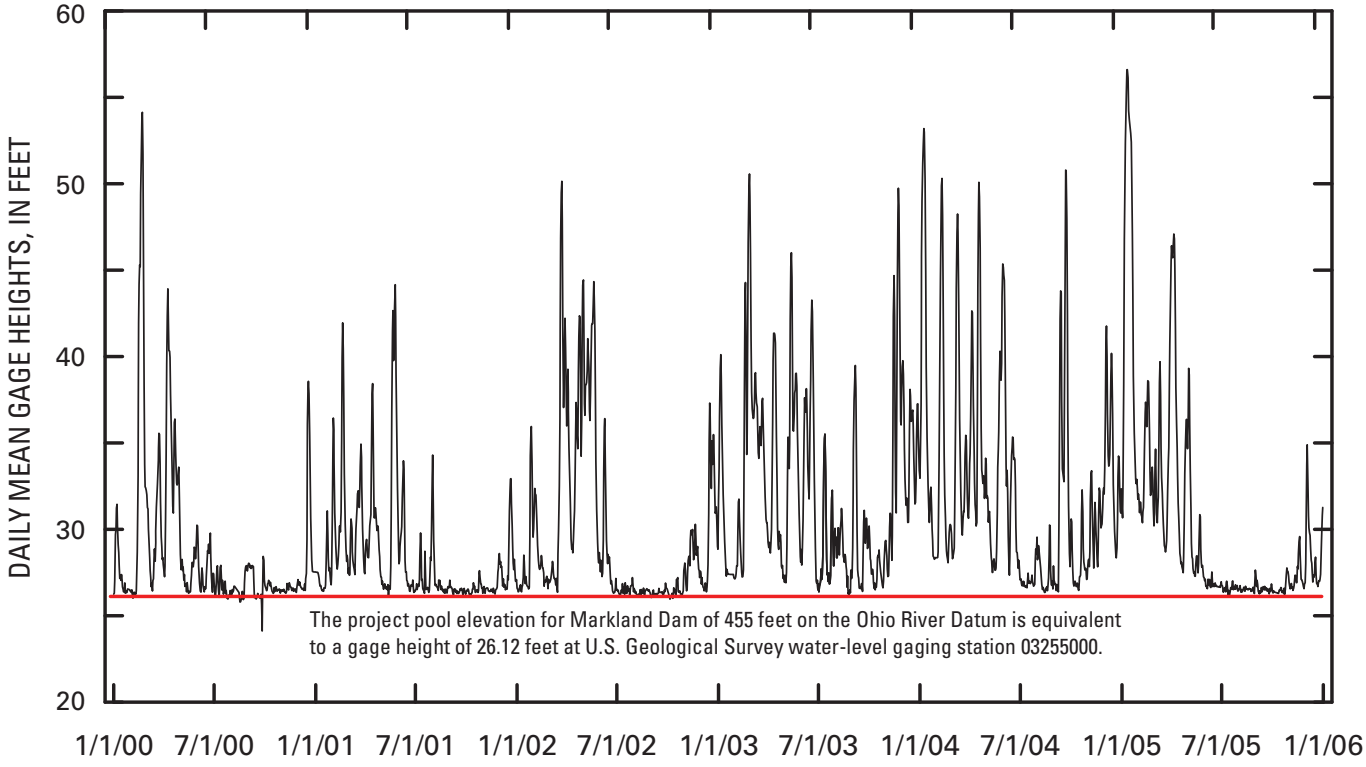

Figure 3. Daily mean gage heights on the Ohio River at Cincinnati, Ohio, at the U.S. Geological Survey water-level gaging station 03255000, January 2000–06.

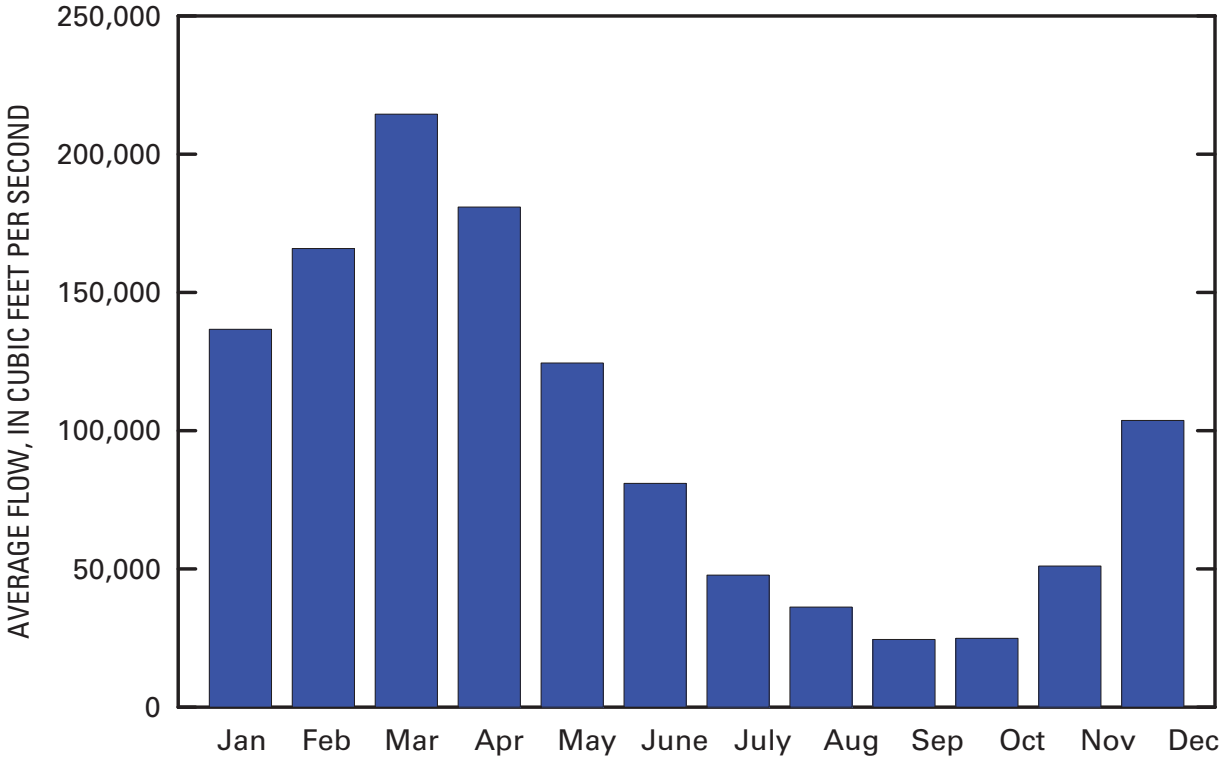

Figure 4. Average monthly flow on the Ohio River at Cincinnati, Ohio, at the U.S. Geological Survey streamgaging station 03255000, 1940–75.

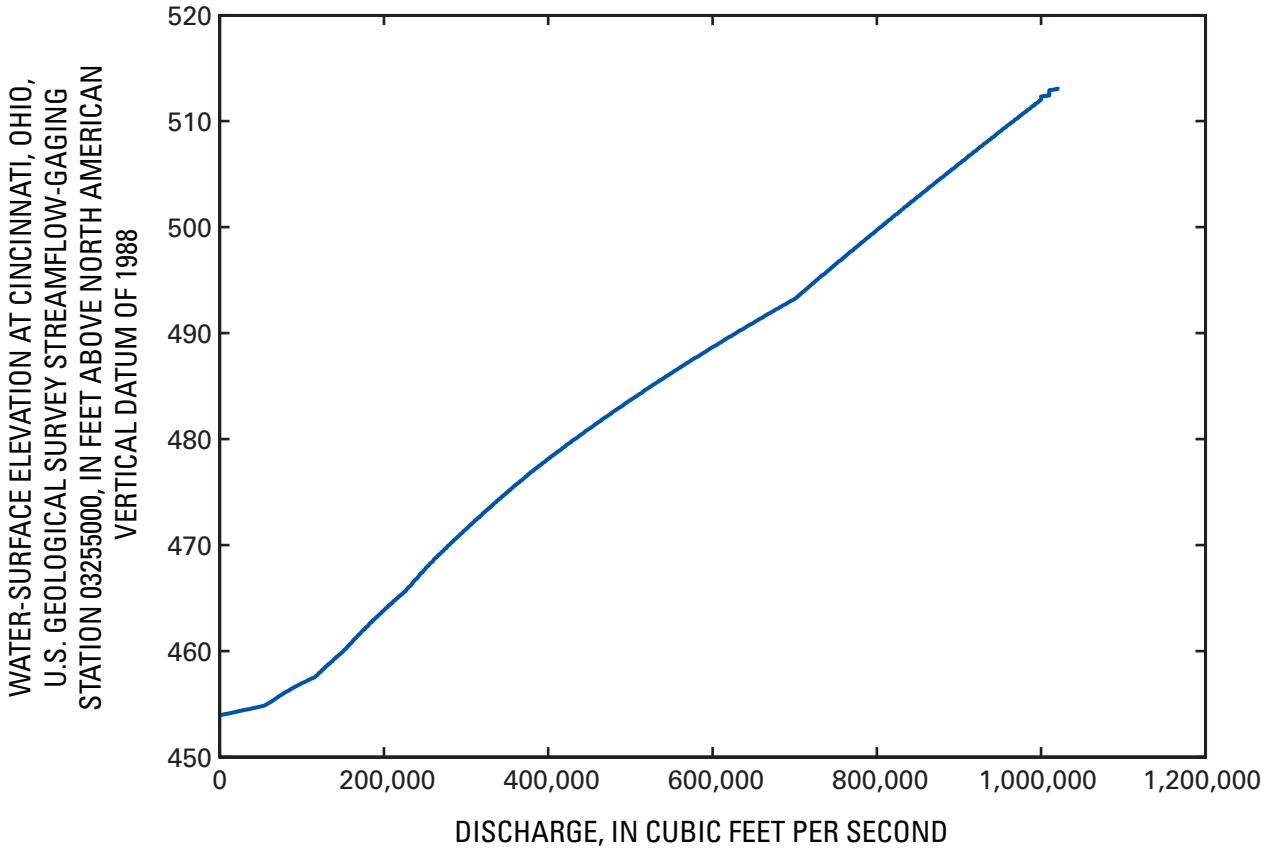

Figure 5. Historical stage-discharge relation at the U.S. Geological Survey streamgaging station at Cincinnati, Ohio, 03255000.

Meldahl Dam is at the upstream limit of the study area. At Meldahl Dam, two parallel locks on the north (Ohio) side of the river facilitate navigation by raising and lowering vessels about 30 ft across the dam (fig. 6). The main lock is 110 ft wide and 1,200 ft long; the shoreward auxiliary lock is 110 ft wide and 600 ft long. Under normal operating conditions when there is a 30-ft difference between water levels on the downstream and upstream sides of the dam, each time the main lock is operated, an equivalent downstream flow of 1,100 ft^3/s for 1 hour results; similarly, use of the smaller auxiliary lock results in 550 ft^3/s for 1 hour. These releases and accompanying surges in the flows were not accounted for in modeling activities described in this report.

Water levels upstream from Meldahl Dam are controlled by the operation of 12 tainter gates south of the locks. A tainter gate is a segment of a cylinder mounted on radial arms that rotates on trunnions anchored to the piers that separate the gates. At Meldahl Dam, each 100-ft-wide gate is separated by piers that are about 15 ft wide. The radial arms are 64 ft long, and the trunnions are set at an elevation of 487 ft above the Ohio River Datum (ORD). When closed, the gates rest on the weir crest that underlies the gate; the weir crests have an elevation of 450 ft above the ORD. The tainter gates are numbered consecutively from gate 1 near the locks on the Ohio side of the river to gate 12 on the Kentucky side.

The tainter gates are operated by a fixed schedule to improve the reaeration of the river (appendix 1). The positions of all tainter gates can be inferred from the reported total gate opening. For example, a total gate opening of 2 ft implies that gates 1 and 4 are raised 1 ft above the weir crest. Each of the gates can be raised a maximum of 30 ft; a gate opening of 360 ft implies that all gates are fully open. A gate opening of 999 implies that all gates as well as the locks are fully open. About 50 percent of the time (fig. 7), a gate opening of 30 ft is needed to maintain the normal pool elevation of 485 ft ORD upstream from Meldahl Dam.

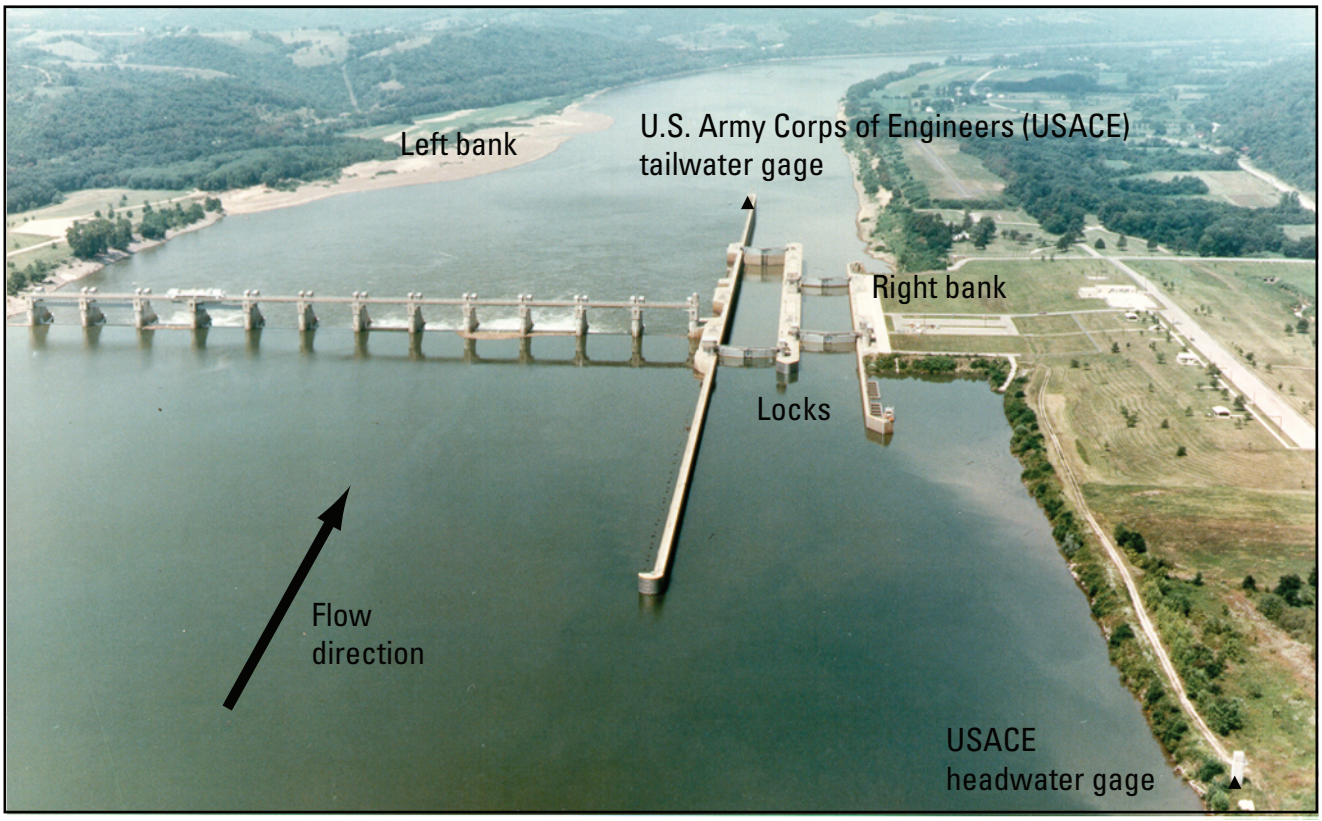

Figure 6. Meldahl Dam on the Ohio River near Neville, Ohio. (Photograph by U.S. Army Corps of Engineers (*http://www.lrh.usace.army.mil/_storage/Photos/1951.jpg*, accessed March 2, 2006). Used with permission.)

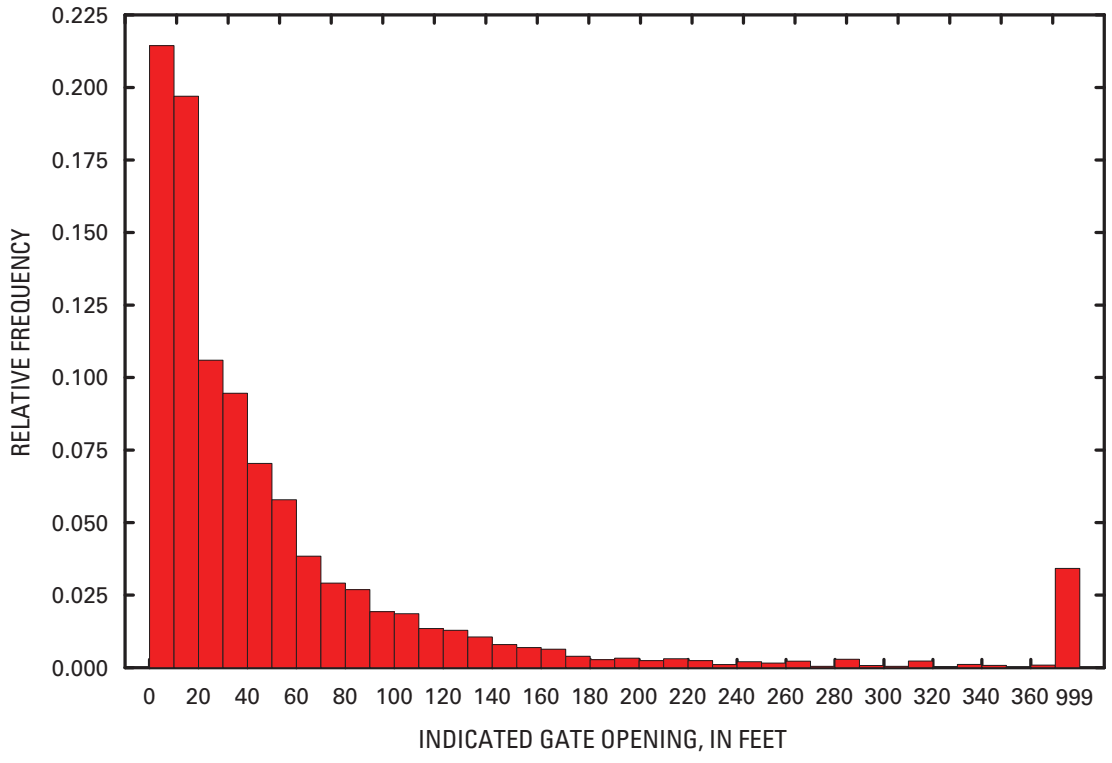

Figure 7. Histogram of hourly gate openings at Meldahl Dam near Neville, Ohio, 2000–05. (Gate-openings analysis based on data provided by Stanley Wisbith, U.S. Army Corps of Engineers, written commun., March 2006).

In the absence of streamflow records derived from up to date ratings based on systematic flow measurements, flow through Meldahl Dam was computed based on the gate rating or the tailwater rating. The USACE commonly computes flow across Meldahl Dam from the gate rating (fig. 8) (Stanley Wisbith, U.S. Army Corps of Engineers, written commun., March 2006). The gate rating does not, however, account for water passing through the locks. Because of their emphasis on high-flow conditions, the Ohio River Forecast Center (OHRFC) bases their estimates of flow exclusively on the tailwater rating, using the downstream pool elevation measured at the USACE water-level gaging station named Ohio River at Meldahl Dam near Neville, Ohio[1].

Gate and tailwater ratings have not been updated in more than 30 years. Some systematic differences between these rated flows occur during high- and low-flow conditions (fig. 9). Discrepancies between rated flows may be attributable to degradation in the accuracy of the tailwater rating as a result of variable backwater conditions from the Markland Dam during low flow. The discrepancies between rated flows result in differences between estimated flow-exceedance characteristics (fig. 10), which were computed by use of hourly values from November 1, 2000 to October 31, 2005. This recent period of record was selected because it contained few periods of missing record and it was considered adequate to provide a context for flow conditions during the ADCP surveys and dye injection studies. Exceedance probabilities indicate the likelihood that hourly flows will exceed a specified magnitude. For example, a flow of 100,000 ft^3/s will be exceeded about 40 percent of the time at Meldahl Dam; 60 percent of the time, flows will be less than [2]100,000 ft^3/s.

Flows were measured with ADCP for model calibration. ADCP units emit acoustic signals into the water and receive returning echoes from suspended particles and the river bottom at a rate of about once per second. Processing these signal pairs provides a basis for determining flow velocity and water depth. By temporally discretizing the returning signal, an ensemble of water velocities was computed at 0.82-ft intervals throughout the water column at that point (physical limitations prevent the measurement of velocities near the surface and near the channel bottom). Flows were determined from about 600 ensembles per transect, which were obtained from an ADCP unit tethered to a boat that traversed the river at about 2 ft/s. Each acoustic signal is coordinated with the measurement of position by a global positioning system (GPS) receiver to provide the ensemble location. Because of the random velocity variations introduced by the pitch, roll, and yaw of the ADCP unit during data collection, the small vertical (upward or downward) velocity component of flow could not be determined effectively from the ADCP data. Therefore, only the variations in horizontal velocity components with flow depth were investigated in this study.

Flows measured during the ADCP surveys were compared with rated flows computed from gate openings (fig. 11) (the gate rating is thought to be less sensitive than the tailwater rating to variable backwater conditions during low-flow periods). Comparison indicates there may be a systematic difference between the measured and rated flows, although this apparent discrepancy diminishes at higher flow rates. A regression equation (fig. 11) provides a basis for adjusting gate-rated flows less than 140,000 ft^3/s to more closely correspond to flows measured at single-transect ADCP measurements obtained during this study. The regression equation is thought to have utility for adjusting boundary inflows at Meldahl Dam to avoid bias in this model calibration. Because the adjustment does not account for the attenuation of flows between the dam and the measurement location, uncertainty in the adjusted flows remains high.

Single-transect ADCP measurements were used primarily to measure local velocity patterns throughout the study area, rather than to measure flows at individual cross sections. To compute flows, USGS guidelines for ADCP measurements (U.S. Geological Survey, 2005) require at least four transects at a cross section. Application of these guidelines to measurements of velocity patterns in this report, however, would have limited the density of information needed to describe flow patterns. Therefore, single-transect data were used to estimate flow for the regression analysis, but the utility of the regression equations for use outside this model calibration effort is uncertain.

Bathymetry and Acoustic Doppler Current Profiler Surveys

Koltun and others (2006) collected bathymetry data at about 800-ft intervals throughout the study area from October 2004 to March 2006 with a boat-mounted NaviSound 210 single-beam echosounder. Horizontal coordinates of the depth measurements were determined with differentially corrected GPS measurements and were referenced to the Ohio State Plane Coordinate System (Ohio South) in feet. Depth measurements were converted to streambed elevations by use of periodic water levels that were referenced to a system of elevation reference marks established by survey-grade GPS units along the study reach. Water levels, thus depths, for locations other than those colocated with the reference marks were determined by assuming a constant water-surface slope between reference marks. These unpublished water-level measurements obtained during bathymetry surveys were quality assured and adjusted by staff from USGS Office of Surface Water (Robert R. Mason, USGS National Center, written commun., 2007) and listed in appendix 2.

[1] For more information on the development or maintenance of the ratings at Meldahl Dam, contact the Huntington District of the U.S. Army Corps of Engineers or the Ohio River Valley Forecast Center.

[2] For more information on the development and maintenance of the gate and tailwater ratings should contact the Huntington District of the U.S. Army Corps of Engineers, or the Ohio River Forecast Center, respectively.

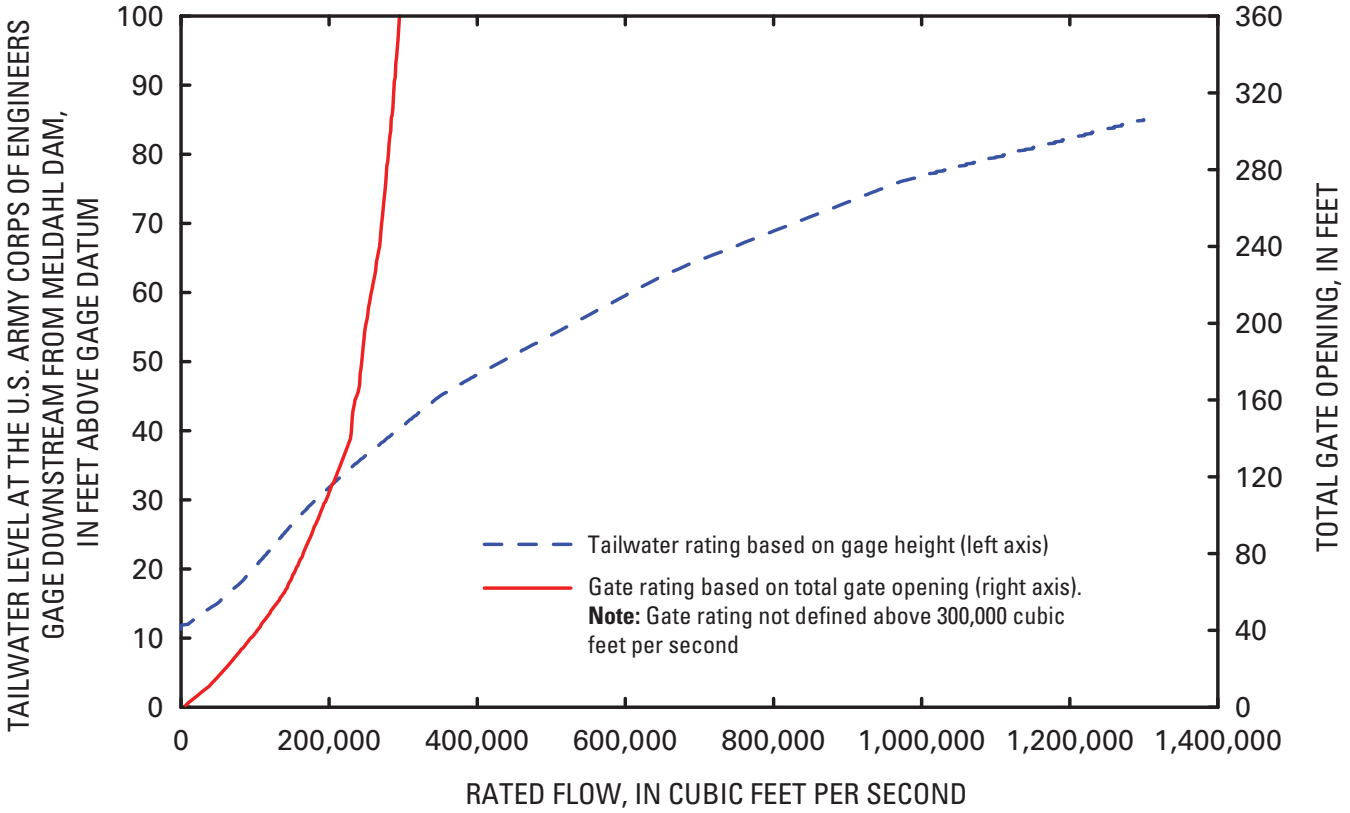

Figure 8. Gate and tailwater ratings at Meldahl Dam on the Ohio River near Neville, Ohio. (Gate and tailwater ratings based on data provided by Stanley Wisbith, U.S. Army Corps of Engineers, written commun., March 2006).

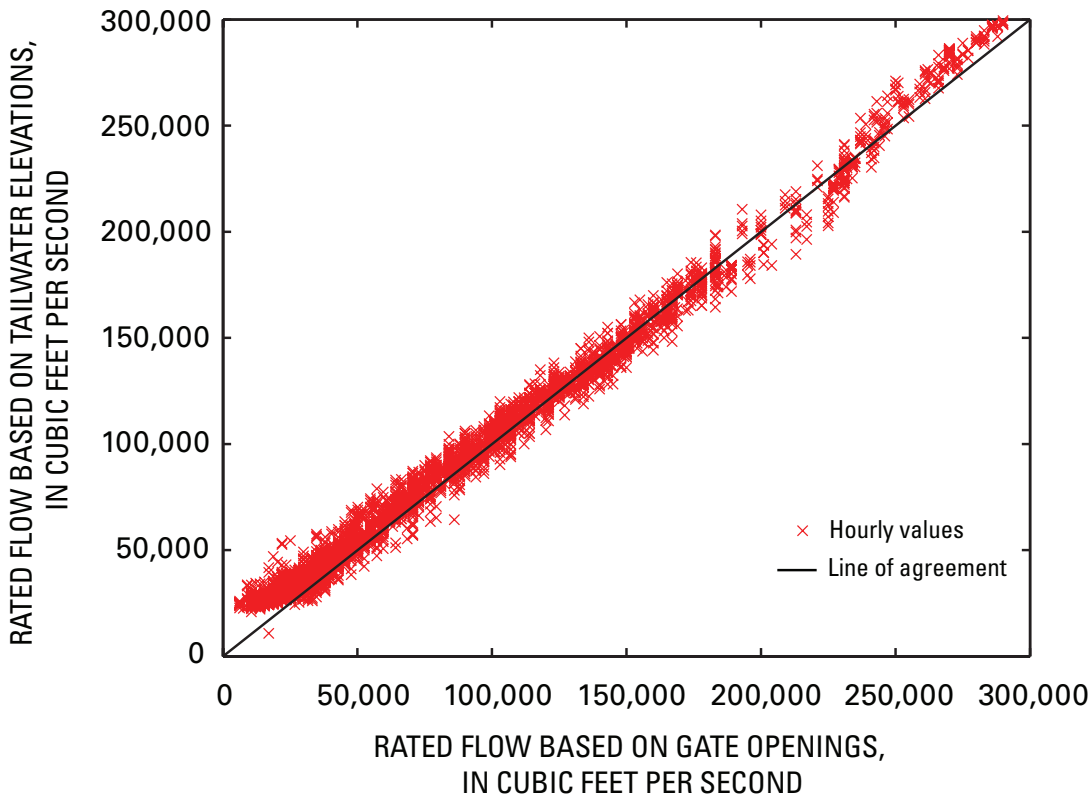

Figure 9. Relation between hourly flows on the Ohio River at Meldahl Dam near Neville, Ohio, estimated from the tailwater and the gate-opening ratings maintained by the U.S. Army Corps of Engineers Huntington District.

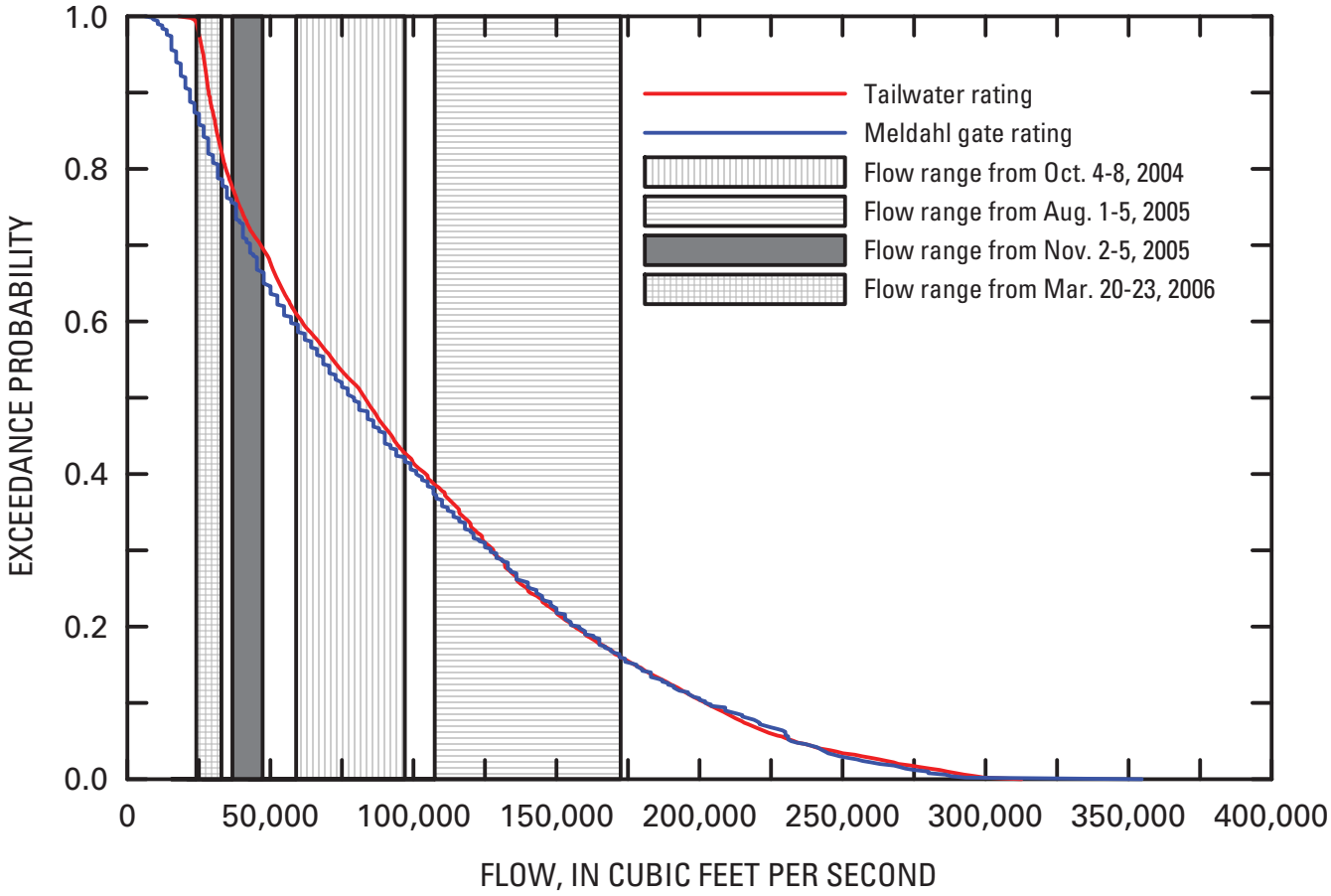

Figure 10. Flow-exceedance characteristics on the Ohio River at Meldahl Dam near Neville, Ohio, estimated by gate and tailwater ratings maintained by the U.S. Army Corps of Engineers Huntington District.

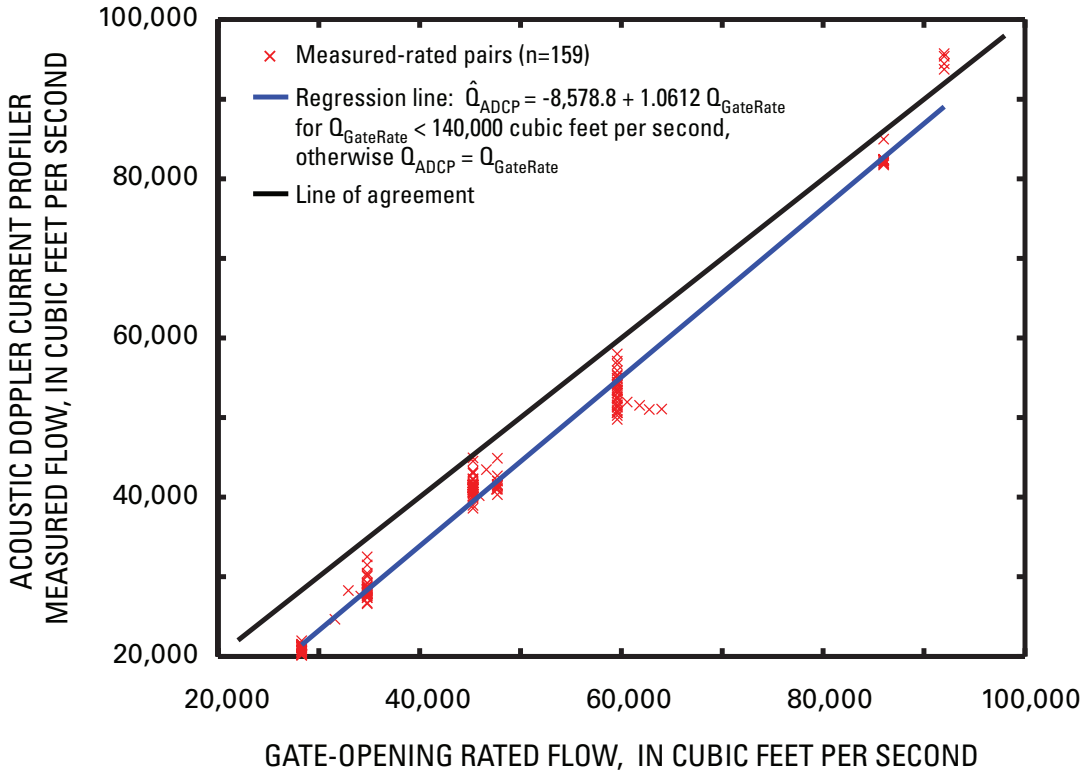

Figure 11. Relation between measured flows and flows estimated from the gate rating on the Ohio River at Meldahl Dam near Neville, Ohio, 2004–06.

Elevations are referenced to the North American Vertical Datum of 1988 (NAVD 88)[3] in feet.

Koltun and others (2006) also used ADCPs in a systematic survey of stream velocities and flows at about 2,200-ft intervals throughout the study reach during three periods of data collection. The upper reach, from RM 437 to 447, was surveyed October 25–November 4, 2005; the middle reach, from RM 447 to 464, was surveyed October 5–7, 2004; and the lower reach, from RM 464 to 470, was surveyed March 21–23, 2006. Additional ADCP transects were measured August 2–4, 2005, to support the dye-injection studies discussed in the following section. Water-level data measured during the bathymetry surveys are mostly from October 2005.

Dye-Injection Studies

Koltun and others (2006) conducted two dye-injection studies on the Ohio River in August 2005. The studies used two injection sites on opposite sides of the river within two overlapping stream reaches to provide dye concentration data needed to estimate transport parameters associated with transverse mixing characteristics. Rhodamine WT dye, a red dye that fluoresces when exposed to light, was used as a tracer because it (1) is nontoxic, (2) is fairly conservative (slowly decaying), (3) fluoresces at a magnitude proportional to its concentration, and (4) is measurable at low concentrations (parts per trillion) (Smart and Laidlaw, 1977). The 20-percent aqueous solution of rhodamine WT dye used in the dye-injection studies had a specific gravity of about 1.15 at 20°C and an active-ingredient concentration of 230,000 mg/L that disperses well in water. As such, rhodamine WT dye is thought to characterize the dispersion of other similar conservative, dissolved constituents in water. In both studies, dye was injected at a nominal rate of 200 mL/min (767 mg/s of active ingredient), starting about 24 hours preceding and throughout the concentration measurements.

Dye concentrations and flows were measured in cross sections downstream from the points of injection, generally spaced 1 to 2 mi apart. Multiple transverses were made at some cross sections to measure dye concentrations. In particular, multiple transverses were used to sample dye concentrations with depth until vertically well-mixed conditions were established. For injections at mid-depth locations, tracers are thought to become vertically well mixed within a distance of about 50 times the depth of water (Rutherford, 1994). In the dye-injection studies, dye was injected about 0.5 to 1 ft below the water surface, where average flow depths are less than 25 ft. ADCP measurements of flow were measured during the first traverse at each cross section. Transects where dye concentrations and flows were measured are shown on figure 12.

Depth-averaged flow-velocity magnitudes, derived from ADCP measurements obtained by Koltun and others (2006), had similar distributions at all dye-measurement transects (fig. 13), indicating slow and uniform velocities within the gently meandering dye-injection reaches. Of the measured depth-averaged velocities, 95 percent ranged from 0.26 to 1.3 ft/s, August 2–4, 2005.

On August 2, 2005, dye was injected about 1,180 ft downstream from the mouth of Twelvemile Creek, about 125 ft east of the Kentucky shoreline at cross section OH 4 (fig. 12). The flow direction in this reach is northerly; the injection point on the west side of the river is on the left as one faces downstream. This injection site and reach, referred to as the Twelvemile Creek (TMC) in this report, and as the "Downstream Dye Study" in the report by Koltun and others (2006), was near RM 451.7, with an injection point near N38°58'23" and W84°18'05." In this report, the TMC injection reach refers to the Ohio River between transects OH 4 and OH 16, approximately RM 451.7 to 463.9 (fig. 2). Vertically well-mixed concentrations were measured at cross section OH 10, about 6 mi downstream from the point of injection. Koltun and others (2006) considered all dye concentrations downstream from OH 10 also to be vertically mixed.

On August 4, 2005, dye was injected about 400 ft downstream from the mouth of Big Indian Creek, about 60 ft west of the Ohio shoreline at cross section OH 0 (fig. 12). This injection site and reach, referred to as Big Indian Creek (BIC) in this report, and as the "Upstream Dye Study" by Koltun and others (2006), was near RM 445.2 (fig. 2), with an injection point near N38°53'38" and W84°14'05," which is near the right bank. The BIC injection reach refers to the Ohio River between transects OH 0 and OH 9, from RM 445.1 to 456.8. Vertically well-mixed concentrations were measured at OH 3, about 5.5 mi downstream from the point of injection; concentrations also were considered vertically mixed downstream from that point.

Modeling Approach

A generalized 2D hydrodynamic code was applied to simulate the time-varying depth-averaged velocities and water levels within the study reach, based on water levels and inflows specified at the boundaries of the model area. Surveys of river bathymetry and channel geometry depicted on navigational charts were used to describe the model area. Hydraulic parameters describing channel friction losses and dispersion characteristics were systematically varied to improve the match between measured flow velocities and depths, flows, and water levels with simulated values for five scenarios.

[3] The velocity, bathymetry, and dye-concentration data can be downloaded as electronic documents from links in USGS Open-File Report 2006–1159 by Koltun and others, 2006, titled Velocity, bathymetry, and transverse mixing characteristics of the Ohio River upstream from Cincinnati, Ohio, October 2004–March 2006, *http://pubs.usgs.gov/of/2006/1159/*, accessed November 2007).

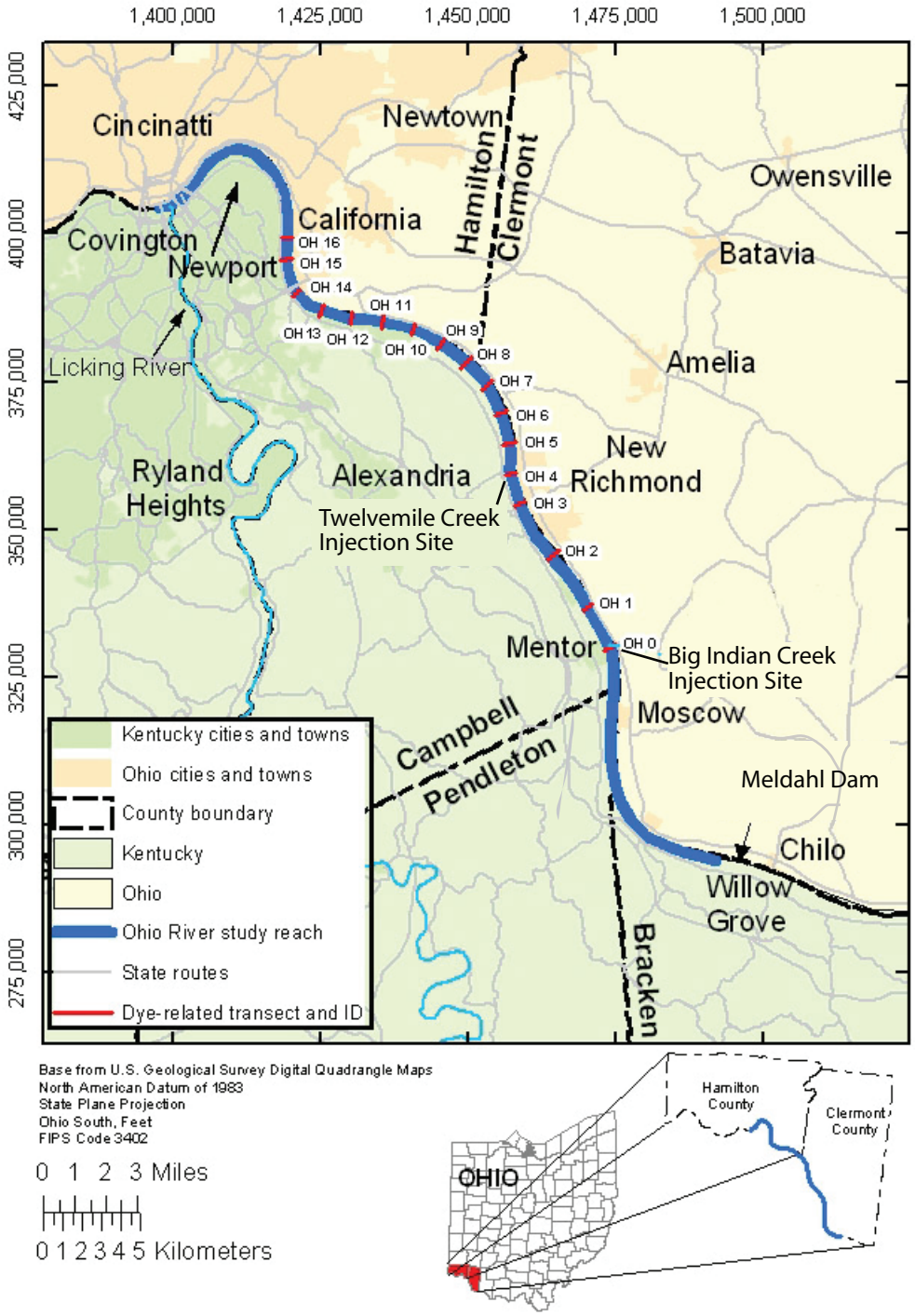

Figure 12. Location of transects related to dye-tracer studies (Koltun and others, 2006, fig. 6).

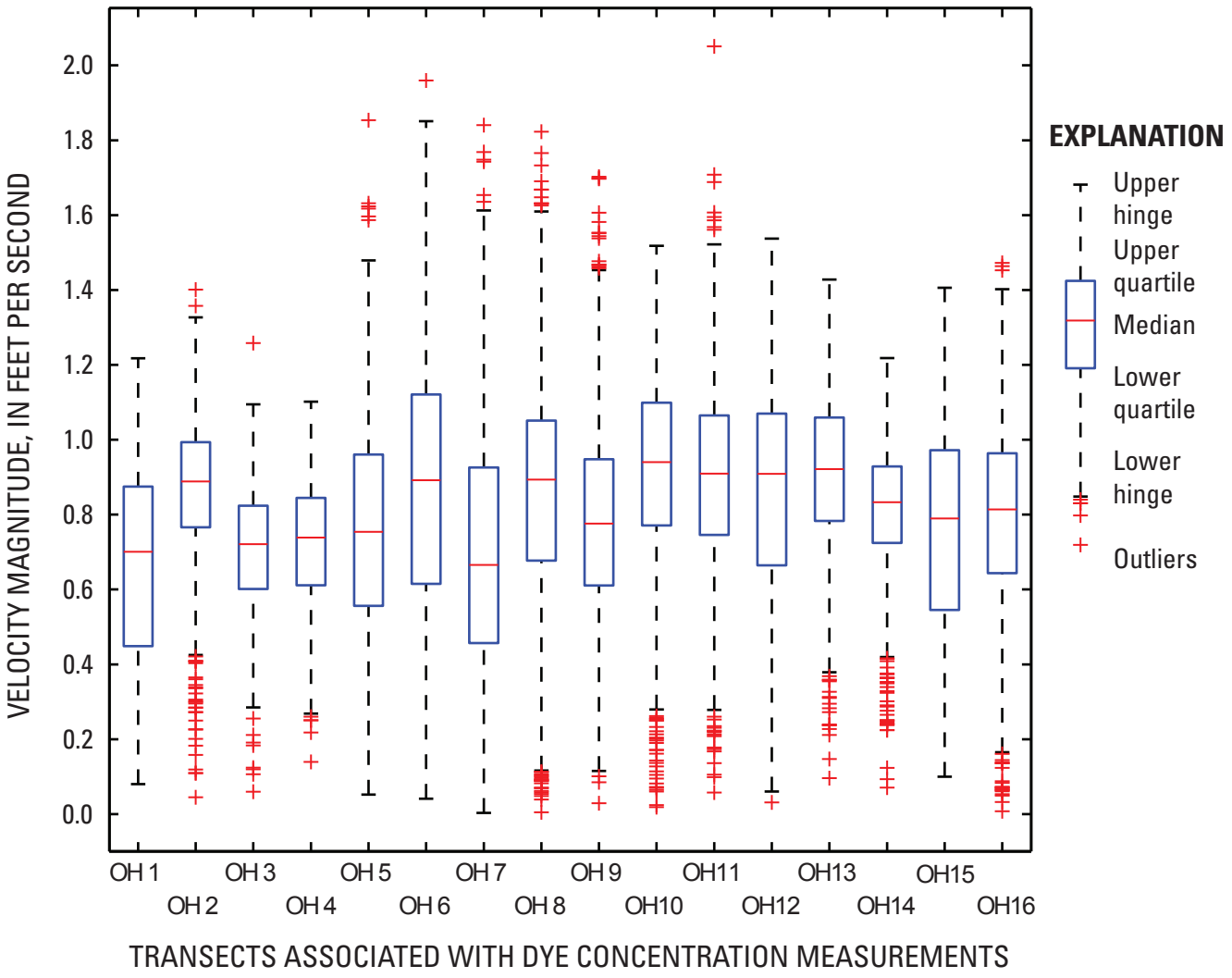

Figure 13. Distribution of depth-averaged flow-velocity magnitudes at dye-measurement transects on the Ohio River, August 2–4, 2005 (data from Koltun and others, 2006).

Simulated flow velocities and water levels provided input to a 2D water-quality transport model to describe the hydrodynamics during the two dye-injection studies (Koltun and others, 2006). Calibration involved estimating water-quality parameters that describe turbulent mixing and dye-decay characteristics by matching measured and simulated dye concentrations. The estimated hydraulic parameter that describes dispersion commonly is used to estimate the water-quality parameter that describes turbulent mixing. These two parameters, estimated from the flow and transport models that use different types of data, are compared.

Dye-Mixing and Transport Rates

Dye concentrations, sampled at a rate of about once in 10 seconds, were obtained along the same transect as ADCP velocity ensembles, sampled at a rate of about once per second. Although the USGS does not ordinarily use single-transect ADCP measurements to compute flow, these measurements were considered the best information available for determining the magnitude and distribution of flow associated with dye-concentration measurements in this study. Therefore, cumulative flows at points of dye concentration measurements were determined from ADCP data. The cumulative flows were used to compute incremental flows for each dye-concentration sample, as shown for flows and dye-concentrations measured on the Ohio River near OH 15 on August 2, 2005, from 13:44 to 13:54 EST (fig. 14).

The flow-weighted mean concentration commonly is defined as $\bar{C} = \frac{1}{Q}\int_0^Q c \cdot dq$, where c is the continuous variation in concentration with flow (Q) across the channel. In this report,the flow-weighted mean concentration was approximated as $\tilde{\bar{C}} = \frac{1}{Q}\sum_i c_m(i) \cdot \Delta q(i)$, where the individual dye-concentration measurements along a transect are indicated by $c_m(i)$ and the corresponding incremental flows centered at points of dye-concentration measurement are indicated by $\Delta q(i)$.

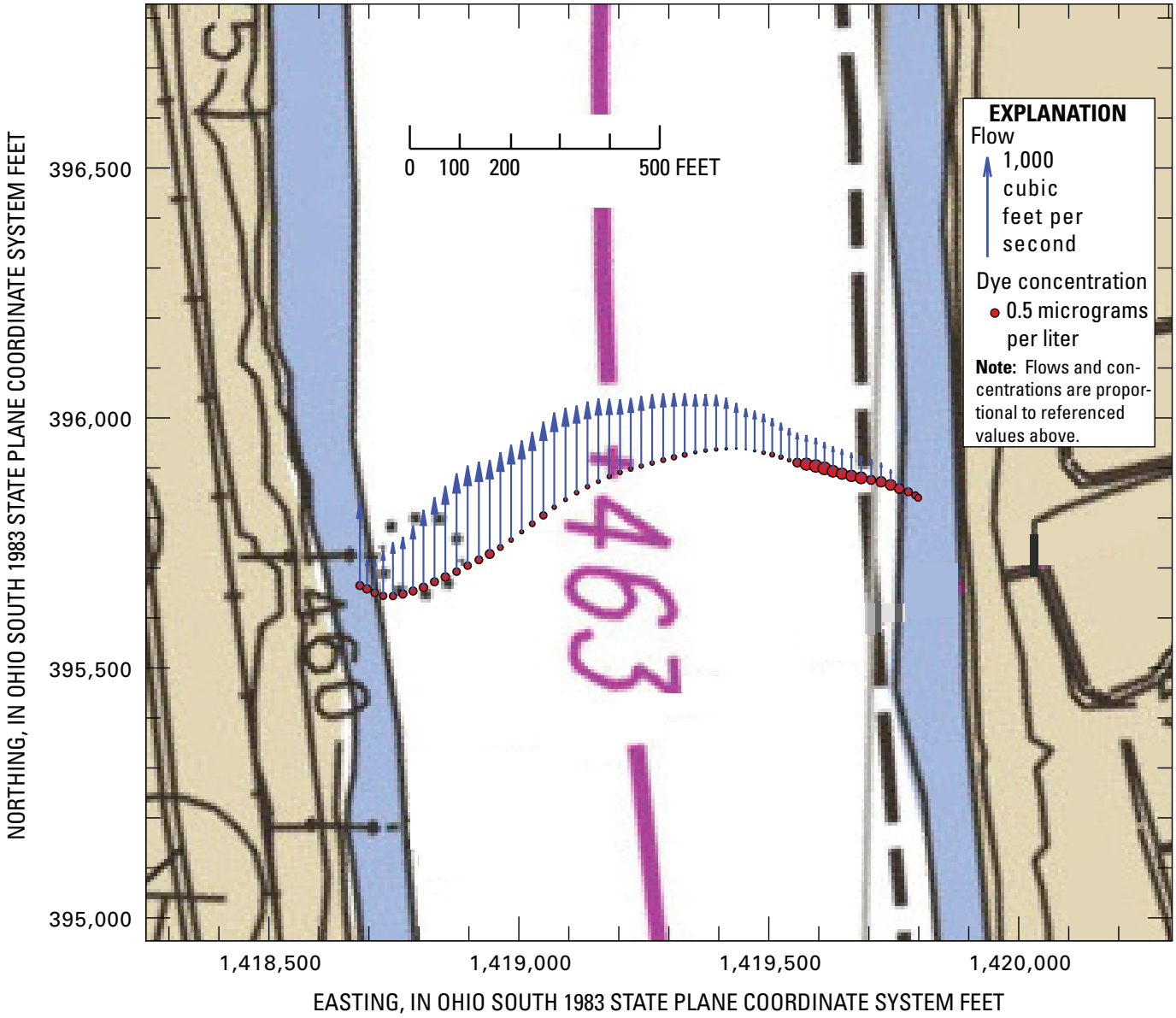

Figure 14. Flows and dye concentrations at OH 15 on the Ohio River from the Twelvemile Creek dye-injection study, near California, Ohio, August 2, 2005, 1344–1354 Eastern Standard Time.

Similarly, the dye-transport rate was computed as $M = \tilde{\bar{C}} \cdot Q$. The percent mixing, which is the degree to which a dispersant is mixed in any cross section of the river, is defined as $P_m = 1 - \frac{1}{2Q}\int_0^Q \left|\frac{c}{\bar{C}} - 1\right| dq$ and approximated as $\tilde{P}_m = 1 - \frac{1}{2Q}\sum_i \left|\frac{c_m(i)}{\tilde{\bar{C}}} - 1\right| \cdot \Delta q(i)$. In general, mean dye concentrations and transport rates decreased with distance downstream from the point of injection, and percent mixing increased (table 1).

Hydrodynamic Simulation

In this report, the hydrodynamic code refers to the generalized RMA2 hydrodynamic FORTRAN (Formula Translation) code; the hydrodynamic model refers to the set of input files describing the geometry, bathymetry, hydraulic characteristics, and boundary conditions of the Ohio River between Meldahl Dam and Cincinnati, Ohio. The code and model are used together to simulate depth-averaged velocities and water levels for flows and water levels specified at the model boundaries.

Table 1. Computed mean dye concentrations, percent mixing, and transport rates at selected Ohio River transects, August 2–4, 2005. (Data from Koltun and others, 2006)

Transect identifier	Distance downstream from injection point, in miles	Dye-measurement start time, Eastern Standard Time	Measured flow, in cubic feet per second	Flow-weighted mean dye concentration, $\tilde{\bar{C}}$, in micrograms per liter	Computed dye-transport rates, *M*, in milligrams per second	Percent mixing, $\tilde{P}_m$	Simulated travel time, in days
Twelvemile Creek injection, August 2, 2005							
OH 10	5.99	10:13	28,200	0.875	700	28.0	0.656
OH 11	7.01	11:01	28,300	.683	549	34.3	.746
OH 12	8.02	11:05	27,900	1.02	803	40.8	.844
OH 13	9.07	11:27	30,300	1.20	1,040	41.7	.948
OH 14	10.1	11:36	28,600	.837	678	70.3	1.058
OH 15	11.2	13:44	32,400	.529	487	89.0	1.167
[1]OH 16a	12.0	12:49	28,600	.507	412	90.7	1.250
[1]OH 16b	12.0	13:07	27,600	.471	386	90.5	1.250
Big Indian Creek injection, August 4, 2005							
OH 3	5.49	9:49	21,200	1.20	653	66.0	0.458
OH 4	6.49	10:09	21,000	1.15	546	72.3	.563
OH 5	7.45	12:39	21,100	1.21	669	77.3	.656
OH 6	8.45	12:50	20,500	.921	535	81.2	.771
OH 7	9.52	13:35	20,100	.897	576	93.0	.865
OH 8	10.5	13:25	18,800	.666	383	92.8	.960
[1]OH 9a	11.5	14:08	20,800	.401	256	87.4	1.063
[1]OH 9b	11.5	14:08	21,800	.432	299	87.7	1.063

[1]Transects labeled with an "a" or "b" suffix were collected at the same location but at different times or by different boat crews.

RMA2 Hydrodynamic Code

RMA2 is a generalized computer code for 2D hydrodynamic simulation of surface-water bodies. The code facilitates the computation of horizontal flow-velocity components and water levels for subcritical, free-surface flow. RMA2 implements a finite-element solution of the Reynolds form of the Navier-Stokes equations for turbulent flows. Donnell and others (2005) provide detailed documentation of the governing equations, their solution by the finite-element method, and recommended uses and limitations of the RMA2 code. RMA2 is under continual development by the USACE at the Waterways Experiment Station, Coastal Hydraulics Laboratory, in Vicksburg, Miss. RMA2 version 4.56, last modified on April 5, 2006, was used in this report. A brief overview of those modeling aspects needed to help understand the simulation and calibration process is provided.

The Reynolds form of the Navier-Stokes equations governing 2D flow that were used consist of a momentum (equation 1) and continuity (equation 2) are

$$h\frac{\partial u}{\partial t}+hu\frac{\partial u}{\partial x}+hv\frac{\partial u}{\partial y}-\frac{h}{\rho}\left[E\frac{\partial^2 u}{\partial x^2}+E\frac{\partial^2 u}{\partial y^2}\right]+gh\left[\frac{\partial a}{\partial x}+\frac{\partial h}{\partial x}\right]+\frac{g\cdot u\cdot n^2}{\left(1.486h^{1/6}\right)^2}\left(u^2+v^2\right)^{1/2}=0$$

$$h\frac{\partial v}{\partial t}+hu\frac{\partial v}{\partial x}+hv\frac{\partial v}{\partial y}-\frac{h}{\rho}\left[E\frac{\partial^2 v}{\partial x^2}+E\frac{\partial^2 v}{\partial y^2}\right]+gh\left[\frac{\partial a}{\partial x}+\frac{\partial h}{\partial x}\right]+\frac{g\cdot v\cdot n^2}{\left(1.486h^{1/6}\right)^2}\left(u^2+v^2\right)^{1/2}=0 \quad (1)$$

$$\frac{\partial h}{\partial t}+h\left[\frac{\partial u}{\partial x}+\frac{\partial v}{\partial y}\right]+u\frac{\partial h}{\partial x}+v\frac{\partial h}{\partial y}=0 \quad (2)$$

where

- h is water depth,
- u,v are velocities in the Cartesian directions,
- x,y,t are Cartesian coordinates and time,
- ρ is the density of water,
- E is the isotropic eddy-viscosity coefficient,
- g is gravitational acceleration,
- a is the elevation of the channel bottom,
- n is Manning's channel roughness value, and
- 1.486 is the conversion from metric to English units of measurement.

Equations 1 and 2 are solved by the finite-element method, using the Galerkin method of weighted residuals (Donnell and others, 2005). Integration in space is performed by Gaussian integration; derivatives in time are evaluated by a nonlinear finite-difference approximation. The solution is fully implicit, and the set of simultaneous equations is solved by Newton-Raphson iteration (Donnell and others, 2005).

To numerically solve the partial differential-flow equations, the channel is discretized into a finite-element mesh, which provides a flexible means to represent an irregularly shaped waterway. Quadrilateral and triangular elements formed by nodes at the vertices and midsides of the connecting arcs compose the mesh. Eight nodes are defined per quadrilateral element; six nodes are defined per triangular element. Contiguous elements forming branches or subreaches of the waterway are grouped into material zones to facilitate characterization of the waterway. Channel-roughness coefficients and eddy-viscosity characteristics are assigned to material zones.

Hydrodynamic simulations compute water levels and flow velocities at interior nodes from boundary conditions specified at exterior (boundary) nodes, the hydraulic characteristics of the waterway, and the flow equations. Boundary conditions include flow (discharge across one or more elements) and water level. Quadratic interpolation is used to determine water levels and velocities within the elemental areas, based on nodal values. Greater densities of nodes provide improved spatial resolution of velocity fields but also require additional computational resources.

Velocity distributions are largely determined by the advection component described by hydrodynamic simulation. Water velocities may decrease in shallow areas because of aquatic vegetation that effectively increases channel roughness; adjacent points may have similar velocities, based on the effectiveness of turbulent exchange in mixing the water. Neither channel roughness nor turbulent exchange (which is the fluid momentum transfer resulting from chaotic motions of fluid particles) (Donnell and others, 2005) can be measured directly in the field; they are inferred from measurements of flow, water level, and velocity.

In RMA2, the eddy-viscosity coefficient represents the effects of molecular viscosity and turbulence on turbulence exchange in which the turbulence component normally dominates. In general, turbulence exchanges depend on the momentum of the flow, spatial gradients of the velocity, and the scale of the flow phenomenon, as described by the length of the element in the direction of flow. For consistency with the physical system, eddy-viscosity coefficients in the mesh should increase with element size and flow velocity. Higher eddy viscosities are associated with greater uniformity of velocity distributions across a channel segment.

Although eddy viscosities may be assigned directly to elements in material zones, greater consistency and flexibility is obtained within RMA2 by assigning eddy viscosities to elements on the basis of the Peclet formula (Donnell and others, 2005) in which the Peclet number is inversely related to the eddy viscosity as

$$E = \frac{\rho \cdot u \cdot dx}{P_{RMA2}} \tag{3}$$

where

E is the eddy viscosity assigned to an element,
ρ is the water density, determined as a function of water temperature,
u is the average elemental velocity,
dx is the length of the element in the streamwise direction, and
P_{RMA2} is the dimensionless Peclet number, which is generally recommended to be between 15 and 40 (Donnell and others, 2005).

Greater Cincinnati Hydrodynamic Model of the Ohio River

The geometry (shoreline) of the Ohio River was based on Ohio River Navigation Charts 115–122, published by U.S. Army Corps of Engineers (2000). The charts were available as map images in Adobe Systems Incorporated's Portable Document Format (PDF). The PDF files were converted to the Joint Photographic experts Group (JPG) graphic format for import into Surface Water Modeling System (SMS) (Environmental Modeling Research Laboratory, 2006). Within SMS, the JPG files were georeferenced to scale and rotate the images. Selected latitude and longitude tic marks shown on the chart images were converted to Ohio South (3402) State Plane Coordinate System of 1983 with Corpscon (U.S. Army Corps of Engineers, 2005) for spatial reference.

The bathymetry of the Ohio River within the model area was based on surveys from 2004 to 2006 by Koltun and others (2006)[4]. Bathymetry data were measured at an average transect spacing of about 800 ft by a boat-mounted single-beam echosounder. To compute streambed elevations, depth information obtained from the echosounder were postprocessed and subtracted from the water surface that was determined from GPS survey techniques or derived from the assumption of constant water-surface slope between surveyed locations. The bathymetry data were written to text files formatted as a series of space-delimited x-, y-, and z-coordinates. Geographic coordinates for bathymetry data in this report are referenced to the North American Datum of 1983 (NAD 83), Ohio State Plane (Ohio South) coordinates, U.S. Survey Feet. Streambed elevations are reported in feet relative to the North American Vertical Datum of 1988 (NAVD 88). Bathymetry data can be downloaded from the Internet at *http://oh.water.usgs.gov/ORreport/data/bathymetry.zip* (accessed December 2006).

[4] Bathymetry data can be downloaded from the Internet at *http://pubs.usgs.gov/of/2006/1159* through a link in the table of contents titled "Retrieval of Data" in U.S. Geological Survey Open-File Report 2006–1159 by Koltun and others (2006).

The surveyed bathymetry data were supplemented with nearshore elevations shown on the Ohio River Navigation Charts (U.S. Army Corps of Engineers, 2008). Charts are referenced to the Ohio River vertical datum (U.S. Army Corps of Engineers, 2005b). Between Meldahl Dam and the Cincinnati water-level gaging station, the USACE communication directs users to subtract an average of 0.73 ft from the Ohio River Vertical Datum to obtain the "1929 General Adjustment," which is interpreted as the National Geodetic Vertical Datum of 1929 (NGVD 29). In the model area, elevations referenced to NAVD 88 can be obtained by subtracting 0.65 ft from elevations referenced to NGVD 29.

SMS software (Environmental Modeling Research Laboratory, 2006) was used to develop the finite-element mesh and to help interpolate the bathymetry between measured transects. In SMS, a map coverage was created that subdivided the study area into 52 polygons defined by 319 arcs. Four arcs typically were used to outline a polygon. Arcs are defined by vertices that initially were located by digitizing straight-line segments that outlined the channel geometry in subreaches about 1-mi long. When the channel geometry was defined, the vertices were redistributed uniformly along the arcs at about 100-ft intervals. Subsequently, the patch-meshing technique was assigned to each polygon. This meshing technique defines elements and nodes throughout the polygon by constructing a partial bicubic Coon's patch. This patch is based on the outlining vertex locations when the map coverage is converted to a finite-element mesh (Environmental Modeling and Research Laboratory, 2006). A material zone was assigned to each polygon; material zones share common channel-roughness and eddy-viscosity characteristics. To allow for possible systematic differences in effective channel roughness between areas of deep and shallow flow, the model contains two material zones. The deep zone corresponds to mid-channel areas shown in white on the navigational charts; the shallow zone corresponds to near-bank areas shown in purple.

Finite-Element Mesh

The finite-element mesh developed for the hydrodynamic study of the Ohio River area (a section of which is shown in fig. 15) includes 29,392 quadrilateral and 359 triangular elements defined by 92,622 nodes. Corner nodes are at the vertices of the elements, and midside nodes are midway along an arc that connects adjacent corner nodes. Each element is about 100 ft on a side, and there is little variability in areas among elements. The entire mesh spans about 10.5 mi^2. Within the finite-element mesh, nodestrings were defined to connect nodes that span the width of a river or a tributary. Nodestrings were used to specify flow and water-level boundary conditions and to specify transects where flow would be computed.

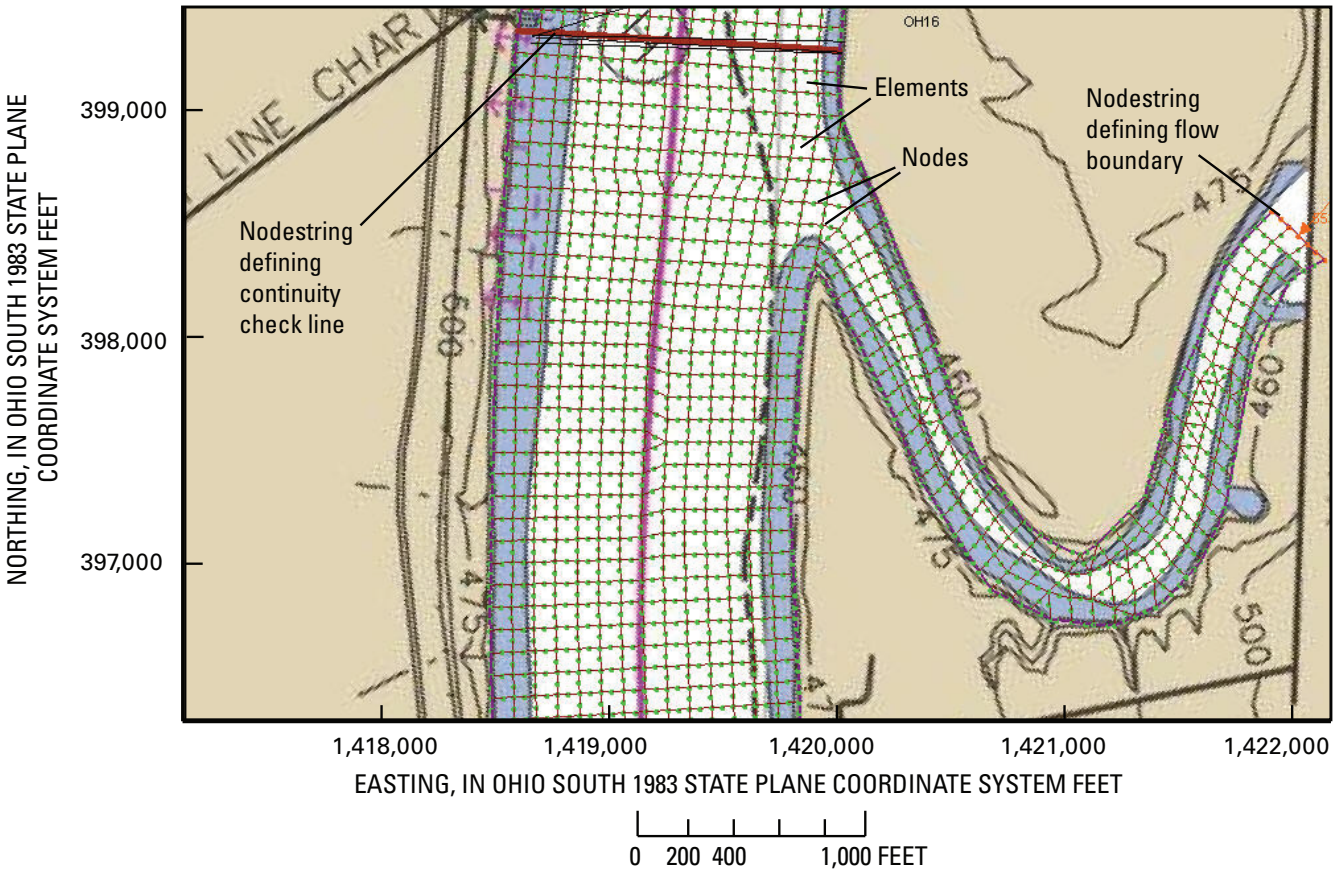

Figure 15. Image of the finite-element mesh near the confluence of Little Miami River and the Ohio River.

Individual nodes within the mesh were repositioned as needed to satisfy mesh quality-assurance criteria that increase the accuracy and reduce numerical instability of finite-element computations. These criteria include a minimum interior angle of 10 degrees for triangular elements (20 degrees for a quadrilateral element), no concave quadrilaterals, and an element-area change restriction that prevents elements from being 50 percent larger or smaller than adjacent elements.

Bathymetry data from measurement at transects and nearshore elevations from topographic maps were interpolated to model nodes in a two-step process. In the first step, a curvilinear grid was superimposed over the model area that followed the curvature of the centerline of the river. The grid was composed of rectangular cells, which had a length of 70 ft in the streamwise direction and 20 ft in the cross-stream direction. The template method (McDonald, Bennett, and Nelson, in press) was used to interpolate river elevations across the grid.

A template consists of a moveable cluster of cells centered at the point of estimation, which for the Ohio River analysis was 4 cells long in the streamwise direction and 1-cell wide in the cross-stream direction. For each cell, the area spanned by the template was used to search adjacent grid cells for bathymetry data. The basic idea of this method is that riverine topography tends to vary more in the cross-stream (transverse) direction than it does in the streamwise (longitudinal) direction (McDonald, Bennett, and Nelson, in press).

At each grid cell, an estimate of the channel bottom is computed as the inverse distance-weighted average of data spanned by the template. If no points were detected in the initial search, the template was doubled in size, preserving the specified ratio of length to width, and searched again until one or more points were found. Up to 3 template expansions were possible. In this analysis, the weighting exponent was one, which is equivalent to simple averaging of bathymetry values.

In the second step, a triangular irregular network (TIN) was formed from the bathymetry values in the curvilinear grid. This grid was overlain on the finite element mesh and linear interpolation was used to estimate the elevation of all model nodes.

Boundary-Condition Scenarios

Boundary conditions were defined for five scenarios that correspond to the periods of the data collection. The scenarios, shown with associated data, are identified as Oct2004 (fig. 16), Aug2005 (fig. 17), Oct2005, (fig. 18), Nov2005 (fig. 19), and Mar2006 (fig. 20) to correspond to the month and year of data collection. One scenario (Oct2005) is associated with the water-level measurements (table 2, fig. 21) obtained during the 2004–06 bathymetry surveys.

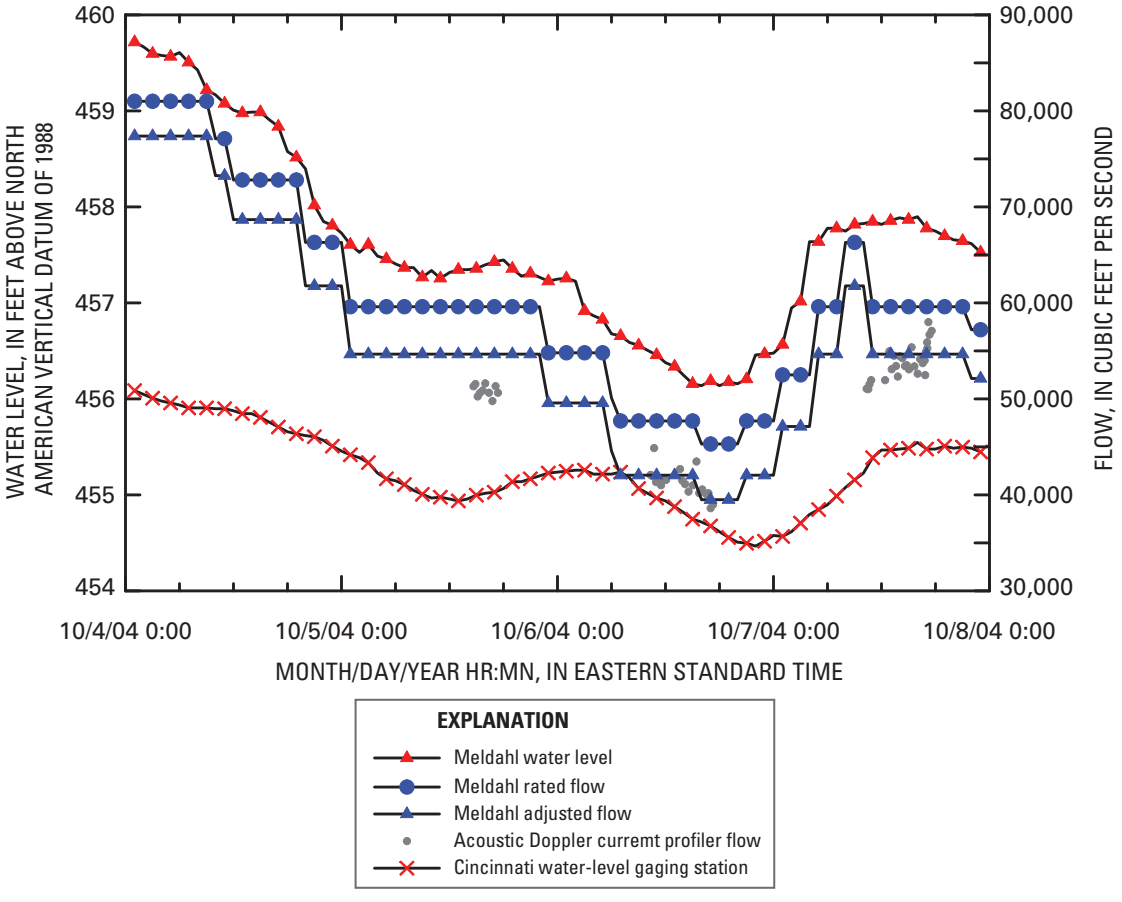

Figure 16. Water levels and flows in the Ohio River model area, October 4–8, 2004, scenario (Oct2004).

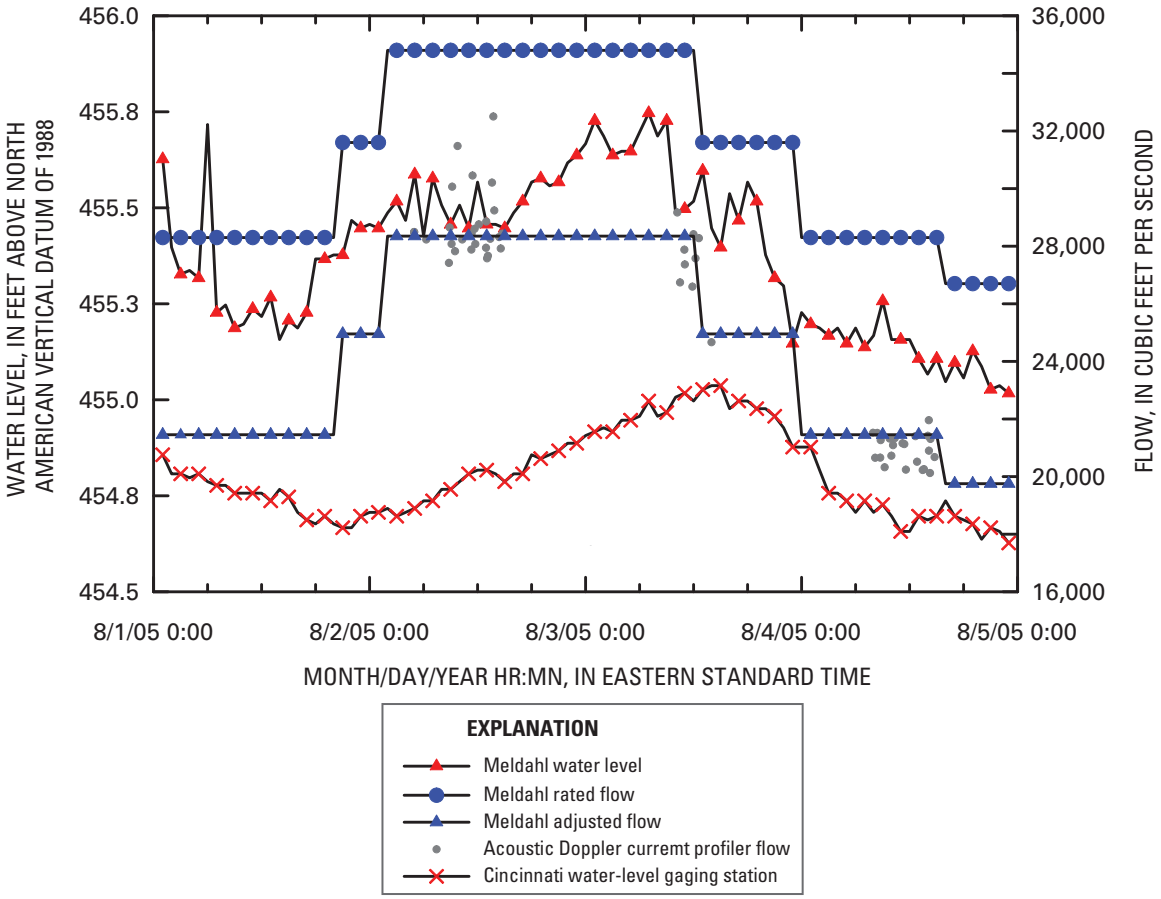

Figure 17. Water levels and flows on the Ohio River, August 1–5, 2005, scenario (Aug2005).

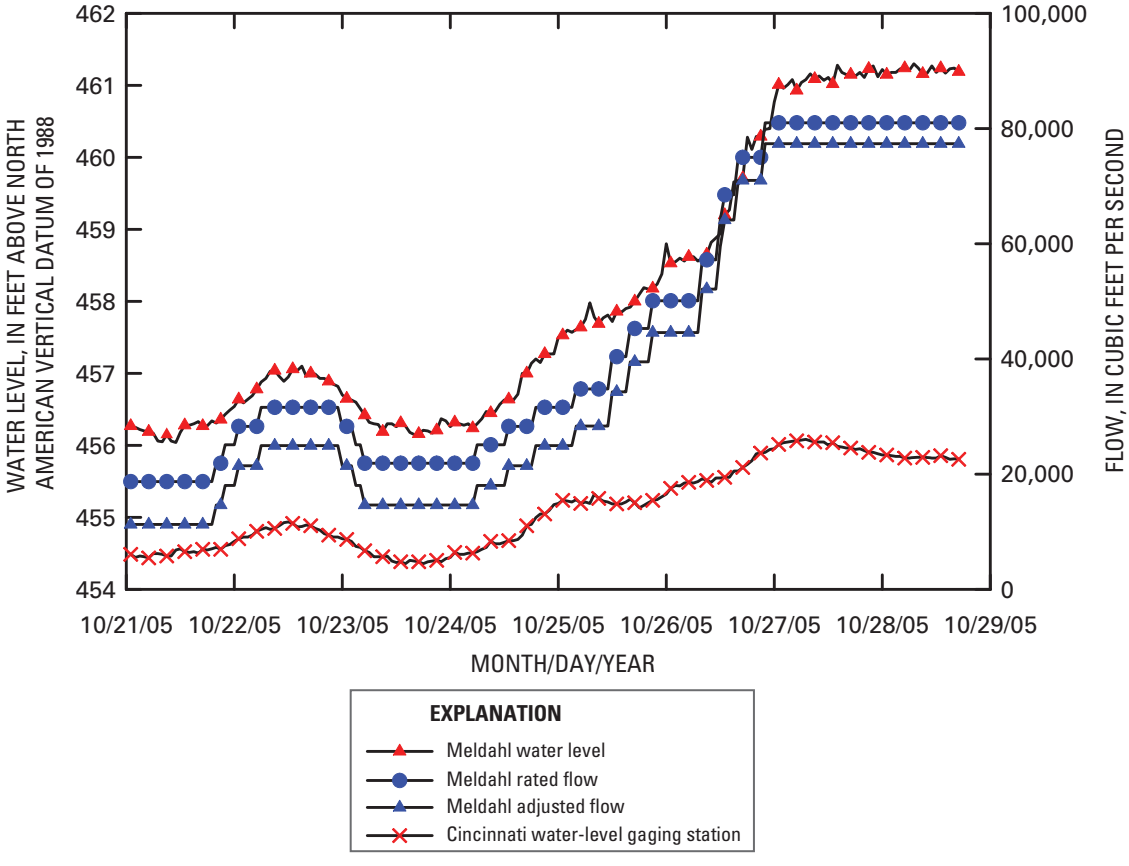

Figure 18. Water levels and flows on the Ohio River, October 21–29, 2005, scenario (Oct2005).

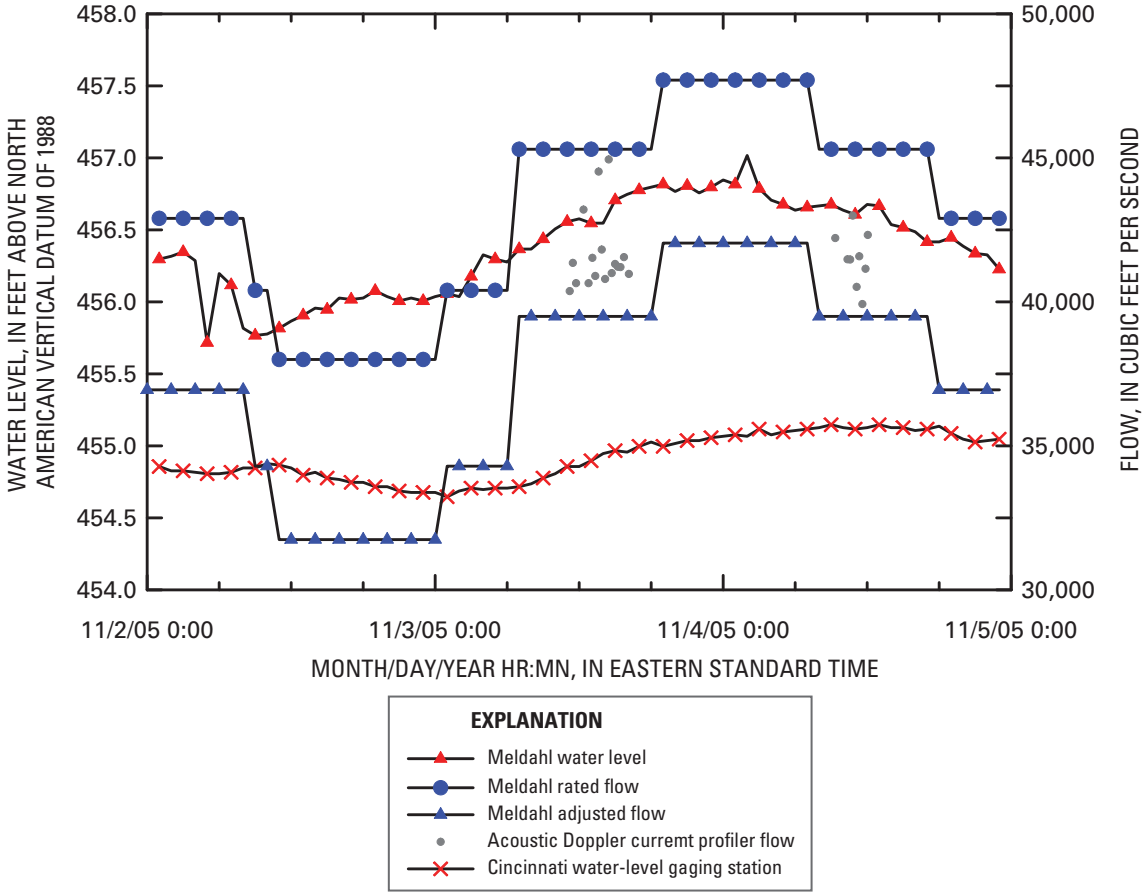

Figure 19. Water levels and flows on the Ohio River, November 2–5, 2005, scenario (Nov2005).

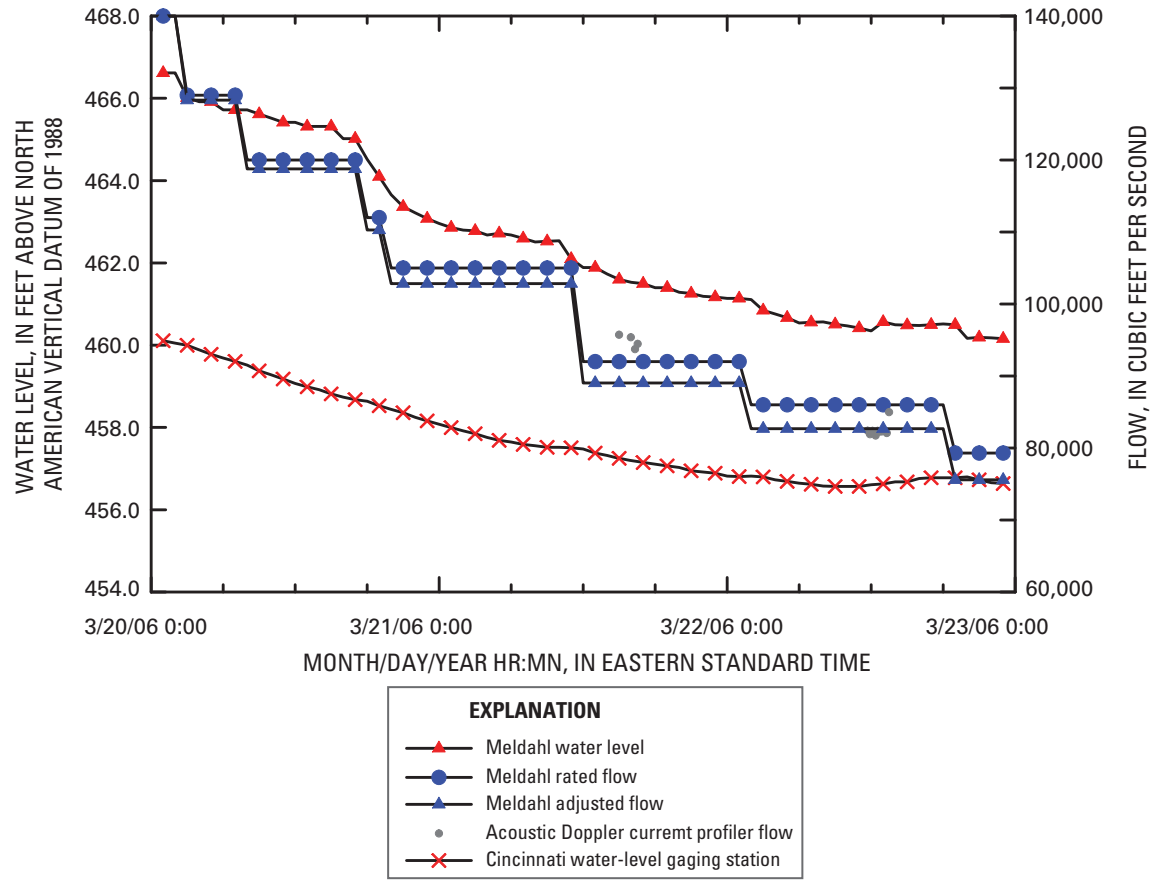

Figure 20. Water levels and flows on the Ohio River, March 20–23, 2006, scenario (Mar2006).

Table 2. Sites of water-level measurements during bathymetry surveys.

River mile	Site reference	Site description	Nearest RMA2 model node	Latitude/ longitude	Northing/easting (Ohio South 1983 State Plane Coordinate System Feet)
436.1	Meldahl Dam	Ohio River downstream from Meldahl Dam	1	38°47'50" 84°10'00"	294,747 1,493,506
438.7	1009	Ohio River at Neville, Ohio	6,359	38°48'25" 84°12'43"	298,529 1,480,670
442.7	1008	Ohio River at Boat Ramp at Moscow, Ohio	16,013	38°51'22" 84°14'00"	316,548 1,474,920
446.9	1007	Ohio River at Bubbers Restaurant near Clermontville, Ohio	27,959	38°54'57" 84°15'05"	338,395 1,470,200
449.4	1006	Ohio River at Skippers Boat Ramp near New Richmond, Ohio	35,604	38°56'44" 84°16'46"	349,374 1,462,433
462.5	1005	Ohio River at the Boat Ramp at California, Ohio	73,875	39°03'52" 84°25'54"	393,571 1,420,083
470.6	Cincinnati water-level gaging station	Ohio River at Cincinnati, Ohio (03255000)	92,573	39°05'40" 84°30'38"	404,966 1,397,923

The flow-exceedance characteristics during these ADCP-related scenarios varied from 0.87 to 0.16 (fig. 10). Transient simulations were used to track time-varying water levels and flows within these scenarios with boundary conditions specifications at 4-hour intervals. The downstream boundary for the simulations was time-varying water levels at the Cincinnati water-level gaging station. The upstream boundary was time-varying flows at Meldahl Dam, which were based on the adjusted gate-rated flows. Flow boundaries for selected tributaries were computed to account for inflows between Meldahl Dam and the Cincinnati water-level gaging station. Flow boundary specifications at tributaries were generally based on simple drainage-area ratio adjustments of flow computed at Meldahl Dam (table 3).

Table 3. Drainage areas of the Ohio River and selected tributaries.

Stream name and location	Drainage area (mi^2)	Ohio river mile (RM)	Basin location	Drainage area ratio	Flow adjustment ratio
Ohio River at Meldahl Dam	70,808	436.5	Ohio and Kentucky	1.00000	1.0000
Big Indian Creek at mouth	40.0	445.1	Ohio	.00056	.00059
Twelvemile Creek at mouth	46.0	451.5	Kentucky	.00065	.00067
Fourmile Creek at mouth	16.4	461.3	Kentucky	.00023	.00024
Little Miami River at mouth	1,757	463.6	Ohio	.02481	.02573
Licking River at mouth	3,707	470.3	Kentucky	.05235	.05429
Subtotal	76,374	--	--	1.07861	11.08152
Ohio River at Cincinnati, Ohio	76,580	471.5	Ohio and Kentucky	1.08152	--

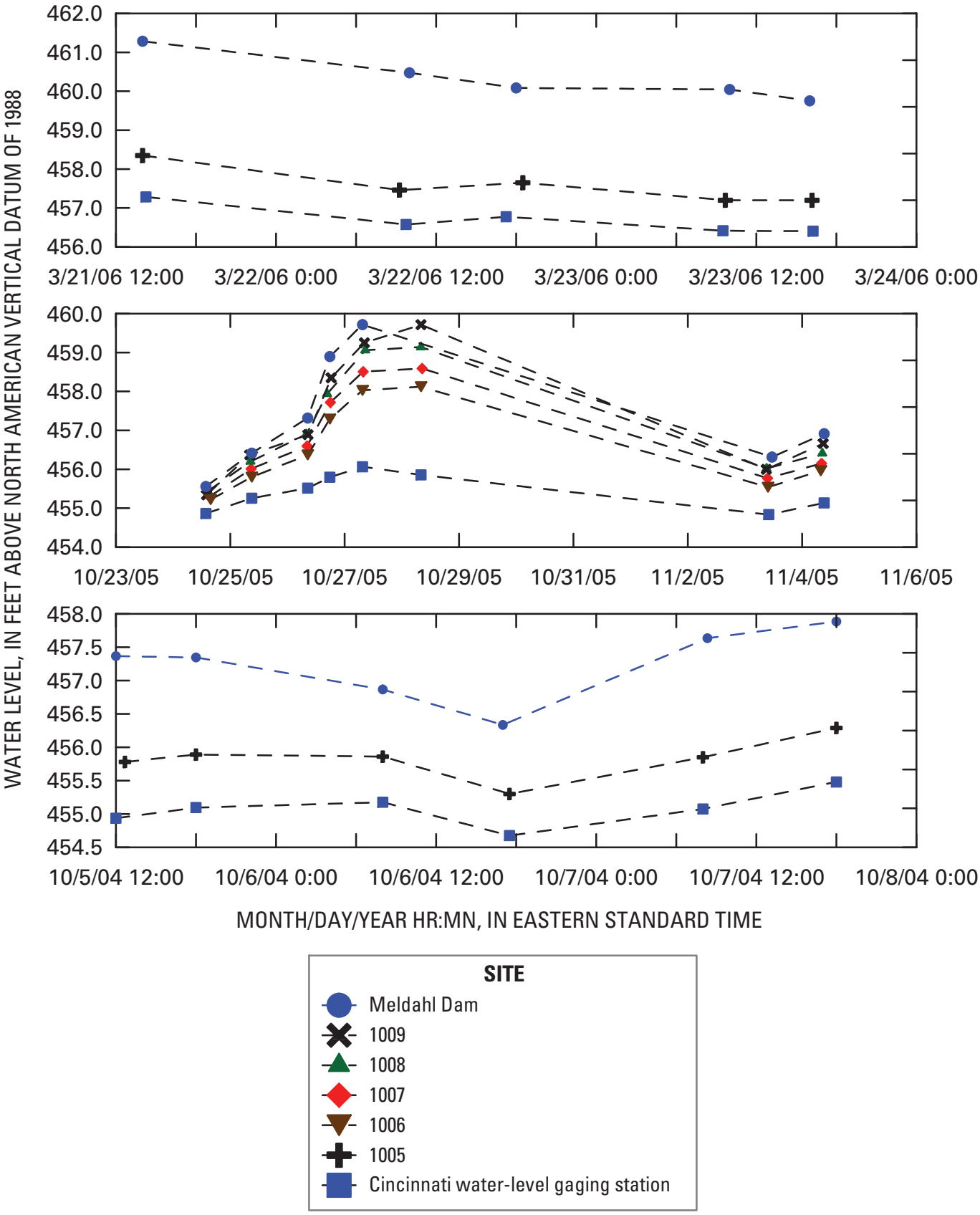

Figure 21. Water-level measurements during the 2004–06 bathymetry surveys.

Water-Quality Simulations

Water-quality simulations were developed to approximate the distribution of dye concentrations measured during two dye-injection studies. Water-quality simulations were based on a water-quality transport code that used the flow velocities and depths simulated by the RMA2 hydrodynamic model of the Ohio River. A dispersion parameter in the transport model was adjusted to improve the match between measured and simulated dye concentrations.

RMA4 Water-Quality Transport Code

The generalized water-quality transport code RMA4 WES (version 4.5), referred to in this report as RMA4 (Letter and others, 2005), was used as a basis for dye-concentration simulations on the Ohio River. RMA4 is designed to simulate depth-averaged advection-diffusion processes in surface-water bodies where flow paths can be approximated by longitudinally integrating their local depth-averaged horizontal-velocity components. The model is applicable to vertically mixed, conservative constituents that are dissolved or neutrally buoyant in water. Non-conservative substances may be described if their mass loss can be approximated by a first-order decay process. The model has been used to identify potential critical areas for the spread of pollutants (Letter and others, 2005).

RMA4 is a finite-element water-quality transport code that simulates 2D (depth-average) equations of transport and mixing, having the form

$$h\left(\frac{\partial c}{\partial t}+u\frac{\partial c}{\partial x}+v\frac{\partial c}{\partial y}-\left[\frac{\partial D_x}{\partial x}\frac{\partial c}{\partial x}\right]-\left[\frac{\partial D_y}{\partial y}\frac{\partial c}{\partial y}\right]-\sigma+kc\right)=0 \quad (4)$$

where

h is water depth,
c is dye concentration,
t is time,
u,v are velocity in the x (easting) and y (northing) directions,
D_x, D_y are turbulent mixing coefficients, which were assumed to be anisotropic such that $D_x = D_y = {}^5D$,
k is first order decay coefficient for dye concentrations, and
σ specifies the loading rate of dye of 767 mg/s for both injections sites.

[5] According to Fischer and others (1979), "Turbulence causes longitudinal mixing presumable at about the same rate as transverse mixing because there is an equal lack of boundaries to inhibit motion. … Rates of turbulent longitudinal mixing have not been measured by dye spreading experiments, because of the difficulty in separating the effects of longitudinal turbulent fluctuations from the results of the shear flow."

The terms in the transport and mixing equation describe local storage, easting and northing advection, easting and northing dispersion, local sources of dye, and exponential decay, respectively. Like RMA2, the transport equation is solved by the finite-element method, using Galerkin weighted residuals (Letter and others, 2005).

In equation 4, the turbulent-mixing coefficients were dynamically assigned on the basis of local simulated velocity and element size as

$$D=\frac{u\cdot dx}{P_{RMA4}} \quad (5)$$

where

D is the turbulent-mixing coefficient,
u is the average elemental velocity,
dx is the element length computed in the direction of flow, and
P_{RMA4} is the RMA4 Peclet number.

RMA4 always is run in transient (dynamic) mode, regardless of whether the RMA2 hydrodynamic results are steady state or transient. If the RMA2 solution is steady state, the hydrodynamics are reapplied at every time step in RMA4. For transient RMA2 simulations, the starting and stopping time for RMA4 can be specified within the duration of the RMA2 run. Letter and others (2005) provide detailed instructions for coding the Timing Control (TC) card in the RMA4 run-control file needed to specify the starting time within the RMA2 simulation, the time step, and the total number of time steps in the simulation, the Boundary Loading (BL) card to constituent loadings at elements, and the Boundary Concentration (BC) card to specify constituent concentrations at the model boundaries.

Greater Cincinnati Water-Quality Transport Model of the Ohio River

The Greater Cincinnati water-quality transport model uses simulated velocities and water level data from the hydrodynamic model as a basis for transport simulations. The finite-element mesh for transport simulations described in this section has been refined from the hydrodynamic version. The refinements were implemented to provide a greater density of velocity and flow-depth information near the dye-injection sites at TMC and BIC and to accommodate minor inflows from Fourmile and Tenmile creeks, small tributaries to the Ohio River near RM 461.4 and 455.0, respectively (fig. 2).

The refinements facilitated estimation of transport parameters associated with turbulent mixing, which were derived from the analysis of dye-concentration data from the two dye-injection studies. Once estimated, the transport parameters were used with the hydrodynamic mesh for transport simulations. The transport model also contains a decay coefficient that is constituent specific and describes the loss of the constituent with time.

Mesh Refinement

In this report, dye-loading rates were specified at selected elements to simulate the discharge of dye from injections at TMC and BIC. So that the dye-injection elements more closely matched the size of the injection points, the finite-element mesh was refined in the vicinity of the dye-injection sites. Within SMS, refinement implies that an element is subdivided into four equally sized (sub) elements, with a corresponding increase in nodes.

A nested, two-stage refinement was applied to elements that surround each dye-injection site (fig. 22). In the first stage, a rectangular array of elements (about eight elements long in the direction of flow and four elements wide) outward from the edge of the channel, was refined. After the initial refinement, unrefined elements along the perimeter of the array were split into two or three elements to avoid excessive area changes between refined and unrefined elements. A second refinement of a subset of the previously refined array was applied similarly. General procedures for mesh refinement are documented within SMS (Environmental Modeling Research Laboratory, 2006).

In addition to mesh refinements near the injection sites, elements and a flow-boundary nodestring were added to represent flow from Fourmile and Tenmile Creeks at the confluence with the Ohio River. The refined mesh comprises 30,398 elements and 94,343 nodes. To maintain numerical efficiency, the nodes and elements were renumbered. Thus between the two hydrodynamic model versions, nodestrings identifying sets of boundary nodes and geometry-continuity check lines may refer to the same nodes but may have different node numbers.

Although mesh refinement can improve the horizontal resolution of water-quality transport simulations, the vertical resolution is fixed as the depth-averaged concentration. At both sites, dye was injected about 0.5 to 1 ft below the water surface. Based on transects downstream from the injection points in which dye was measured at multiple depths, Koltun and others (2006) indicate that dye concentrations were vertically mixed 5 mi downstream from the injection points.

Boundary-Condition Scenarios

Two scenarios were used to represent the two dye-injection studies. In each scenario, a loading rate of 767 mg/s was specified at the element corresponding to the dye-injection site, and zero was assigned to constituent concentrations at all flow boundaries. Hydrodynamic boundaries and parameters were consistent with those that were specified in the Aug2005 hydrodynamic scenario. In contrast to 4-hr hydrodynamic-simulation time steps, however, water-quality transport was simulated at 1-hr time steps to accommodate rapid temporal and spatial changes in concentrations downstream from the points of injection. Transport rates expressed in milligrams per second result in simulated concentrations in milligrams per cubic meter or micrograms per liter, which is consistent with measured dye-concentration units (Koltun and others, 2006).

In the refined mesh, element 16642 was selected to represent the TMC dye-injection site, and element 23087 represents the BIC injection site. The area of these elements is about 282 ft^2, which is a closer approximation to a point injection than the average element area of about 10,000 ft^2. As the distance from the point of injection to the area of interest increases, the impact of refining the injection element on simulated concentrations near the target area diminishes. In this report, dye transects where vertical mixing had occurred about 5.5 mi or more downstream from the point of injection were selected for use in calibrating the transport model.

Simulations with the water-quality model may be done in all English or all metric units. The hydrodynamic model was developed in English units so that the more familiar system of units in the United States could be used to specify the geometry, bathymetry, and boundary conditions of the system. Dye concentrations, however, were measured in metric units of micrograms per liter. To provide consistency between units of measured and simulated dye concentrations, scaling factors were applied to the hydrodynamic model to convert the English units to metric units.

Within the water-quality model, unit conversion is accomplished by changing three input-card images in the run-control file of the water-quality model, which by default has the extension *trn*. The SI Card, for the International System of units, is coded as "SI 1" to identify the card type and specify a value of 1 (true) for the variable METRIC; this indicates that metric units are expected as input and used for output. The GS Card, for converting the river geometry and bathymetry data, is coded as "GS 0.3048 0.3048" to identify the card type and specify values for the variables XSCALE and YSCALE, respectively, which provide the feet-to-meter conversion. The HS Card, for hydrodynamic conversion, is coded as "HS 0.3048 0.3048 0.3048" to identify the card type and specify a scaling factor for variable USCALE, applied to the simulated easting velocity components; the variable VSCALE, applied to the simulated northing velocity components; and the variable WSCALE, applied to the simulated depths of flow. Letter and others (2005) provide detailed instructions on coding RMA4.

Parameter Estimation and Model Calibration

Inverse modeling techniques were used in this report to estimate RMA2 and RMA4 parameters that have physical significance for describing flow and dispersion but, unlike geometry and bathymetry, cannot be measured directly. Parameters had to be inferred from measurements of other attributes by comparing simulated with measured values. A nonlinear-regression technique embedded within UCODE_2005 (Poeter and others, 2005) was used with measurements of water level, flow, water depth, water velocity, and dye concentrations to estimate RMA2 parameters associated with channel roughness and eddy viscosity and RMA4 Peclet numbers associated with turbulent mixing and decay rate. Parameters in RMA2 were estimated independently of parameters in RMA4.

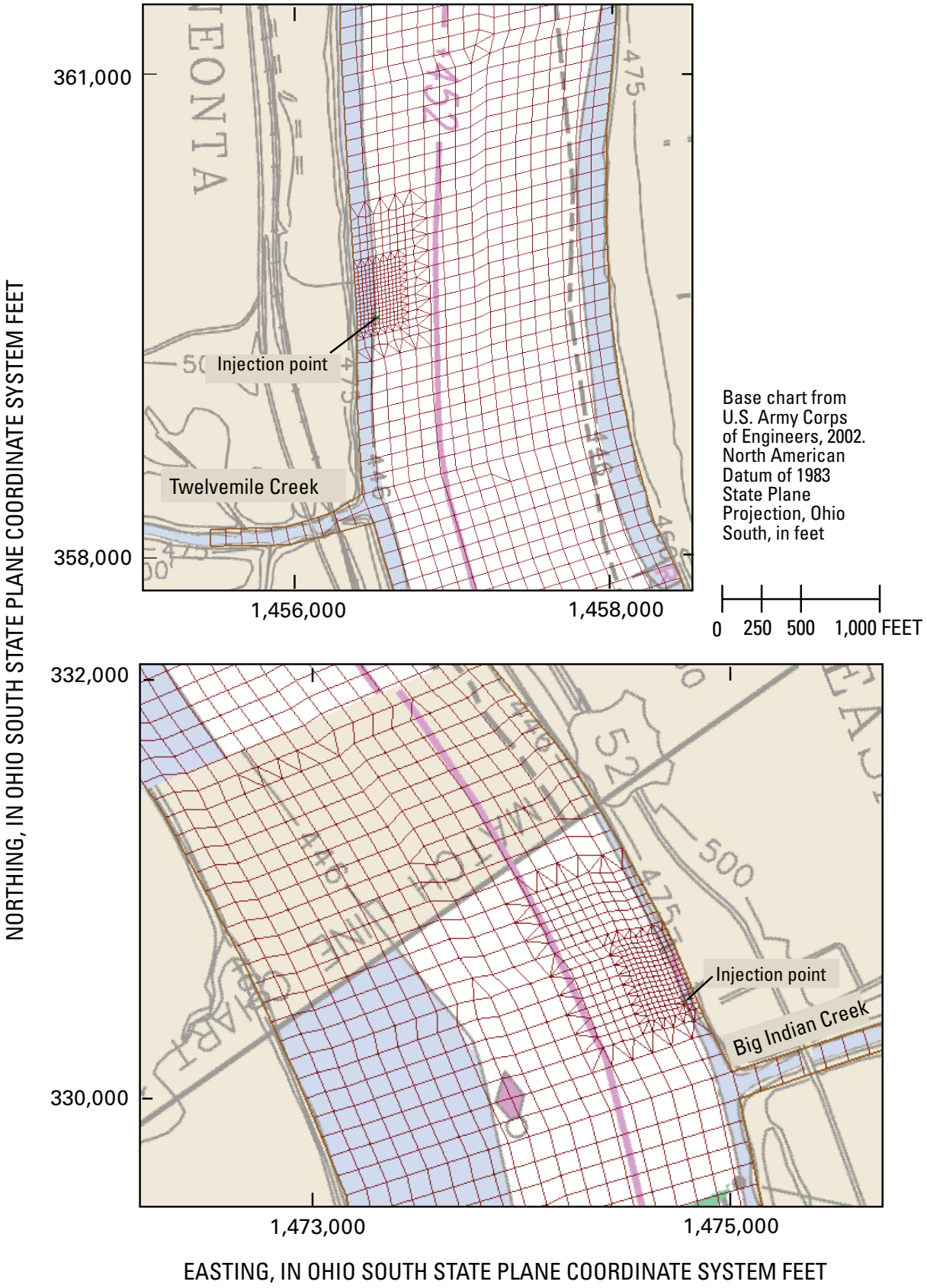

Figure 22. Refined mesh areas that surround dye-injection sites near Twelvemile Creek and Big Indian Creek on the Ohio River.

Nonlinear Regression

Nonlinear regression provides a generally applicable method for calibrating models in which simulated values vary nonlinearly with model parameters (Hill, 1998). In this study, the objective was to minimize the sum of the weighted-squared differences between measured and simulated values as

$$S(\underline{b}) = \sum_{i=1}^{N} \omega_i \left[y_i - \tilde{y}_i(\underline{b}) \right]^2 \qquad (6)$$

where

$S(\underline{b})$ is the sum of weighted-squared differences between measured and simulated values,

$\underline{b}$ is a vector of model parameters of length p,

N is the number of measurements,

y_i is the i^{th} measurement,

$\tilde{y}_i(\underline{b})$ is the i^{th} simulated value, which is a function of the underlying model and associated parameters, and

ω_i is the weight for the i^{th} measurement.

The difference $\left[y_i - \tilde{y}_i(b) \right]$ is referred to as a residual; the difference $\omega_i^{1/2} \left[y_i - \tilde{y}_i(\underline{b}) \right]$ is a weighted residual. Measurement weights ω provide a mechanism for expressing the uncertainty of individual measurements and for including measurements in different scales (for example, flow, in cubic feet per second and water level, in feet) within the same objective function. In this report, the weight matrix Ω was approximated as a diagonal matrix with elements ω_{ii}, which does not account for correlations among measurement errors.

Initial values of model parameters $\underline{b}_0$ were assigned physically plausible values. After the first model simulation was completed with the initial (reference) parameter vector, each parameter was, in turn, varied by a small amount (perturbed) and the model was rerun. The collection of *p+1* simulations was used to compute a forward approximation of the sensitivity matrix $X_{N \times p}$, which describes the sensitivity of each simulated value for which there is a matching observation to each parameter. The *i,j*th element in the forward sensitivity matrix is computed as

$$\frac{\Delta \tilde{y}_i}{\Delta b_j} = \frac{\tilde{y}_i\left(\underline{b} + \Delta \underline{b}_j\right) - \tilde{y}_i\left(\underline{b}\right)}{\left(\underline{b} + \Delta \underline{b}_j\right) - \left(\underline{b}\right)} \qquad (7)$$

where

Δb_j is the change in j^{th} parameter estimate, and

$\Delta \underline{b}_j$ is a zero vector of length p except for the j^{th} element, which contains Δb_j.

To facilitate the comparison of sensitivities among parameters and measurements in different scales, a dimensionless scaled sensitivity is calculated as

$$ss_{ij} = \left(\frac{\Delta \tilde{y}_i}{\Delta b_j} \right) b_j \cdot \omega_{ii}^{1/2}$$

The composite scaled sensitivity *css* provides a measure of the total sensitivity of the estimated parameters to the measured data. Parameters associated with higher *css* values are more sensitive to the data. Values of *css* are independent of the measured values and the model fit. Hill (1998) calculates *css* for each parameter as $css_j = \sqrt{\sum_{i=1}^{N} \left(ss_{ij} \right)^2 \Big|_{\underline{b}} / N}$.

When the sensitivity matrix is computed, based on the initial parameter estimates and perturbation results, all parameter estimates are updated simultaneously using an iterative process of the modified Gauss-Newton optimization method (Hill, 1998) as

$$\begin{aligned} \underline{d}_r &= C_r \cdot \left(C_r^T \cdot X_r^T \cdot \Omega \cdot X_r \cdot C_r + I_{p \times p} \cdot m_r \right)^{-1} \\ &\quad C_r^T \cdot X_r^T \cdot \Omega \cdot \left(\underline{y} - \underline{\tilde{y}}(\underline{b}_r) \right) \\ \underline{b}_{r+1} &= \rho_r \cdot \underline{d}_r + \underline{b}_r \end{aligned} \qquad (8)$$

where

$\underline{d}_r$ is the computed change in the parameter vector for the r^{th} regression iteration,

X_r is the sensitivity matrix evaluated with parameter estimates $\underline{b}_r$,

Ω is a diagonal weight matrix with nonzero elements ω_{ii},

C_r is a p dimensional diagonal scaling matrix with elements $c_{r(jj)} = \sqrt{\left(X_r^T \cdot \Omega \cdot X_r \right)_{jj}}$

$I_{p \times p}$ is an identity matrix, and

m_r is the Marquardt parameter, which improves regression performance for ill-posed problems (Hill, 1998),

$\underline{b}_{r+1}$ is the updated parameter vector, and

ρ_r is a damping parameter between 0 and 1 that is used to reduce parameter oscillations.

Values in the updated parameter vector can be modified because of parameter constraints before use as the reference parameter vector for the calculation of revised model simulations and perturbation analyses. Regression iterations continue until convergence is achieved and changes in the objective function are less than the specified amount and parameters are stable, or the maximum number of regression iterations is exceeded or other difficulties are encountered.

For regressions that converge, several overall statistical measures of fit are computed. In particular, the estimated error variance is computed as

$$s^2 = S(\underline{b}_f)/(N-p) \quad (9)$$

where

$S(\underline{b}_f)$ is the weighted sum of squared residuals computed with the final estimate of the parameter vector.

This variance, together with the final estimate of the sensitivity matrix, is used to compute the symmetrical covariance matrix of the parameter vector as $V(\underline{b}_f) = s^2\left(X_f^T \cdot \Omega \cdot X_f\right)^{-1}$. The standard error of the regression is the square root of the estimated error variance. The diagonal elements are the variances of the individual parameters $s_{b_j}^2$, and the off diagonal elements are covariances between parameter pairs. An (1-α)-level linear confidence interval is computed for each parameter as $b_j \pm t_{N-p,1-\alpha/2} \cdot s_{b_j}$, where t is the Student-t statistic with N-p degrees of freedom. Finally, the parameter-correlation matrix is computed from covariance elements of $\mathrm{cov}_{ij} = V(\underline{b}_f)_{ij}$ and the correlation between the i^{th} and j^{th} parameter $cor_{ij} = \mathrm{cov}_{ij} \Big/ \sqrt{\mathrm{cov}_{ii} \cdot \mathrm{cov}_{jj}}$. Parameter correlations can vary in the interval [-1, 1]. Parameter correlations with an absolute value greater than 0.85 indicate that some degradation in parameter estimates may have occurred because of the ambiguity of the effects caused by two model parameters on simulated results.

UCODE Analyses

UCODE provides for parameter estimation, using nonlinear regression by controlling the execution of the regression analysis, defining the magnitudes and uncertainties of measured data, providing instructions for extracting simulated values from model output files and, in some cases, deriving simulated values that better correspond with points of measured data. Commonly, derived values were spatially or temporally interpolated from simulated values to improve the match to locations of measured data.

Parameters in the hydrodynamic model were estimated before parameters in the water-quality transport model were. Hydrodynamic model parameters for channel roughness or resistance to flow were targeted at determining whether there were significant differences in average roughness characteristics between zones of flow depth. The eddy-viscosity parameter, estimated from the dimensionless RMA2 Peclet number, was used to characterize the variability of velocities across the river. In general, higher RMA2 Peclet numbers are associated with lower eddy viscosities and more local variability in velocities; lower Peclet numbers are associated with higher eddy viscosities and more uniform local velocities. In RMA2, hydrodynamic simulations can become numerically unstable if Peclet numbers are too high.

Results of hydrodynamic model calibration are passed to the water-quality transport model in the form of simulated velocities and depths of flow. In addition, the (RMA2) Peclet number estimated in the hydrodynamic-model calibration P_{RMA2} provides an initial estimate of the (RMA4) Peclet number in the water-quality transport model P_{RMA4}, which was updated on the basis of dye-concentration data. Eddy viscosities, E in lb-s/ft, derived from the P_{RMA2} have different units than turbulent mixing coefficients (D in ft^2/s) derived from the P_{RMA4}. This sequential calibration strategy provided an opportunity to test the possibility that $P_{RMA2} = P_{RMA4}$, which would imply that dye-concentration data may not be needed for estimating turbulent mixing characteristics in the water-quality model; thus, dye injection-studies might not be needed.

Hydrodynamic-Model-Calibration Strategy

Five transient-flow scenarios were used to estimate hydrodynamic-model parameters in equation 1. Two parameters were used to describe possible systematic differences in channel resistance to flow among shallow and deep zones. On navigational charts (fig. 15), shallow zones of the river are shown with a blue tint; deep zones are shown in white. Each element was assigned to the shallow or deep zone. One additional parameter in equation 4, referred to as the RMA2 Peclet number, is used to assign eddy-viscosity values as a function of flow velocities and element sizes.

The Greater Cincinnati hydrodynamic model simulates flow depths $\tilde{y}_d(\underline{b})$ and easting $\tilde{y}_{VelE}(\underline{b})$ and northing $\tilde{y}_{VelN}(\underline{b})$ velocity components at nodes, monitored water levels $\tilde{y}_H(\underline{b})$, and flows $\tilde{y}_Q(\underline{b})$ for comparison with measured values. The following text describes how corresponding measurements y_d, y_{VelE}, y_{VelN}, y_H, and y_Q were computed and how weighting factors ω were assigned to individual measured values and measurement types to represent their corresponding precisions.

During the five scenarios used in model calibration, water depths and flow velocities were measured at each ADCP ensemble throughout numerous transects across the Ohio River (Koltun and others, 2006). Although few ensembles were colocated with nodes for direct comparison, numerous nodes were located near one or more ensembles. In this report, a node N was considered estimable if one or more ensembles E were within 50 ft of a model node. If a node was determined to be estimable, the closest of up to 10 ensembles was used to compute an inverse, distance-weighted average and standard deviation for the flow depth and velocity components at that node. Water depths and flow velocities computed by the transformation of measured values described in the following text are referred to as measured water depths and flow velocities.

Inverse distance weighting factors $\alpha_{i(j)}$ were computed for each of the $i = n \le 10$ closest ensembles to the j^{th} node as

$$\alpha'_{i(j)} = 1 \Big/ \sqrt{(N(j)_{Easting} - E(i)_{Easting})^2 + (N(j)_{Northing} - E(i)_{Easting})^2}$$
$$A_{N(j)} = \sum_{i \le 10} \alpha'_{i(j)} \qquad (10)$$
$$\alpha_{i(j)} = \alpha'_{i(j)} \Big/ A_{N(j)}$$

where

$N(j)_{Easting}$ and $N(j)_{Northing}$ indicate the easting and northing coordinates for the j^{th} node, respectively, with

$E(i)_{Easting}$ and $E(i)_{Northing}$ defined similarly for the i^{th} ADCP ensemble.

When the weighting factors were computed, the estimate of depth at the j^{th} node was computed as $y_{d(j)} = \sum_{i=n} \alpha_{i(j)} \cdot y_{d(E(i))}$

Similar computations were used to determine the easting $y_{VelE(j)}$ and northing $y_{VelN(j)}$ velocity components at the j^{th} node. The standard deviation of the inverse, distance-weighted averages of flow depths was computed at estimable nodes as

$$\hat{\sigma}_{d(j)} = \sqrt{\sum_{i=1}^{n} \frac{\left(y_{d(E(i))} - y_{d(j)}\right)^2}{n-1} \cdot \sum_{i=1}^{n} \alpha_{i(j)}^2} \qquad (11)$$

Measurement weights for depths were computed as a function of measurement uncertainty and the number of depth measurements, as

$$\omega_{d(j)} = 1 \Big/ \left(\hat{\sigma}^2_{d(j)} \cdot NumMeaSet\right) \qquad (12)$$

where

$NumMeaSet$ is the number of depth measurements.

For depth and velocity data, the number of measurements in the set is the number of estimable nodes. Adjusting measurement weights for the number of measurements in the set prevented the parameter-estimation analysis from being too heavily weighted by any particular type of measurement. Similar computations were used to compute measurement weights for easting and northing velocity components $\omega_{VelE(j)}$ and $\omega_{VelN(j)}$. Linear interpolation was used to temporally adjust simulated depths and velocities to match measured values near nodes.

During the five scenarios, water-level data y_H were obtained at 4-hour intervals from tailwater measurements at Meldahl Dam and from miscellaneous water-level obtained during the October 2005 bathymetry survey. A standard deviation of 0.15 ft was specified (Robert R. Mason, Jr., USGS Office of Surface Water, written commun., 2008) as the uncertainty of the water-level data.

Flow data y_Q were based on single-transect ADCP flow measurements during the five scenarios. Although the accuracy of single-transect measurements is uncertain, they were considered to be of fair to poor quality with an uncertainty of about 10 percent. Within UCODE_2005, this was expressed as a coefficient of variation of 0.10; the corresponding measurement weights were computed as

$$\omega_{Q_i} = 1 \Big/ \left((0.10 \cdot Q_i)^2 \cdot NumMeaSet\right),$$

where

Q_i is the measured flow.

Simulated flows were linearly interpolated with time for comparison with measured flows. The number of measurements of each type used in the estimation of the RMA2 parameters varied from 116 to 7,174 (table 4).

Water-Quality-Transport Model-Calibration Strategy

Two water-quality-transport scenarios were used with UCODE_2005 to estimate turbulent-mixing coefficients in equation 6. Turbulent mixing coefficients are assigned as a function of the RMA4 Peclet number parameter, simulated flow velocities, and element sizes (equation 7). The two scenarios are based on the TMC and BIC dye-injection studies and provide a basis for independently estimating RMA4 Peclet numbers in the two overlapping study reaches. Consistent parameter estimates for the studies would support the use of a single RMA4 Peclet number to represent dispersion and mixing throughout the study area. The RMA4 Peclet number initially was set to the RMA2 Peclet number.

Table 4. Number of measurements used in the estimation of RMA2 parameters for the hydrodynamic model of the Ohio River near Cincinnati, Ohio, by scenario, 2004–06.

[ADCP, acoustic Doppler current profiler]

Scenario (Month and year of ADCP survey)	Number of observations used in the parameter-estimation analysis, by measurement type			
	Water levels	Flows	Water depths	Easting and northing velocities
Oct2004	16	59	1,742	3,484
Aug2005	17	23	729	1,458
Oct2005	61	0	0	0
Nov2005	10	26	791	1,582
Mar2006	12	14	324	650
Total	116	122	3,586	7,174

In addition to the RMA4 Peclet numbers, the transport model contains a decay coefficient to describe the loss of non-conservative constituents with time. Decay coefficients were estimated independently for the two scenarios on the basis of simulated traveltimes and measured dye-transport rates at measured transects. In contrast, the decay coefficients describing any dye losses within the study area were considered constituent specific and sensitive to environmental conditions. As such, estimated decay coefficients may have limited transfer value to other investigations.

In comparison to ADCP ensembles, dye-concentration measurements are relatively sparse. Typically, 50 to 90 concentration measurements were obtained in one dye transect. Therefore, the strategy for matching measured and simulated values differed from that used with depths and velocities in the hydrodynamic model. Rather than inverse, distance-weighted averages of measured values as approximations to simulate values at nodes, a quadratic interpolation scheme was used to compute a simulated value at a point within an element where a concentration measurement was made. The details of the procedure are discussed in the following text.

The element *J* containing the k^{th} measured dye concentration (c_k) and all its associated nodes, indexed by *j,* was identified for each measured concentration. The point of the dye-concentration measurement was considered the local origin, and the easting and northing of the dye-measurement location was subtracted from those in the surrounding nodes to form localized easting and northing coordinate pairs $\tilde{x}_j, \tilde{y}_j$ for all nodes defining element *J*.

For quadrilateral elements, the interpolating function was of the form

$$\breve{c}_j(\tilde{x}_j, \tilde{y}_j \,|\, \underline{b}) = \beta_0 + \beta_1 \cdot \tilde{x}_j + \beta_2 \cdot \tilde{y}_j + \beta_3 \cdot \tilde{x}_j^2 + \beta_4 \cdot \tilde{y}_j^2 + \beta_5 \cdot \tilde{x}_j \cdot \tilde{y}_j + \beta_6 \cdot \tilde{x}_j^2 \cdot \tilde{y}_j + \beta_7 \cdot \tilde{x}_j \cdot \tilde{y}_j^2 \quad (13)$$

where

$\breve{c}_j$ is the simulated concentration at the j^{th} node, given the parameter vector $\underline{b}$, and

β are values estimated for the interpolating function.

From this equation, the design matrix corresponding to a quadrilateral element was

$$Z_{Quad} = \left[1_{8\times1} \quad \tilde{\bar{x}} \quad \tilde{\bar{y}} \quad \tilde{\bar{x}}^2 \quad \tilde{\bar{y}}^2 \quad \tilde{\bar{x}} \cdot \tilde{\bar{y}} \quad \tilde{\bar{x}}^2 \cdot \tilde{\bar{y}} \quad \tilde{\bar{x}} \cdot \tilde{\bar{y}}^2 \right] \quad (14)$$

The 8 by 8 *Psi* matrix $\Psi_{8\times8}$ was computed as $\Psi_{8\times8} = \left[Z'_{Quad} \cdot Z_{Quad} \right]^{-1} \cdot Z'_{Quad}$, which is only a function of the unit vector $1_{8\times1}$ and localized easting $\tilde{x}$ and northings $\tilde{y}$ of the static node coordinates and not a particular set of simulated concentrations. Typically, the Ψ matrix together with a vector of simulated dye concentrations $\tilde{\bar{c}}$ would be used to compute a full beta vector $\vec{\beta}_{8\times1} = \Psi_{8\times8} \cdot \tilde{\bar{c}}_{8\times1}$, which provides a means to estimate simulated values of concentrations anywhere in the element as $\hat{\tilde{c}}(\tilde{x}, \tilde{y}) = \left[1 \quad \tilde{x} \quad \tilde{y} \quad \tilde{x}^2 \quad \tilde{y}^2 \quad \tilde{x}\tilde{y} \quad \tilde{x}^2\tilde{y} \quad \tilde{x}\tilde{y}^2 \right] \cdot \vec{\beta}_{8\times1}$. In this analysis, however, the only simulated point of interest in the element is at the k^{th} measured dye concentration for which $\tilde{x}_k = \tilde{y}_k = 0$. This restriction provides a basis to precompute the top row of the Psi matrix $\Psi_{1,1:8}$, which together with the simulated concentrations in the surrounding j^{th} element $\tilde{\bar{c}}_{\forall j \in J}$, provides a basis for quadratic interpolation as $\hat{\tilde{c}}_k\left(\tilde{x}_j = 0, \tilde{y}_j = 0\right) = \left[1\right] \cdot \Psi_{1,1:8} \cdot \vec{\tilde{c}}$. This computed concentration is unbiased as $\sum_{j=1:8} \Psi_{1,j} = 1$. For triangular elements, the quadratic interpolation function is

$$\breve{c}_j(\tilde{x}_j, \tilde{y}_j \,|\, \underline{b}) = \beta_0 + \beta_1 \cdot \tilde{x}_j + \beta_2 \cdot \tilde{y}_j + \beta_3 \cdot \tilde{x}_j^2 + \beta_4 \cdot \tilde{y}_j^2 + \beta_5 \cdot \tilde{x}_j \cdot \tilde{y}_j \quad (15)$$

The corresponding design and Psi matrices for triangular elements are defined similarly to those of the quadrilateral elements. The standard deviations of the measured dye concentrations were computed as $\hat{\sigma}_{c_k} = 0.1 \cdot c_k + 0.05$, and the corresponding measurement weights ω_{c_k} were computed as $1 / \hat{\sigma}_{c_k}^2$.

Greater Cincinnati Hydrodynamic Model of the Ohio River

When the geometry and bathymetry of the Ohio River study reach were described and boundary conditions for the five calibration scenarios were specified, hydraulic parameters describing channel resistance to flow and eddy viscosity were estimated by minimizing the differences between measured and simulated depths of flow, heads, flows, and velocities. The following discussion characterizes the results of the parameter-estimation analysis and the correspondence between simulated and measured values.

Parameter Estimation

Estimation for the hydrodynamic-model parameters of effective channel roughness for shallow and deep zones and the Peclet number converged at a weighted sum of squared residuals *S(b)* equal to 47.329. The estimated effective Manning's "*n*" value for the shallow zone (0.02751) was about 17.3 percent higher than that for the deep zone (0.02345) (table 5). Parameter estimates were consistent with the range of Manning's "*n*" values associated with materials expected on the Ohio River (Barnes, 1967). The estimated RMA2 Peclet number of 38.3 was within the recommended range of 15–40 (Donnell and others, 2005).

Table 5. Parameter estimates for the two-dimensional hydrodynamic and transport models of the Ohio River near Cincinnati, Ohio.

Parameter statistic	Manning's "*n*"		Peclet number RMA2	Twelvemile Creek RMA4 Peclet number	Big Indian Creek	
	Deep zone	Shallow zone			RMA4 Peclet number	Decay coefficient
Upper 95 percent confidence limit	0.02361	0.02806	46.13	190.5	38.26	0.342
Expected value	.02345	.02751	38.33	173.3	37.19	.323
Lower 95 percent confidence limit	.02329	.02697	30.52	157.6	36.15	.342
Standard deviation	.0000835	.0002763	3.984	[1]85.08	.305	.0000993
Coefficient of variation	.003559	.0104	.1040	.4910	.00821	.000307
Composite scaled sensitivity	.2587	.07918	.00728	4.002	3.969	1.968

[1]RMA4 Peclet numbers were determined under a $\log_{10}$ transformation. The standard deviation shown was applied to $\log_{10}$ estimates of the Peclet numbers and transformed back to arithmetic space by power transformation.

Absolute values of correlation among parameter pairs exceeding 0.85 can create ambiguity among parameter estimates and degrade the interpretability of parameter estimates (Poeter and others, 2005). The maximum correlation between parameters was 0.5565 between Manning's "*n*" for the deep zone and the RMA2 Peclet number. The minimum correlation between parameters was -0.6120 between Manning's "*n*" values in the deep and shallow zones. Thus, parameter correlation is not expected to degrade parameter estimates. As indicated by the scaled sensitivity values (table 5), Manning's "*n*" parameters were more sensitive to the data than the Peclet parameter.

Simulation

The relation between measured and simulated flow depths, heads, flows, and velocities is shown by scenario in table 6. Across all scenarios, the average coefficient of determination (r^2) was greater than or equal to 0.90 for all measurement types. Also, the interval computed about the bias, plus or minus twice the standard deviation of residuals, included zero for all measurement types and scenarios, except for the Mar2006 flows. This bias may have been smaller if the time step for the hydrodynamic simulations would have been smaller to better account for rapidly changing boundary conditions. Figures 23 through 28 show the relation between computed and simulated values for all scenarios. These results indicate that point measurements of flow depths, heads, flows, and velocities generally are consistent with corresponding simulated values.

Greater Cincinnati Water-Quality-Transport Model of the Ohio River

Application of the RMA4 transport model to the Ohio River study area requires estimation of dye-decay and RMA4 Peclet number (turbulent-mixing) parameters. Comparison between measured and simulated dye concentrations demonstrates the effectiveness of the water-quality transport model. In the following section, model-parameter estimates are presented and discussed, and comparisons between measured and simulated dye concentrations are provided.

Parameter Estimation

Parameters in the water-quality transport model were estimated independently for each dye study. Independent estimation of parameters provided a means to assess their consistency and reproducibility for different injection sites. Initially, least squares estimates of dye-decay parameters were determined from computed dye-transport rates and simulated travel times. Subsequently, an attempt was made to simultaneously estimate dye-decay and RMA4 Peclet numbers describing turbulent-mixing by use of UCODE with transport simulations and measured dye concentrations.

Table 6. Summary statistics describing the match between simulated and computed flow depths, heads, flows, and velocities for the hydrodynamic model of the Ohio River near Cincinnati, Ohio, October 2004–March 2006.

Parameter	Scenario	Count	Coefficient of determination	Residuals	
				Bias	Standard deviation
Flow depth	Oct2004	1,742	0.9204	-0.3626	2.006
	Aug2005	729	.9342	-.0385	1.850
	Nov2005	791	.9283	.0344	1.575
	Mar2006	324	.9499	.3155	1.841
	All	3,586	.9353	-.1479	1.885
Head	Oct2004	16	.8516	-.0431	.2298
	Aug2005	17	.7659	-.0520	.1025
	Oct2005	61	.9882	.0879	.2281
	Nov2005	10	.5568	.2293	.1714
	Mar2006	12	.9961	.0708	.2281
	All	116	.9004	.0598	.1980
Flow	Oct2004	59	.928	-1,880	1,623
	Aug2005	23	.910	475	1,508
	Nov2005	26	[1].000	1,709	1,393
	Mar2006	14	.990	-2,607	581
	All	122	.988	-755.0	1,467
Easting velocity	Oct2004	1,742	.8996	.0162	.1888
	Aug2005	729	.8851	-.0120	.1195
	Nov2005	791	.9523	-.0566	.1228
	Mar2006	325	.9109	.1158	.2334
	Total	3,587	.9093	.0034	.1747
Northing velocity	Oct2004	1,742	.9041	-.0031	.1609
	Aug2005	729	.8022	.0103	.1165
	Nov2005	791	.8374	.1122	.1922
	Mar2006	325	.9746	.0109	.2771
	Total	3,587	.9401	.0263	.1804

[1]Flows showed little variability during the period.

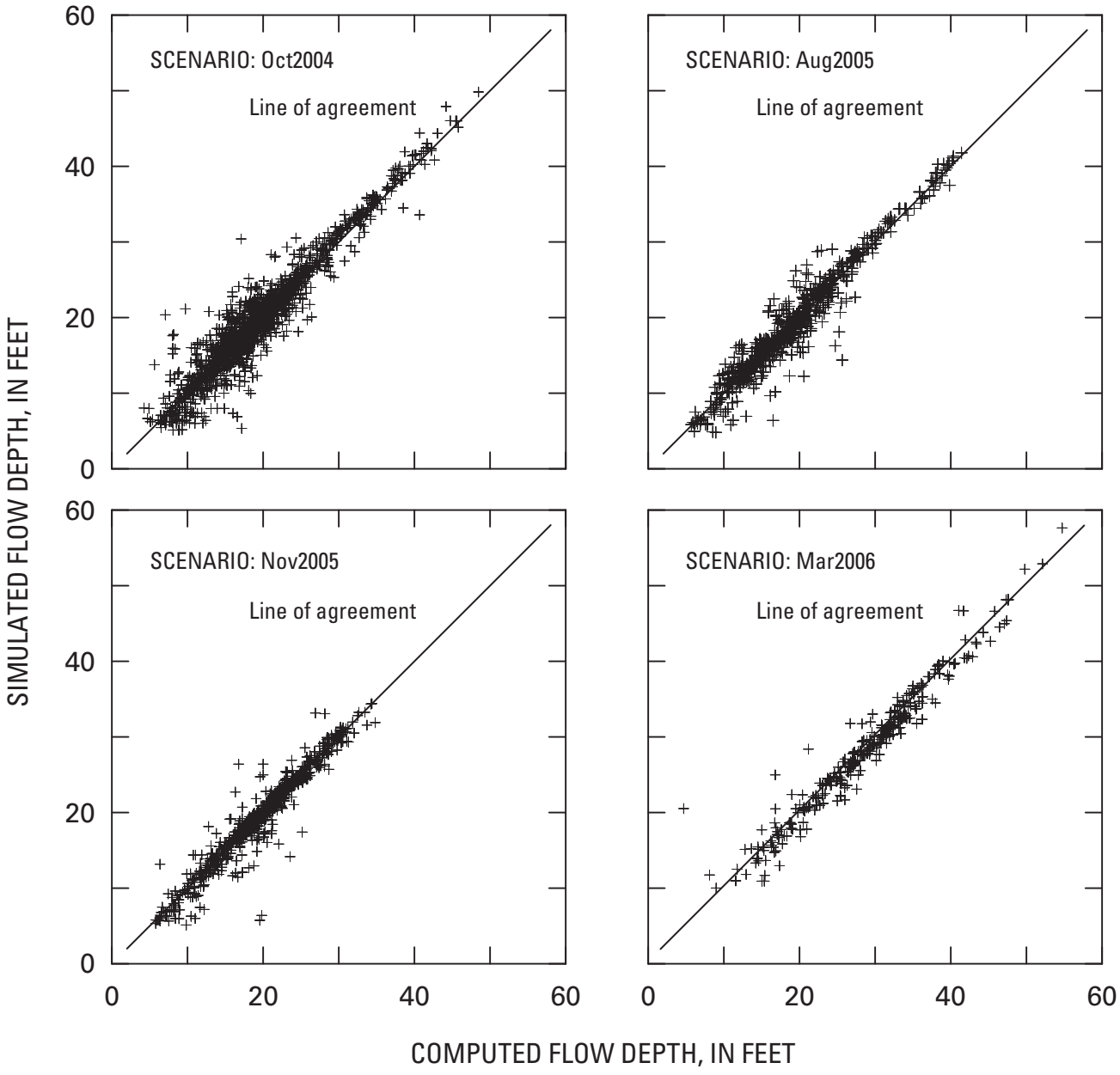

Figure 23. Relation between computed and simulated flow depths on the Ohio River near Cincinnati, Ohio, October 2004–March 2006.

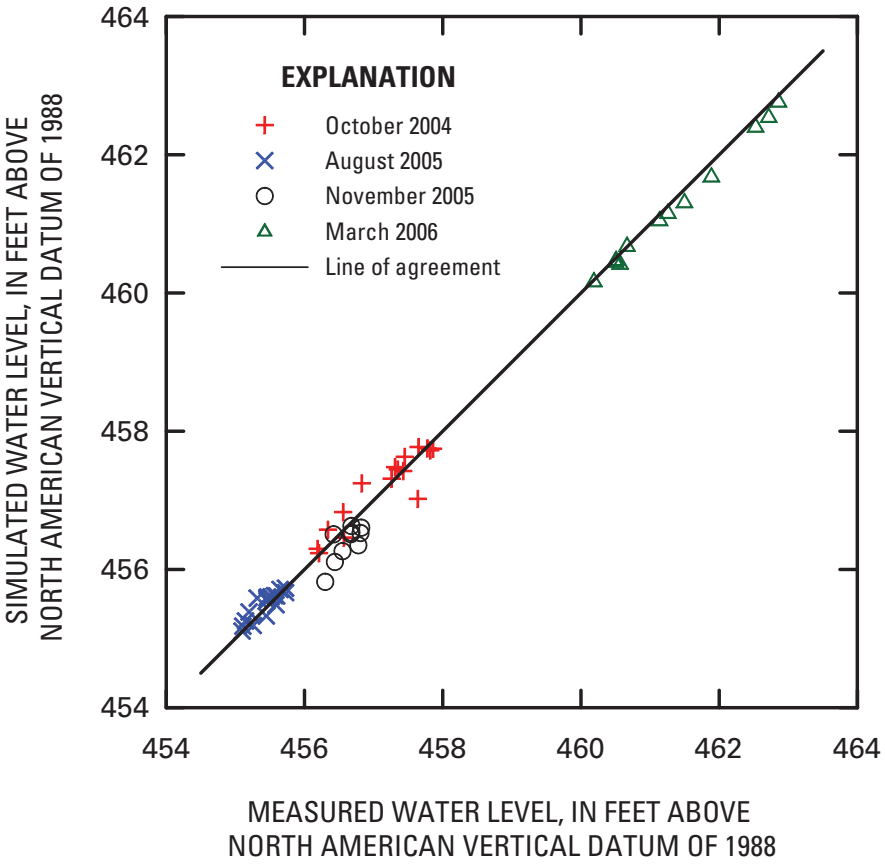

Figure 24. Relation between systematically measured and simulated water levels on the Ohio River downstream from Meldahl Dam near Neville, Ohio, October 2004–March 2006.

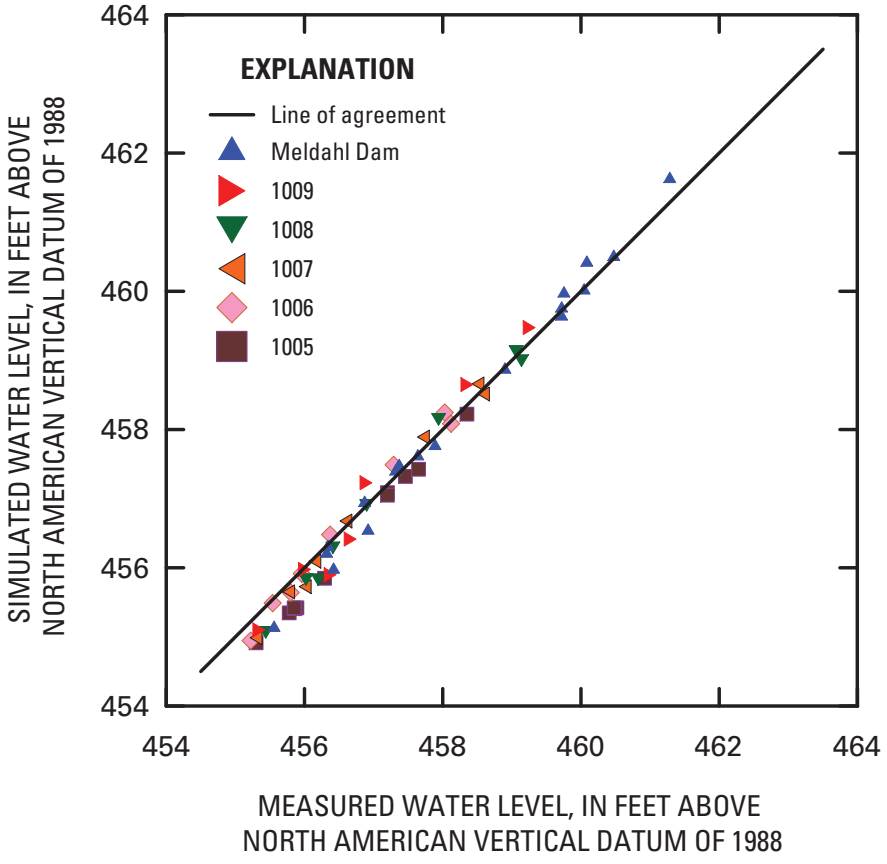

Figure 25. Relation between miscellaneous measurements and simulated water levels at miscellaneous sites measured during bathymetry surveys.

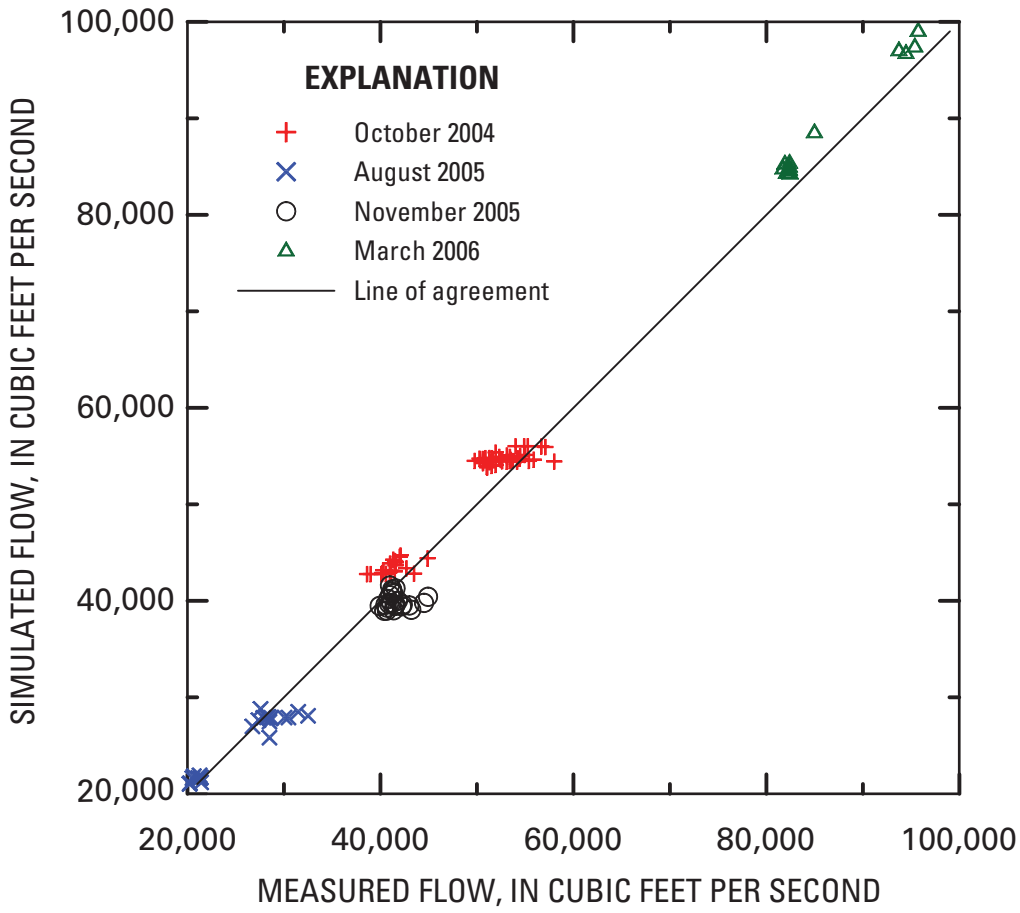

Figure 26. Relation between measured and simulated flows on the Ohio River near Cincinnati, Ohio, October 2004–March 2006.

Dye-Decay Parameters

Rhodamine WT dye is a conservative constituent, although some losses can occur as a result of degradation associated with sunlight and sorption on particles in water. Dye-transport rates were determined at several transects downstream from the dye-injection points to assess possible losses. Resulting transport rates showed variability within both injection reaches (table 1). In the TMC dye-injection study, the computed transport rates exceeded the injection rate at two transects. Sources of variability in transport rates are uncertain but may include unsteadiness of flow, transport measurements occurring before steady-state concentrations were established, and dye- and flow-measurement uncertainties. Measurement uncertainties, for example, were evident in near-simultaneous measurements of transport rates by two boat crews at OH 9a and OH 9b that differed by about 15 percent (table 1).

Constituent losses may be accounted for by the exponential decay equation

$$M(t-t_o) = M(t_o) \cdot e^{-[k_1 \cdot (t-t_o)]} \qquad (16)$$

where

$M(t)$ is the transport rate at time t, and

k_1 is the estimated decay parameter, with units of day^{-1}.

In this report, the product of the flow-weighted mean concentration $\tilde{\tilde{C}}(t)$ and measured flow at a transect downstream from the point of injection was used to estimate the transport rate $M(t)$.

The traveltimes from the TMC dye-injection site to dye-measurement transects were estimated with SMS drogue-tracking capabilities. In particular, a hypothetical massless particle was placed in the simulated transient-flow field for the Aug2005 scenario near the TMC dye-injection point. The drogue was tracked at 0.5-hour intervals during an interval corresponding approximately to the dye-injection period, August 1, 2005, at 12:00 EST to August 2, 2005, at 13:00 EST. The traveltime to individual transects was estimated by interpolating between drogue positions at 0.5-hour intervals. Measurements of dye-transport rates at transects OH 16 (a and b) were not used to estimate the decay coefficient because concentrations may not have reached near-steady-state concentrations before dye concentrations were measured. The relatively low transport rates computed at transects OH 15 and OH 16 may be partially explained by dye measurements being made before concentrations reached their near-steady-state values.

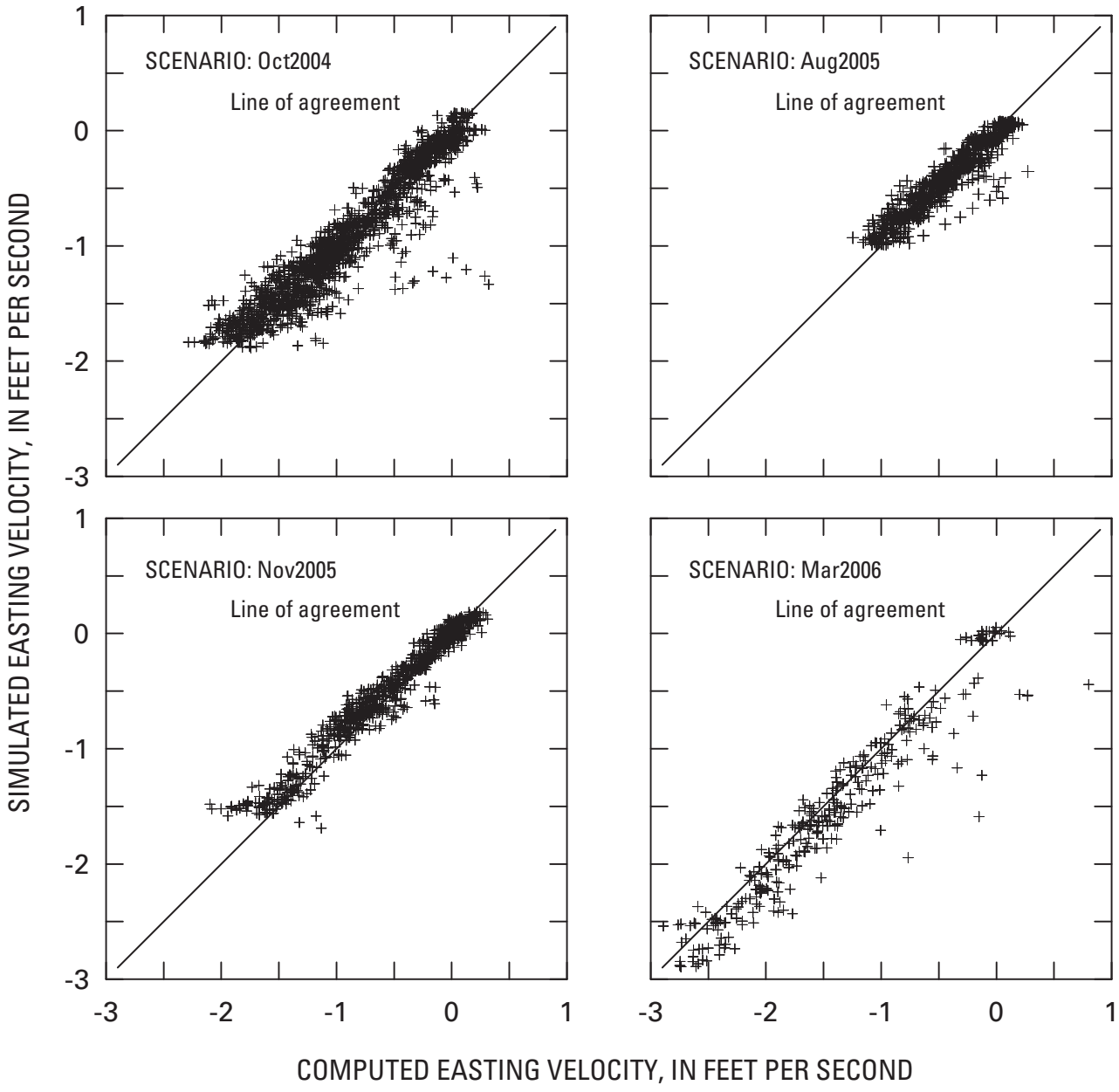

Figure 27. Relation between computed and simulated easting velocities on the Ohio River near Cincinnati, Ohio, October 2004–March 2006.

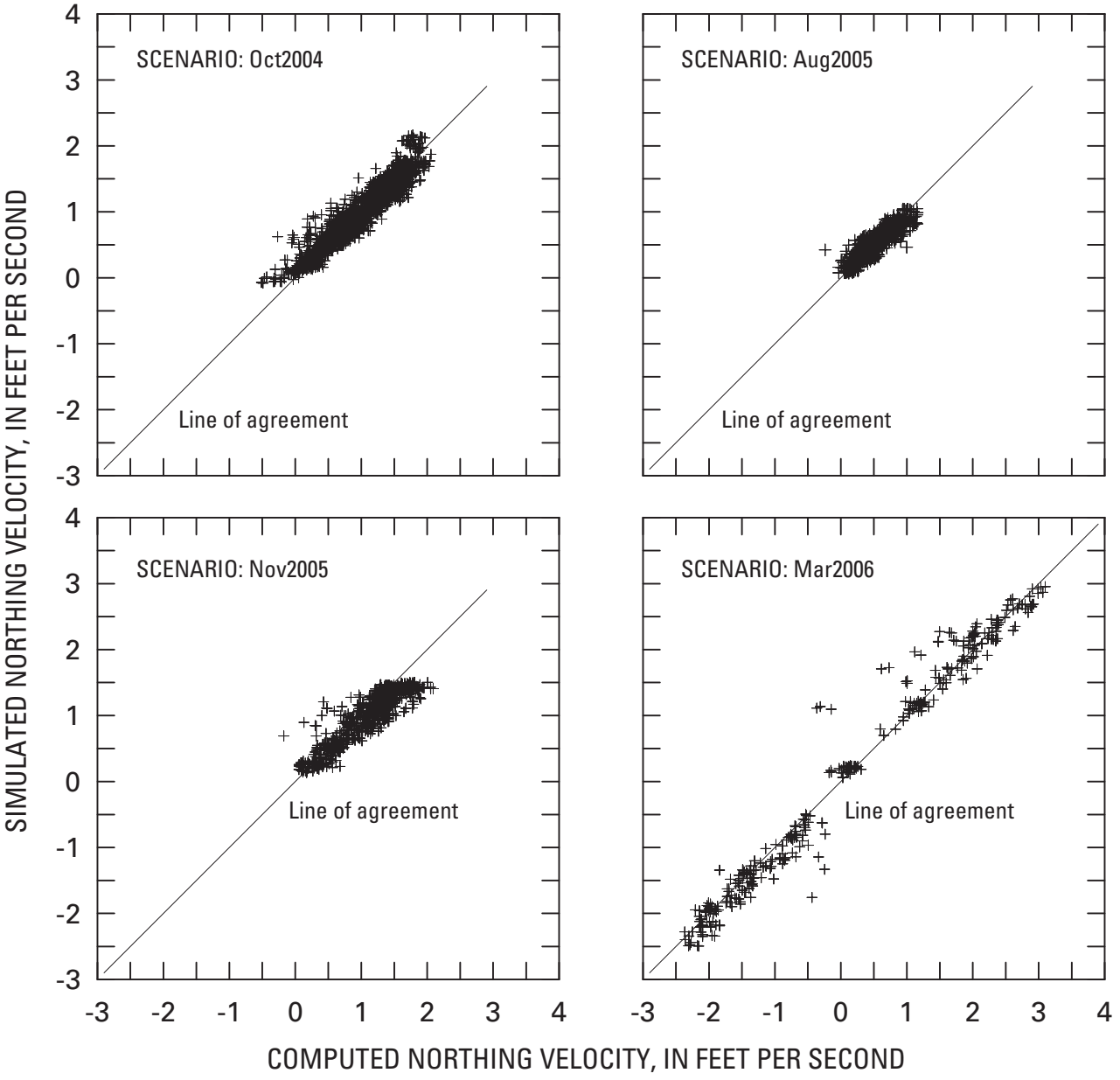

Figure 28. Relation between computed and simulated northing velocities on the Ohio River near Cincinnati, Ohio, October 2004–March 2006.

Drogue tracking also was used to estimate traveltimes along the BIC dye-injection-flow path. Again, with simulations from the Aug2005 scenario, drogue tracking was approximately constrained to the injection interval that was initiated on August 3, 2005, at 1300 EST and continued through August 4, 2005, at 1400 EST at 0.5-hour intervals. Based on this traveltime analysis, concentrations at transect OH 9 may have been measured before near-steady-state concentrations developed and were not used in the estimation of the decay coefficient for the BIC reach. Again, the relatively low transport rates computed at transects OH 8 and OH 9 may be related to insufficient traveltimes.

Measured transport rates were generally lower within the BIC dye-injection reach than those in the TMC injection reach for the same traveltimes, even though loading rates were the same for the two injection studies. Part of these differences may be associated with the greater magnitude of the estimated decay coefficient for the BIC injection reach. Transport rates used to estimate these parameters, however, were highly variable (fig. 29).

RMA4 Peclet Numbers

In RMA4, Peclet numbers are used to dynamically compute turbulent-mixing parameters. To assess the reproducibility of the transverse-mixing characterization provided by the two dye-injection studies, Peclet numbers were allowed to vary between the TMC and the BIC dye-injection sites. Higher RMA4 Peclet numbers are associated with lower turbulent mixing, which causes slower rates of simulated transverse and longitudinal mixing with distance downstream from the point of injection.

An initial attempt to simultaneously estimate dye-decay and RMA4 Peclet number parameters for the TMC dye-injection study was not successful. In particular, the dye-decay parameter estimate tended to 1, indicating a complete loss of dye. Subsequently, the least-squares estimate of the dye-decay parameter (0.218) was used with UCODE to estimate the RMA4 Peclet number within the TMC dye-injection reach. UCODE results converged to an RMA4 Peclet number of 173 (table 5), which is not consistent with the recommended (or physically plausible) range of 15 to 40, or with the estimated RMA2 Peclet number of 38.3. Thus, the utility of the parameter estimate, and corresponding simulated concentrations, are considered highly uncertain. The sum of squares weighted residuals, *S(b)*, was 13,775, based on 607 dye concentration measurements. The standard error of the parameter regression is 4.77.

In contrast, estimates of the dye-decay and RMA4 Peclet number parameters for the BIC reach converged simultaneously in UCODE to 0.323 and 37.2, respectively (table 5). The correlation between the two parameter estimates was -0.152, indicating that the pair of estimates is not degraded because of correlation. The final value of *S(b)* was equal to 1,044, based on 571 concentration measurements; this corresponds to a standard error of the regression of 1.35. The composite scaled sensitivities for the RMA4 Peclet number and the decay coefficient was 3.97 and 1.97, respectively, indicating sensitivity to the measured BIC concentrations. The decay coefficient estimated by use of UCODE is considered to supersede the estimate based on measured dye transport rates (fig. 30). The RMA4 parameter estimate is consistent with the expected parameter range and does not differ significantly from the RMA2 Peclet number. The discrepancy between the final estimates of RMA4 Peclet numbers at the two dye-injection sites makes application of the water-quality model to spills at new locations problematic because the RMA4 Peclet number cannot be consistently estimated.

Simulation

On August 2, 2005, measured dye concentrations within the TMC dye-injection reach were initially higher near the left bank, which is consistent with the side of the river where dye was injected in the TMC study. Maximum concentrations of about 8 µg/L were measured near the left bank at transect OH 10, which was about 6 mi downstream from the site of injection, and the first transect where dye concentrations were considered to be vertically mixed. Generally, these maximum concentrations attenuated with distance downstream, although this attenuation was not uniform with distance. In particular, maximum concentrations near the left bank decreased about 1 µg/L per mile along the four transects from OH 10 to OH 13 (fig. 30). Measured and simulated dye concentrations were generally consistent in these transects. From OH 13 to OH 14, however, maximum measured concentrations along the left bank decreased about 2.5 µg/L per mile, and a second concentration mode appeared mid channel. At transect OH 14, maximum dye concentrations in the mid-channel mode were greater than concentrations near the left bank. From transect OH 14 to OH 15, the measured mid-channel concentration mode appears to have continued its translation to the right bank, while maximum measured concentrations near the left bank again decreased at a rate of about 1 µg/L per mile downstream. Simulated concentrations do not indicate the presence or translation of a mid-channel model of elevated concentrations near OH 14 or OH 15. At OH 15, maximum concentrations were near the right bank, and these concentrations increased about 0.5 µg/L between samples collected starting at 12:56 PM and those samples collected starting 48 minutes later. Average concentrations elsewhere in transect OH 15 appeared unchanged during the two periods of measurements. Measured dye concentrations at transect OH 16 were approximately uniformly distributed, except near the right bank where average concentrations were about 0.5 µg/L lower than average. These concentrations may have been lowered by inflows of dye-free water from Little Miami River, which discharges into the Ohio River on the right bank between transects OH 15 and OH 16. Simulated dye concentrations at transects OH 15 and OH 16 exceeded 1.5 µg/L near the left bank and were near zero near the right bank.

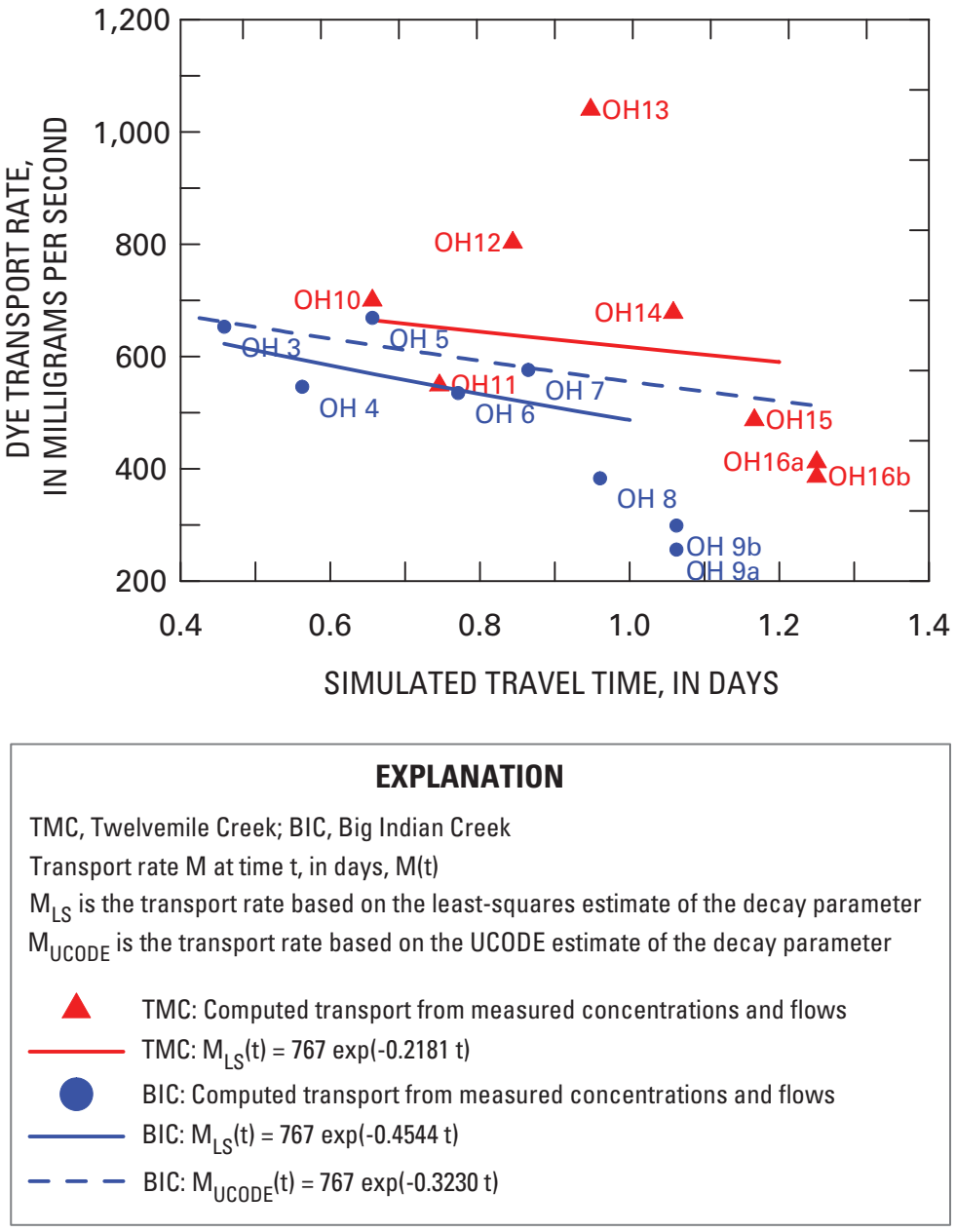

Figure 29. Dye-decay characteristics inferred from dye-injection sites near Twelvemile and Big Indian Creeks on the Ohio River upstream from Cincinnati, Ohio, August 2005.

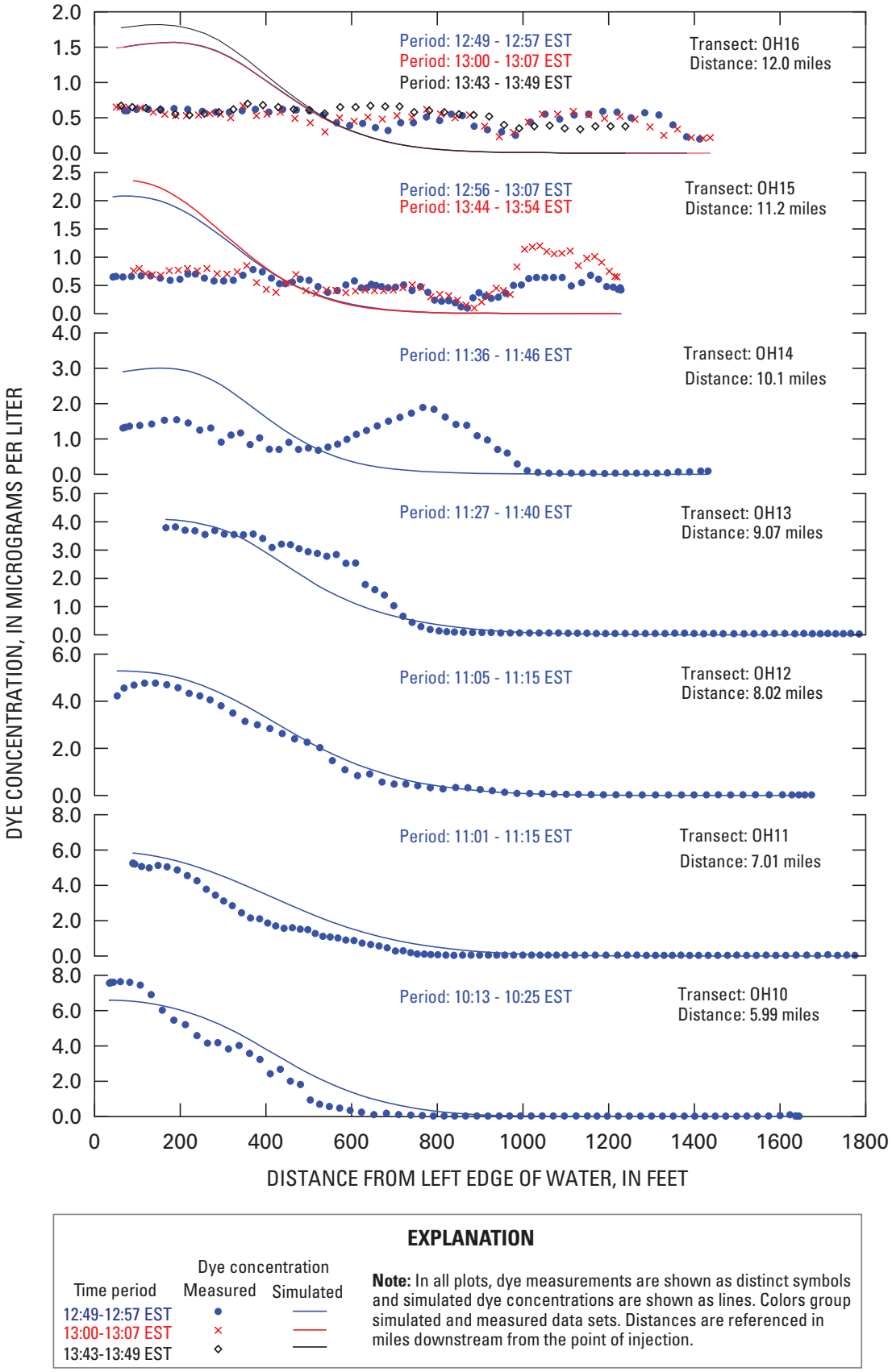

Figure 30. Measured and simulated dye concentrations at vertically mixed transects within the Twelvemile Creek injection reach of the Ohio River near Cincinnati, Ohio, August 2, 2005.

The inability to simulate the measured bimodal distribution of dye concentrations is an inherent limitation of a 2D transport model under any parameterization. The bimodal distribution of concentrations is thought to be associated with transport phenomena that are not sufficiently described by a 2D flow model. Investigation of 3D flow and transport characteristics within the TMC injection reach would provide a more comprehensive theoretical framework for simulation, and additional flow and concentration data from transects OH 4–OH 9 would support additional parameter estimation.

On the August 4, 2005, dye-injection study of the BIC reach, maximum measured dye concentrations were on the right side of the river, which is consistent with the location of the dye injection site. Transect OH 3, which is about 5.5 mi downstream from the BIC injection site, was the first transect where dye concentrations were considered vertically mixed. Maximum measured concentrations at OH 3 were about 2.6 µg/L (fig. 31), in contrast to maximum measured concentrations of about 8 µg/L at transect OH 10 during the TMC injection study. The lower maximum initial concentrations during the BIC study occurred despite a 19 percent decrease in flow from August 2–4, 2005, and a BIC injection site that was less than half the distance to the shoreline (60 ft) as the distance from the TMC injection site to the shoreline (125 ft). (Dye injection rates were the same for both injection studies.) Thus, dye concentrations during the TMC injection study might be considered initially under dispersed with respect to concentrations measured during the BIC injection study.

Maximum measured dye concentrations decreased with distance downstream at a rate of less than 0.5 µg/L per mile during the BIC injection study, which is a rate less than half the corresponding rate measured during the TMC injection study. The lower initial concentrations during the BIC study combined with the lower rate of decrease resulted in similar maximum concentrations of about 0.6 µg/L at the terminal transects of both injection studies, which were both about 12.0-mi downstream from their corresponding injection sites.

In contrast to bimodal distribution of dye concentrations that developed during the TMC injection study, the distribution of dye concentrations during the BIC injection study was unimodal, although asymmetric, with maximum concentrations consistently on the right side of the river. Concentrations at the right bank, however, were commonly lower than maximum concentrations. This near-shore affect was attributed to inflows of dye-free water from local tributaries, including Tenmile Creek.

Given the quantitative and qualitative differences between the distributions of dye concentrations measured during the two injection studies, differences between transport model parameters were inevitable. Dye concentrations simulated for the BIC injection study generally tracked the attenuation of measured dye concentrations with distance downstream from the point of injection. (fig. 31).

Despite the general consistency between measured and simulated dye concentrations in the BIC injection reach, some anomalies occurred. For example, measured dye concentrations near the left bank at transect OH 7 were higher than left-bank dye concentrations at all upstream transects; which did not follow the general pattern of dye concentrations decreasing with downstream distance. In particular, at upstream transect OH 6, near RM 8.5, left-bank dye concentrations were about 0.3 µg/L; downstream at OH 7, near RM 9.5, concentrations increased to about 0.7 µg/L but then decreased to 0.25 µg/L at OH 8, near RM 10.5. This discrepancy in measured dye concentrations may be attributable to transients in flow that were not measured or accounted for in hydrodynamic time steps used for all scenarios.

In addition, simulated dye concentrations generally tracked measured concentrations at transects OH 8 and OH 9, although measured dye concentrations near the right bank were markedly lower than simulated values. In this area, unmeasured inflows to the Ohio River from creeks on the Ohio side of the river may have diluted local dye concentrations. The fluctuations of flows near the mouths of ungaged tributaries to the Ohio River are difficult to quantify; these effects were not included in the hydrodynamic or transport models. The slight discontinuity in the simulated concentrations at transect OH 8, about 1,600 ft from the left edge of water, is attributed to simulations that transitioned at 13:30 EST from conditions at 13:00 EST to the right of this point to conditions at 14:00 EST to the left of this point. The transition indicates that simulated concentrations were still increasing with time when this transect was measured.

Dye concentrations and flows were measured almost simultaneously at OH 9 by two boat crews that were following slightly different paths across the transect (Koltun and others, 2006). The slight discrepancy between simulated flows for the two dye transects is the result of interpolating simulated concentrations at the same time step to different boat paths used to measure the dye.

The relation between percent mixing and distance downstream from the dye-injection point differed substantially between the TMC and BIC dye-injection studies (fig. 32). For the most upstream transects in the vertically mixed reaches, the computed mixing within the TMC reach was 28 percent at a point 6.0 mi downstream from the injection point. In contrast, the computed mixing within the BIC reach was 66 percent at a point 5.5 mi downstream from the injection point. At points greater than 11.5 mi downstream from the injection, however, both reaches showed mixing greater than 87 percent. Thus, the rate of mixing in the TMC reach increased about 2.5 times faster with downstream distance than mixing in the BIC reach, based on linear approximations to the relation between percent mixing and distance from the injection point. Extrapolation of either linear relation upstream through the unmixed reaches is unsatisfactory because neither relation has an intercept near zero-percent mixing. The differences between the rates of mixing during the TMC and BIC injection studies indicate sensitivity to the location of dye injection. This sensitivity may indicate that transverse flow components, not described by the 2D hydrodynamic model, affect transverse mixing characteristics in the study reach.

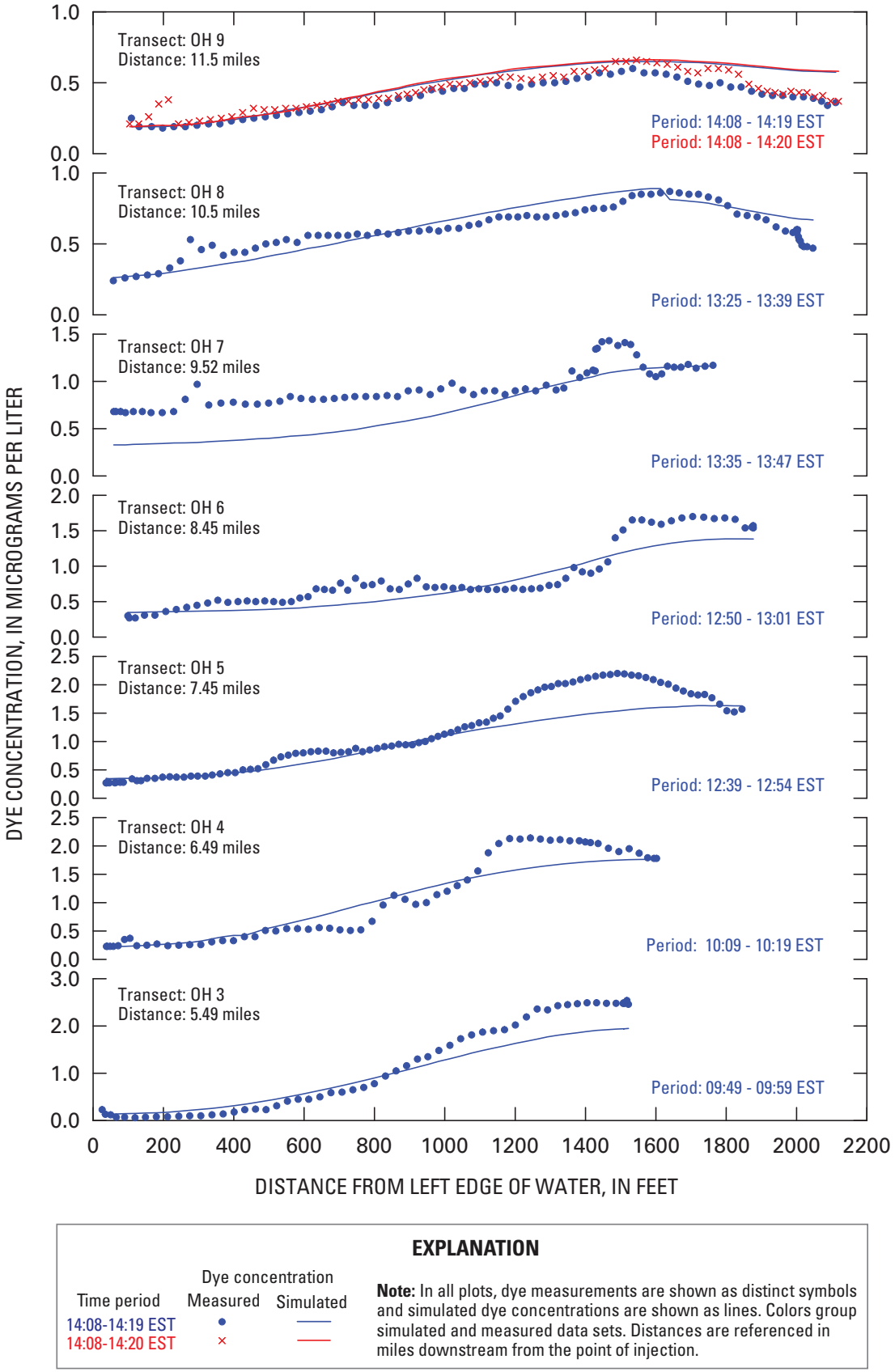

Figure 31. Measured and simulated dye concentrations at vertically mixed transects within the Big Indian Creek dye-injection reach of the Ohio River near Cincinnati, Ohio, August 4, 2005.

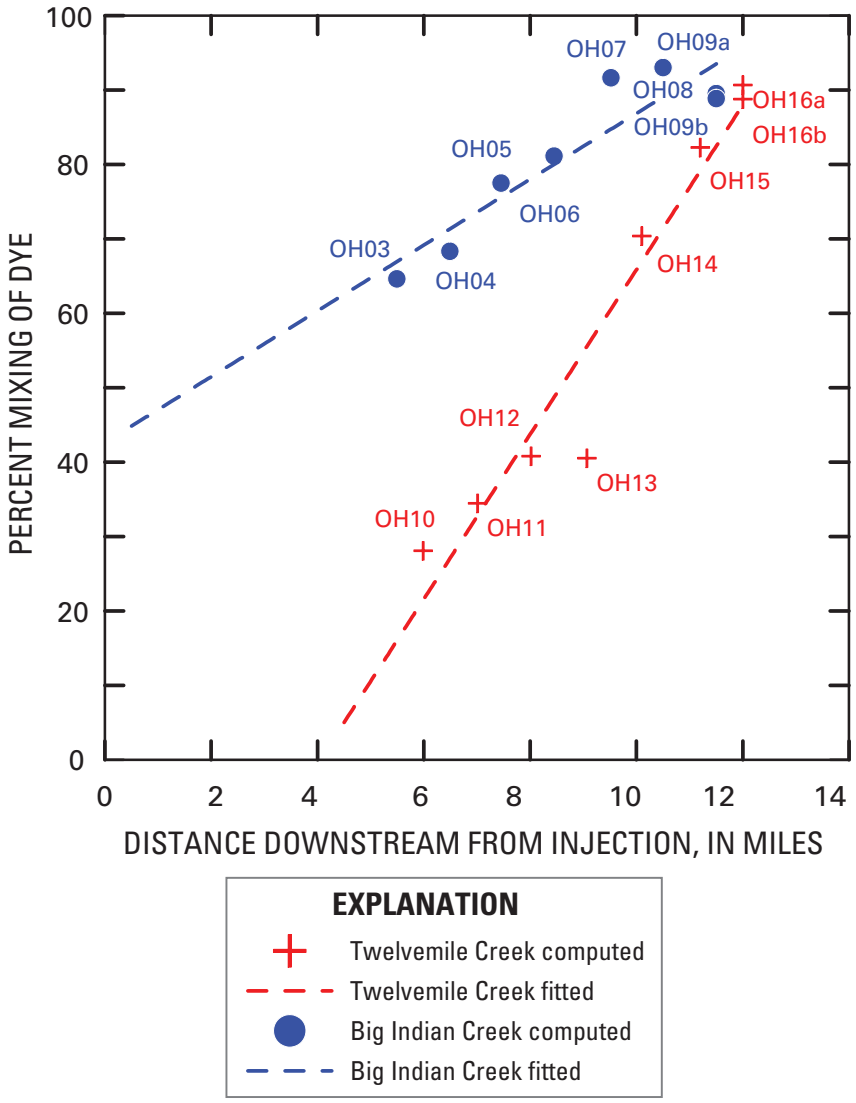

Figure 32. Relation between distance downstream from dye-injection points near Twelvemile Creek and Big Indian Creek and percent mixing on the Ohio River near Cincinnati, Ohio, August 2–4, 2005.

Hydrodynamic Model Limitations and Impacts on Water-Quality-Transport Simulations

RMA2 and RMA4 are based on the assumption that vertically averaged velocities are adequate to describe the variations of flow velocities with depth. The 2D hydrodynamic model developed in this report closely matches local depth-averaged velocities, flows, depths, and water levels along the modeled reach of the Ohio River. The 2D water-quality-transport model effectively integrates these local depth-averaged velocities longitudinally to define flow paths for transport simulations. Where vertical profiles of velocity deviate systematically from depth-averaged velocities, however, integration of velocities can result in a cumulative departure between simulated and actual flow paths with increasing longitudinal distances. This discussion uses ADCP velocity data collected on the Ohio River to illustrate how departures from 2D model assumptions may impact the accuracy of water-quality transport simulations.

Two-dimensional hydrodynamic-model simulations describe horizontal variations in depth-averaged velocities. In reaches that curve toward the left in the downstream direction, however, maximum velocities tend to be closer to the right bank (fig. 33). In straight reaches, maximum velocities tend to be near the center of the channel (fig. 34). In reaches that curve toward the right, maximum simulated velocities tend to be closer to the left bank (fig. 35). The general horizontal pattern of simulated velocities is consistent with depth-averaged ADCP velocity data; these data are computed by averaging horizontal velocities in 0.25-m bins that are available throughout the water column from individual ADCP ensembles.

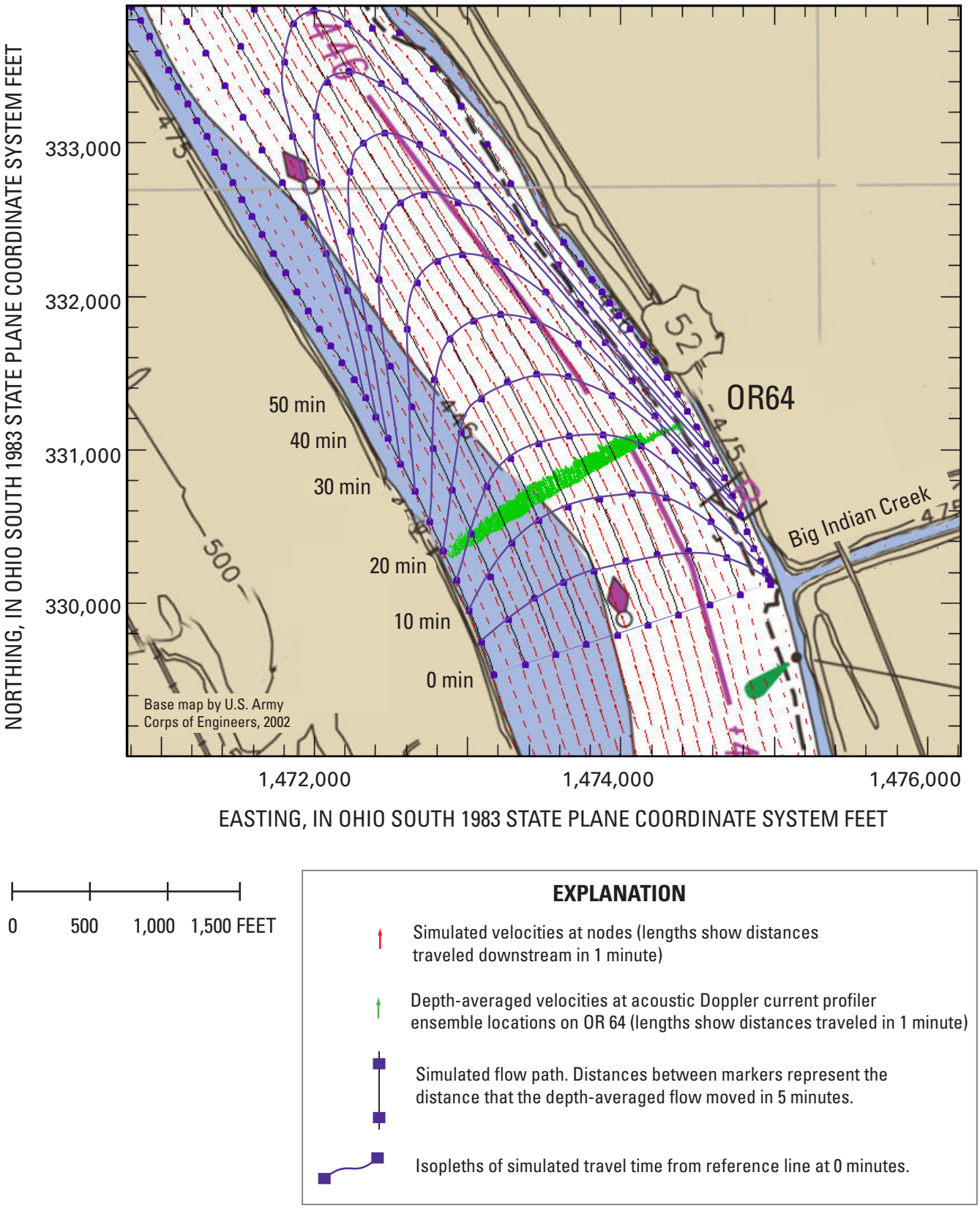

Figure 33. Variation in depth-averaged velocities, November 3, 2005, near acoustic Doppler current profiler transect OR 64 in a reach of the Ohio River near Cincinnati, Ohio, that curves to the left.

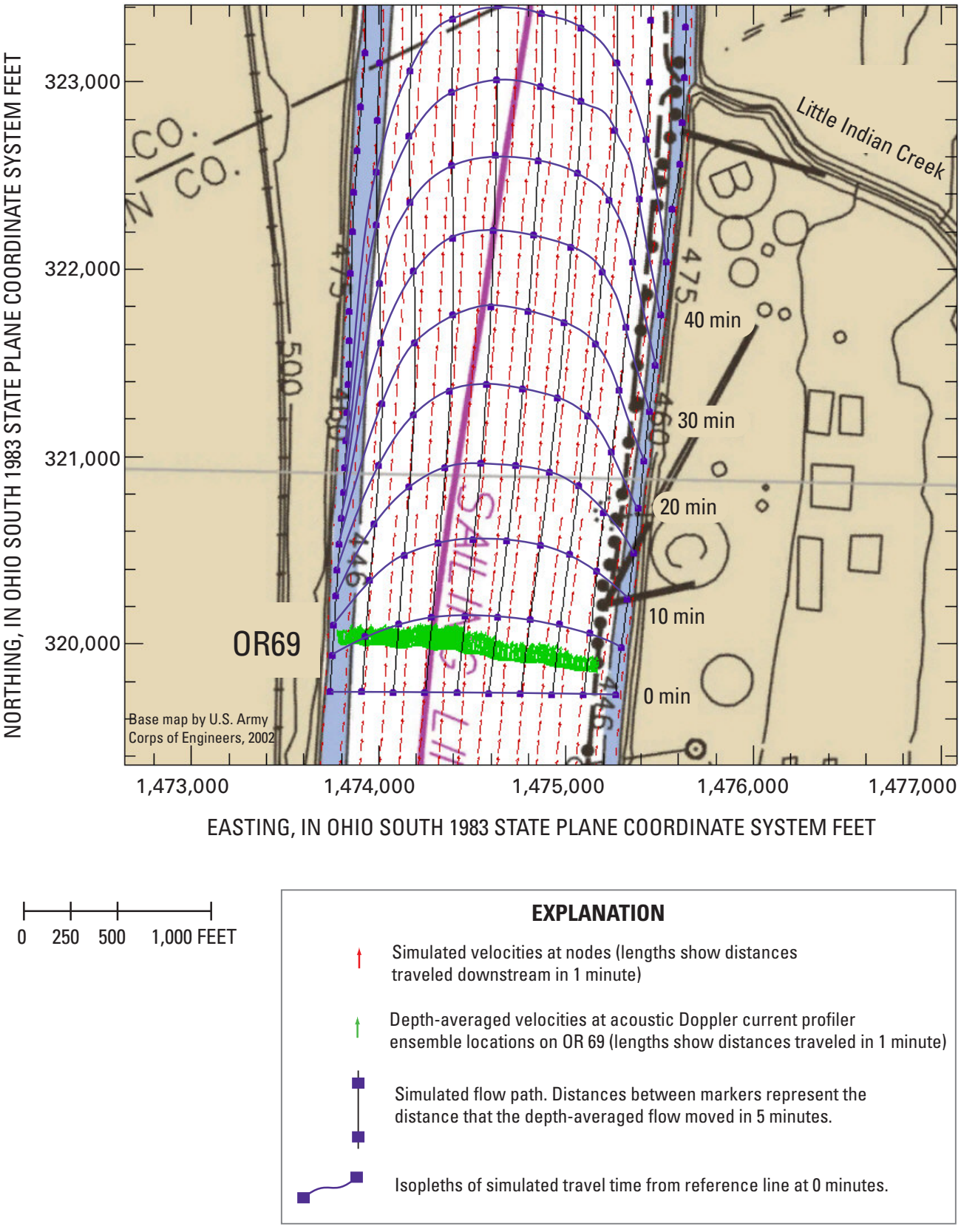

Figure 34. Variation in depth-averaged velocities, November 3, 2005, near acoustic Doppler current profiler transect OR 69 in straight reach of the Ohio River near Cincinnati, Ohio.

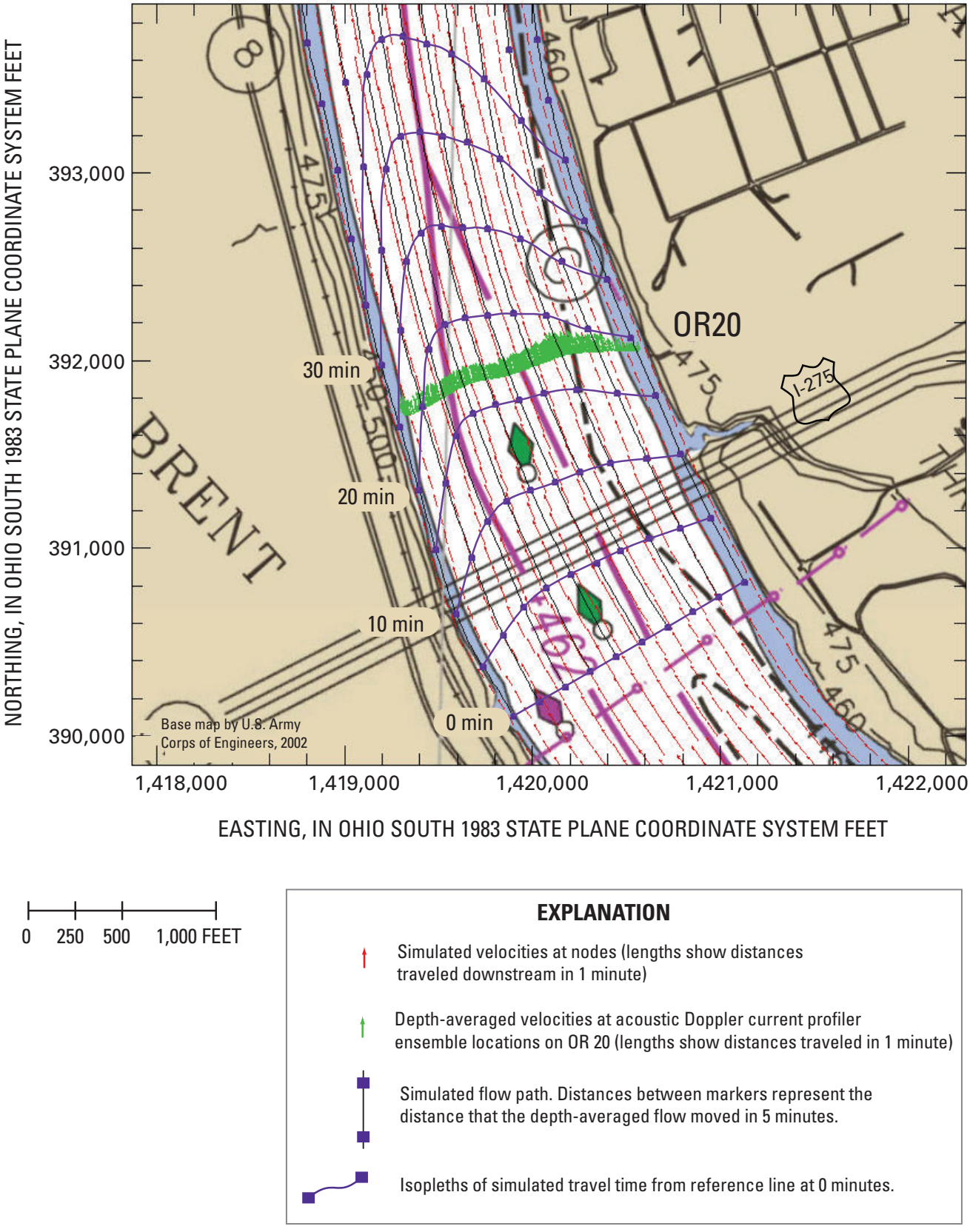

Figure 35. Variation in depth-averaged velocities, October 7, 2004, near acoustic Doppler current profiler transect OR 20 in a reach of the Ohio River near Cincinnati, Ohio, that curves to the right.

As an alternative to depth-averaged velocities, horizontally averaged velocities also can be computed by depth intervals from ADCP velocity data. These horizontally averaged velocities provide insight into the 3D variations in flow velocities. In the following paragraphs, variations in horizontal water speeds and directions with depth are discussed.

The average velocity magnitude (speed) was computed for each 0.25-m bin interval from 24 adjacent ensembles near the deepest part of the channel at OR 20 from data obtained during the ADCP survey, October 7, 2004 (Koltun and others, 2006). Because of the effects of vertical shear, the average speed varies approximately linearly with the depth below the water surface across the range of depths where velocity data were available (fig. 36). In particular, the average water speed increases about 59 percent from 1.16 ft/s in the lowest bin of the ensemble set at 43.1 ft below the water surface to 1.85 ft/s at 2.89 ft below the water surface.

Longitudinal mixing is determined by the vertical shear velocity and the longitudinal turbulent diffusive components. In contrast, transverse mixing is determined primarily by transverse turbulent mixing, except where significant transverse velocity shear occurs from secondary circulation. Within the study reach, secondary circulation patterns are thought to be restricted primarily to areas immediately downstream from Meldahl Dam; these may form as a result of the asymmetric release of flows across the gates and locks. According to Fischer and others (1979), rates of turbulent longitudinal mixing have not been measured by dye experiments because of the difficulty in separating the effects of longitudinal turbulent fluctuations from the results of shear flow. Presumably, turbulence causes longitudinal mixing at about the same rate as transverse turbulent mixing because there is an equal lack of boundaries to inhibit motion (Fischer and others, 1979); this is consistent with the assumption of an isotropic eddy-viscosity coefficient used in this report (equation 2).

Unlike transverse velocity shear in areas of secondary circulation, vertical shear velocity is integrated with depth (eliminated) in these 2D hydrodynamic and transport models. Thus, although an isotropic eddy-viscosity coefficient may be appropriate for describing the turbulent dispersion component, longitudinal mixing may be underestimated because the effect of vertical shear is not reflected in the simulations. Thus, concentrations simulated downstream from slug releases—for example, short-duration spills—may be overestimated because the longitudinal mixing associated with vertical shear is not taken into account. Use of a constant dye-injection rate and delaying dye sampling until near-steady-state concentrations developed at each transect facilitated data collection; however, the design made it difficult to quantify longitudinal mixing characteristics.

ADCP survey data also were used to investigate the variation of flow direction with depth through channel reaches with different curvatures (fig. 37). The ADCP data were subdivided into four quartiles corresponding to the cumulative flow from the left bank. At transect OR 64, which curves to the left, velocity azimuths in all flow quartiles tend to increase with depth. Given this general tendency, velocity azimuths span the largest range (about 19 degrees) with depth in the fourth quartile of flow $Q_{75–100}$, near the right bank. At transect OR 69, which has little curvature, velocity azimuths tend to have little relation to depth of flow. At transect OR 20, which curves to the right, azimuths tend to decrease with flow depth; this trend spans the largest range (about 14 degrees) with depth in the first quartile of flow $Q_{0–25}$, near the left bank. Thus, transverse-flow components in the vicinity of channel bends may significantly affect the transverse mixing of constituents; the significance of this effect may vary with the depth of the constituent in the water column.

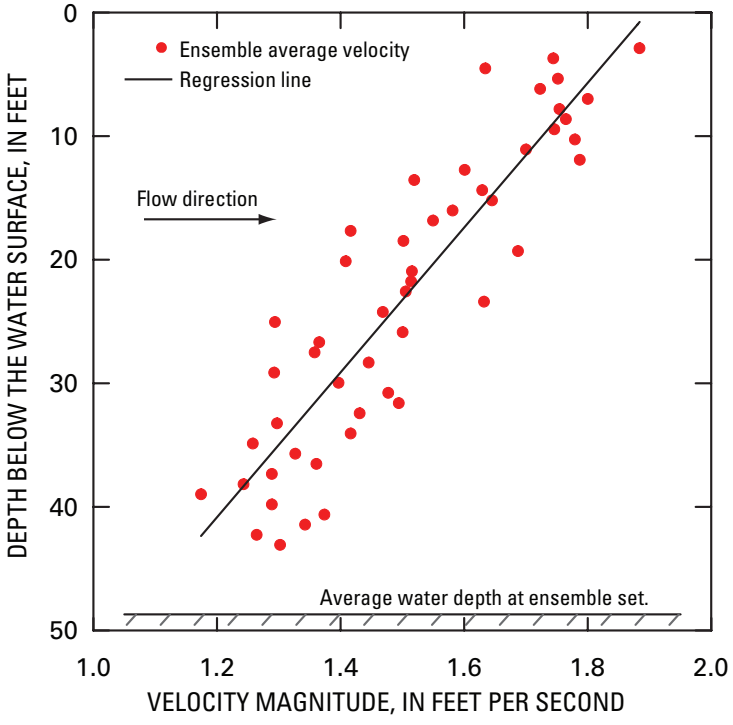

Figure 36. Variation of speed of flow with depth below the water surface at OR 20, Ohio River near Cincinnati, Ohio, October 7, 2004.

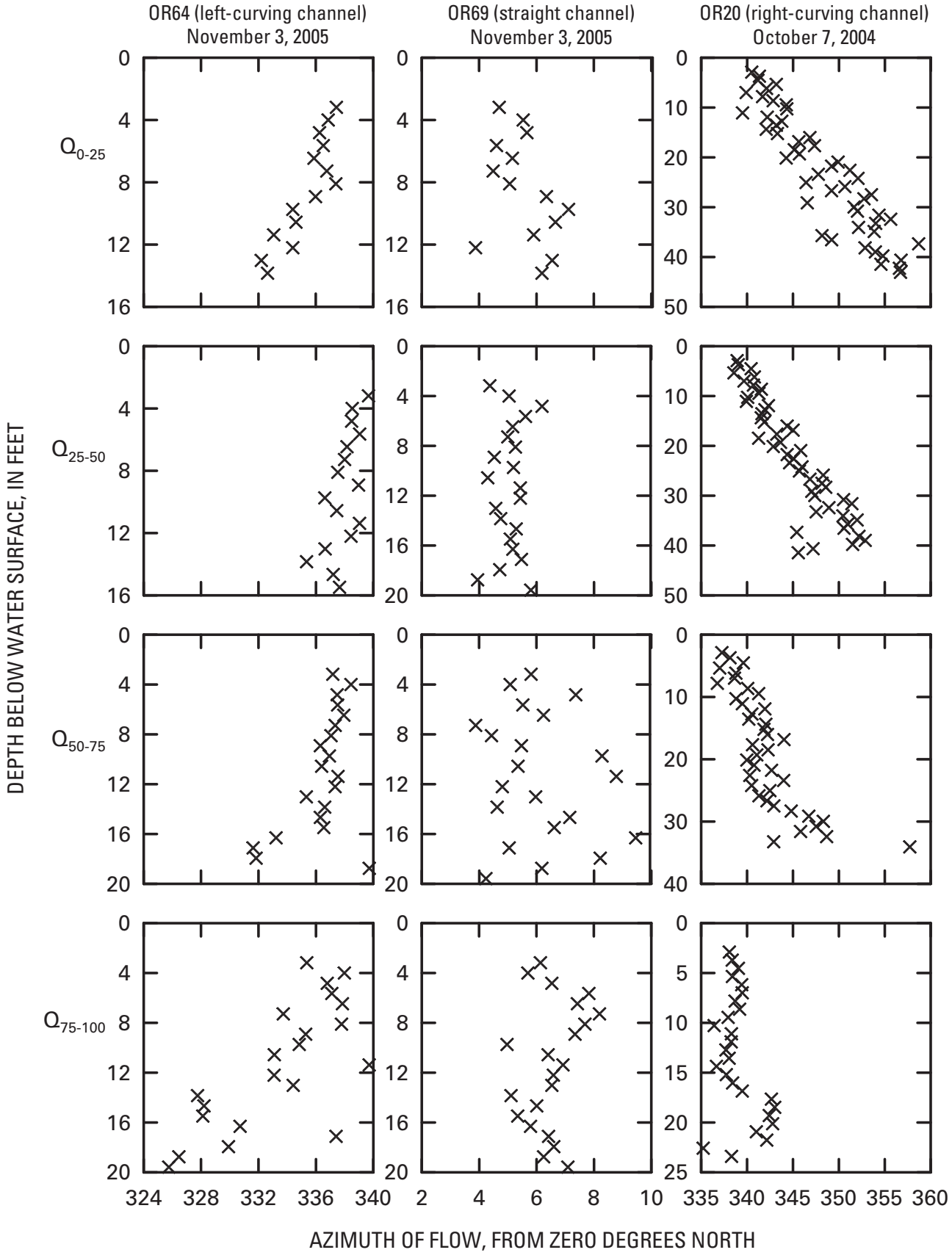

Figure 37. Relation between flow depth and flow-velocity azimuth from selected acoustic Doppler current profiler surveyed cross sections on the Ohio River near Cincinnati, Ohio, 2004–05.

The 2D flow and transport model applied in this report do not account for transverse-flow components. Transverse-flow components, however, may be associated with an anomalous distribution of dye from the TMC dye injection and the associated estimate of RMA4 Peclet number that is far outside the recommended range for this parameter. The inconsistency between measured velocity variations with depth and 2D model assumptions of depth-averaged flow impose restrictions on the application or interpretation of simulation results.

The lack of consistency between turbulent-mixing characteristics in the TMC and BIC reaches leaves significant uncertainty as to the appropriate turbulent-mixing characteristics for other reaches in the study area. Simulations of flows with RMA2 and concentration distributions with RMA4 (using the RMA4 Peclet number of 37.3 determined from the BIC dye-injection study), however, may be helpful for emergency planning of responses to contaminant spills. Areas likely to be affected by actual contaminant spills, however, would be identified more reliably from real-time flow measurements and water-quality sampling. Finally, implementation of a 3D flow and transport model within the Cincinnati reach of the Ohio River may reduce the uncertainty of simulated concentrations. The ADCP velocity and dye-concentration data such as that used in this model development, plus improved streamflow information as might be obtained from an operational streamgage may provide a basis for 3D model implementation and calibration.

Summary and Conclusions

Beginning in 2005, two-dimensional hydrodynamic and water-quality models were developed for a 34-mi reach of the Ohio River from Cincinnati, Ohio, upstream to Meldahl Dam, near Neville, Ohio. The models were developed on the basis of bathymetry, flow information, water-levels, and dye concentration measurements made by Koltun and others (2006). The study was done in cooperation with the Greater Cincinnati Water Works (GCWW) and the American Water Works Association Research Foundation (AwwaRF) to better understand flow and transport in the Ohio River.

Channel boundaries were digitized from georeferenced images of navigational charts of the Ohio River. Bathymetry of the channel was based on surveys from 2004-06 conducted by the U.S. Geological Survey. Based on these data, a finite-element mesh was developed to discretize the study reach, which is needed to facilitate the solution of hydrodynamic and transport equations. The mesh comprises 29,751 elements, averaging 100 ft on a side, defined at their vertices and mid-side edges by 92,622 nodes. Groups of contiguous elements define three material zones. Hydrodynamic and transport simulations compute water levels, velocities, and constituent concentrations at nodes; quadratic interpolation is used to estimate corresponding quantities within the interior of the elements.

Five scenarios representing transient flow conditions were used to calibrate the hydrodynamic model. Boundary conditions described time-varying flow and water-surface elevations at the model limits. In this report, Ohio River flows at the upstream model boundary were specified on the basis of the gate rating at Meldahl Dam, developed by the U.S. Army Corps of Engineers, and modified on the basis of flow measurements made in conjunction with this study. Flows near the mouths of Big Indian Creek, Twelvemile Creek, Little Miami River, and Licking River on the Ohio River also were specified as a proportion of the flows at Meldahl Dam. Water-surface elevations were specified on the basis of water levels recorded at the USGS water-level gaging station on the Ohio River at Cincinnati, Ohio.

The hydrodynamic model was based on the generalized finite-element hydrodynamic code RMA2 to simulate depth-averaged velocities and flow depths. The hydrodynamic model contains parameters that characterize the channel's resistance to flow and eddy viscosity, which controls the local variability of velocities that affect turbulent exchange and mixing. Unlike channel geometry, parameters cannot be measured directly but must be inferred from other measurements. In this report, measurements of flow, velocity, and water depth obtained during USGS ADCP surveys, measurements of tailwater elevation at Meldahl Dam, and miscellaneous measurements of water-surface elevation were used to estimate parameters in the hydrodynamic model. The parameter-estimation process, based on a nonlinear regression technique embedded within UCODE_2005, produced estimates for the hydrodynamic parameters that were considered physically plausible. Also, simulation results were consistent with measured flows, water levels, flow depths, and depth-averaged velocities.

The generalized water-quality code RMA4, using hydrodynamics simulated with RMA2, was used to simulate the transport of vertically mixed dye, which is a water-soluble constituent having a density similar to water. Two water-quality scenarios, representing two USGS dye-injection studies on Twelvemile Creek (TMC) and Big Indian Creek (BIC), were used to estimate dye-loss rates and turbulent-mixing characteristics for the two overlapping reaches. The two studies used the same dye-injection rates and were conducted two days apart under similar flow conditions. The transverse distribution of dye concentration was measured in several transects downstream from the injection sites. Minor dye losses within the injection reaches were described with an exponential decay formula; coefficients were estimated on the basis of simulated travel times and computed dye-transport rates at transects downstream from the points of injection. Both dye-injection studies showed more than 87-percent mixing of dye concentrations along transects more than 11.5 mi downstream from the point of injection. The rates of turbulent mixing and the ability to match simulated and measured dye concentrations, however, differed widely between the two reaches.

In the TMC injection study, maximum dye concentrations exceeded 7.5 µg/L in the upstream transects, starting at about 6 mi downstream from the injection site, and were less than 0.8 µg/L in some downstream transects. To simulate the measured distribution of dye concentrations in the more-upstream transects, a RMA4 Peclet number of 173 was estimated, which is far outside the recommended range from 15 to 40 and is considered implausible. This parameter estimate, however, resulted in simulations that underestimated the attenuation in the downstream transects and resulted in less-uniform concentrations than were measured. In the BIC dye-injection reach, the attenuation of maximum dye concentrations from 2.5 µg/L at OH 3 (the first measured transect about 5.5 mi downstream from the injection) to 0.6 µg/L at OH 9 (the last measured transect about 11.5 mi downstream from the injection) were approximated by a RMA4 Peclet number of 37.2, which is within the recommended range from 15 to 40.

The 2D models used in this report assume that depth-averaged velocities are adequate to describe flow and transport within the study reach. This assumption was investigated by examining the variation of horizontal velocity components with depth from ADCP measurements. Comparisons indicate that in the vicinity of channel bends, variations in velocity directions with depth are not well approximated by depth-averaged values. Departures from model assumptions associated with flow and transport are thought to be associated with the anomalous parameter estimate obtained for the RMA4 Peclet number at the TMC dye-injection reach. Although the estimated RMA4 Peclet number of 37.2 for the BIC injection reach is within the recommended range and produces a consistent match with measured concentrations in downstream transects, the model application may be restricted to emergency planning. In particular, the lack of consistency between turbulent-mixing characteristics in the TMC and BIC reaches leaves significant uncertainty as to the appropriate turbulent-mixing characteristics for other reaches in the study area. Application of 3D flow and transport models using the existing ADCP and dye-concentration data may help address some of this ambiguity. The dye-injection studies provided critical information needed to calibrate and assess the validity of the transport model. Although the RMA2 Peclet number and the RMA4 Peclet number for the BIC dye-injection study were similar, ADCP velocity data, as applied in this study, could not be substituted for dye-concentration data.

Acknowledgments

This study was done in cooperation with the Greater Cincinnati Water Works (GCWW) and the AWWA Research Foundation (AwwaRF). Mr. Ramesh Kashinkunti, Supervising Engineer with GCWW, and Dr. Kenan Ozekin, Senior Account Manager with AwwaRF, provided technical assistance and coordination. Dr. Richard W. Gullick, Environmental Engineering & Technology, Inc.; Dr. Eugene J. LeBoeuf, Vanderbilt University; Dr. Morton W. Reed, Columbus Water Works; and Mr. Ed Roehl, Advanced Data Mining International, served on AwwaRF's Project Advisory Committee and provided technical review and oversight. Mr. Stan Wisbith, U.S. Army Corps of Engineers, Great Lakes and Ohio River Division, provided data on flows, water levels, operations, and conditions that were critical in modeling the river. Mr. Michael Griffin, USGS Kentucky Water Science Center, provided unpublished water-level data obtained during the bathymetry surveys. Graphical and editorial assistance was provided by Ms. Sharon Baltusis and Ms. Patricia Long of the U.S. Geological Survey. Mr. Chad Wagner, U.S. Geological Survey, also provided technical review. Mr. Robert R. Mason, Jr. and staff at the USGS Office of Surface Water, quality assured miscellaneous water-level data obtained by the USGS Kentucky Water Science Center during the bathymetry surveys.

References Cited

Barnes, H.H., Jr., 1967, Roughness characteristics of natural channels: U.S. Geological Survey Water-Supply Paper 1849, 213 p.

Donnell, B.P., Letter, J.V., Jr., McAnally, W.H., and others, 2005, Users guide to RMA2 WES Version 4.5: Vicksburg, Miss., U.S. Army, Engineer Research and Development Center, Waterways Experiment Station, Coastal and Hydraulics Laboratory, 277 p.

Environmental Modeling Research Laboratory, 2006, SMS Surface-Water Modeling System Reference Manual, Version 9: Provo, Utah, Environmental Modeling Systems, Inc., 342 p.

Fischer, H.B., List, E.J., Koh, R.C.Y., Imberger, Jörg, and Brooks, N.H., 1979, Mixing in inland and coastal waters: New York, Academic Press, 483 p.

Hill, M.C., 1998, Methods and guidelines for effective model calibration; with application to UCODE, a computer code for universal inverse modeling, and MODFLOWP, a computer code for inverse modeling with MODFLOW: U.S. Geological Survey Water-Resources Investigations Report 98–4005, 90 p., accessed December 1, 2007, at *http://pubs.er.usgs.gov/usgspubs/tm/tm6A11/*.

Koltun, G.F., Ostheimer, C.J., and Griffin, M.S., 2006, Velocity, bathymetry, and transverse mixing characteristics of the Ohio River upstream from Cincinnati, Ohio, October 2004–March 2006: U.S. Geological Survey Open-File Report 2006–1159, accessed December 3, 2007, at *http://pubs.usgs.gov/of/2006/1159/*.

Letter, J.V., Donnell, B.P., and others, 2005, Users guide to RMA4 WES Version 4.5: Vicksburg, Miss., U.S. Army, Engineer Research and Development Center, Waterways Experiment Station, Coastal and Hydraulics Laboratory, 173 p.

McDonald, R.R., Nelson, J.M., and Bennett, J.P., in press, Multi-dimensional surface-water modeling system user's guide: U.S. Geological Survey Techniques and Methods, 6–B2, 136 p.

Ohio River Valley Water Sanitation Commission, 2006, Ohio River Facts, accessed December 3, 2007, at *http://www.orsanco.org/rivinfo/facts.asp*

Poeter, E.P., Hill, M.C., Banta, E.R., Mehl, Steffen, and Christensen, Steen, 2005, UCODE_2005 and six other computer codes for universal sensitivity analysis, calibration, and uncertainty evaluation: U.S. Geological Survey Techniques and Methods 6–A11, 283 p., accessed December 3, 2007, at *http://www.mines.edu/igwmc/freeware/ucode/UCODE_2005_Manual_USGS-TM6-A11.pdf*

Rutherford, J.C., 1994, River mixing: New York, John Wiley & Sons, 347 p.

Smart, P.L., and Laidlaw, I.M.S., 1977, An evaluation of some fluorescent dyes for water tracing: Water Resources Research, v. 13, no. 1, p. 15–33.

U.S. Army Corps of Engineers, 2005a, Coordinate Conversion Program Corpscon (v. 6.0.1): Alexandria, Va., Engineer Research and Development Center, Topographic Engineering Center, accessed December 1, 2006, at *http://crunch.tec.army.mil/software/corpscon/corpscon.html*

U.S. Army Corps of Engineers, 2005b, Difference between "1929 General Adjustment" and "Ohio River" datum planes: Louisville, Ky., Louisville District, accessed December 1, 2007, at *http://www.lrl.usace.army.mil/optm/article.asp?id=231*

U.S. Army Corps of Engineers, 2008, Ohio River and Green River Navigation Charts: Louisville, Ky., U.S. Army Corps of Engineers, Louisville District, accessed December 12, 2008, at *http://www.lrl.usace.army.mil/optm/article.asp?id=145&MyCategory=41*

U.S. Geological Survey, 2005, Policy and guidance for archiving electronic discharge measurement data: U.S. Geological Survey Office of Surface Water Technical Memorandum No. 2005.08, September 26, 2005 5 p., accessed June 23, 2009, at *http://hydroacoustics.usgs.gov/memos/OSW2005-08.pdf*

Appendixes 1 and 2

Appendix 1. Regimen of the gate-opening sequence for individual gates as a function of total gate opening at Meldahl Dam, near Neville, Ohio.

[Feet of gate opening for individual gates, which are numbered sequentially starting from 1 at the northern-most gate next to the main lock and ending at 12 at the gate closest to Kentucky shoreline. Gate opening data were provided by Stanley Wisbith, U.S. Army Corps of Engineers, written commun., March 2006]

Total gate opening, in feet	Gate 1	Gate 2	Gate 3	Gate 4	Gate 5	Gate 6	Gate 7	Gate 8	Gate 9	Gate 10	Gate 11	Gate 12
1	0	0	0	0	0	0	0	0	0	0	0	1
2	0	0	0	1	0	0	0	0	0	0	0	1
3	0	0	0	2	0	0	0	0	0	0	0	1
4	0	0	0	2	0	0	0	0	1	0	0	1
5	0	0	0	2	0	0	0	0	2	0	0	1
6	0	0	0	2	0	0	0	0	3	0	0	1
7	0	0	0	3	0	0	0	0	3	0	0	1
8	0	0	0	3	0	0	0	0	3	1	0	1
9	0	0	0	3	0	0	0	0	3	2	0	1
10	0	0	0	3	0	0	0	0	3	3	0	1
11	0	0	1	3	0	0	0	0	3	3	0	1
12	0	0	2	3	0	0	0	0	3	3	0	1
13	0	0	3	3	0	0	0	0	3	3	0	1
14	0	0	3	3	0	1	0	0	3	3	0	1
15	0	0	3	3	0	2	0	0	3	3	0	1
16	0	0	3	3	0	3	0	0	3	3	0	1
17	0	0	3	3	0	3	1	0	3	3	0	1
18	0	0	3	3	0	3	2	0	3	3	0	1
20	0	0	3	3	1	3	3	0	3	3	0	1
22	0	0	3	3	3	3	3	0	3	3	0	1
24	0	0	3	3	3	3	3	2	3	3	0	1
26	0	1	3	3	3	3	3	3	3	3	0	1
28	0	3	3	3	3	3	3	3	3	3	0	1
30	0	3	3	3	3	3	3	3	3	3	2	1
32	1	3	3	3	3	3	3	3	3	3	3	1
34	3	3	3	3	3	3	3	3	3	3	3	1
36	3	3	3	3	3	3	3	3	3	3	3	3
36	3	3	3	3	3	3	3	3	3	3	3	3
38	3	3	3	3	3	4	4	3	3	3	3	3
40	3	3	3	3	4	4	4	4	3	3	3	3
42	3	3	3	4	4	4	4	4	4	3	3	3
44	3	3	4	4	4	4	4	4	4	4	3	3
46	3	4	4	4	4	4	4	4	4	4	4	3
48	4	4	4	4	4	4	4	4	4	4	4	4
50	4	4	4	4	4	5	5	4	4	4	4	4
52	4	4	4	4	5	5	5	5	4	4	4	4
54	4	4	4	5	5	5	5	5	5	4	4	4
56	4	4	5	5	5	5	5	5	5	5	4	4
58	4	5	5	5	5	5	5	5	5	5	5	4

Appendix 1. Regimen of the gate-opening sequence for individual gates as a function of total gate opening at Meldahl Dam, near Neville, Ohio. —Continued

[Feet of gate opening for individual gates, which are numbered sequentially starting from 1 at the northern-most gate next to the main lock and ending at 12 at the gate closest to Kentucky shoreline. Gate opening data were provided by Stanley Wisbith, U.S. Army Corps of Engineers, written commun., March 2006]

Total gate opening, in feet	Gate 1	Gate 2	Gate 3	Gate 4	Gate 5	Gate 6	Gate 7	Gate 8	Gate 9	Gate 10	Gate 11	Gate 12
60	5	5	5	5	5	5	5	5	5	5	5	5
62	5	5	5	5	5	6	6	5	5	5	5	5
64	5	5	5	5	6	6	6	6	5	5	5	5
66	5	5	5	6	6	6	6	6	6	5	5	5
68	5	5	6	6	6	6	6	6	6	6	5	5
70	5	6	6	6	6	6	6	6	6	6	6	5
72	6	6	6	6	6	6	6	6	6	6	6	6
76	6	6	6	6	6	8	8	6	6	6	6	6
80	6	6	6	6	8	8	8	8	6	6	6	6
84	6	6	6	8	8	8	8	8	8	6	6	6
88	6	6	8	8	8	8	8	8	8	8	6	6
92	6	8	8	8	8	8	8	8	8	8	8	6
96	8	8	8	8	8	8	8	8	8	8	8	8
100	8	8	8	8	8	10	10	8	8	8	8	8
104	8	8	8	8	10	10	10	10	8	8	8	8
108	8	8	8	10	10	10	10	10	10	8	8	8
112	8	8	10	10	10	10	10	10	10	10	8	8
116	8	10	10	10	10	10	10	10	10	10	10	8
120	10	10	10	10	10	10	10	10	10	10	10	10
124	10	10	10	10	10	12	12	10	10	10	10	10
128	10	10	10	10	12	12	12	12	10	10	10	10
132	10	10	10	12	12	12	12	12	12	10	10	10
136	10	10	12	12	12	12	12	12	12	12	10	10
144	12	12	12	12	12	12	12	12	12	12	12	12
148	12	12	12	12	12	14	14	12	12	12	12	12
152	12	12	12	12	14	14	14	14	12	12	12	12
156	12	12	12	14	14	14	14	14	14	12	12	12
160	12	12	14	14	14	14	14	14	14	14	12	12
168	14	14	14	14	14	14	14	14	14	14	14	14
172	14	14	14	14	14	16	16	14	14	14	14	14
176	14	14	14	14	16	16	16	16	14	14	14	14
180	14	14	14	16	16	16	16	16	16	14	14	14
184	14	14	16	16	16	16	16	16	16	16	14	14
192	16	16	16	16	16	16	16	16	16	16	16	16
196	16	16	16	16	16	18	18	16	16	16	16	16
200	16	16	16	16	18	18	18	18	16	16	16	16
204	16	16	16	18	18	18	18	18	18	16	16	16
208	16	16	18	18	18	18	18	18	18	18	16	16
216	18	18	18	18	18	18	18	18	18	18	18	18

Appendix 1. Regimen of the gate-opening sequence for individual gates as a function of total gate opening at Meldahl Dam, near Neville, Ohio. —Continued

[Feet of gate opening for individual gates, which are numbered sequentially starting from 1 at the northern-most gate next to the main lock and ending at 12 at the gate closest to Kentucky shoreline. Gate opening data were provided by Stanley Wisbith, U.S. Army Corps of Engineers, written commun., March 2006]

Total gate opening, in feet	Gate 1	Gate 2	Gate 3	Gate 4	Gate 5	Gate 6	Gate 7	Gate 8	Gate 9	Gate 10	Gate 11	Gate 12
220	18	18	18	18	18	20	20	18	18	18	18	18
224	18	18	18	18	20	20	20	20	18	18	18	18
228	18	18	18	20	20	20	20	20	20	18	18	18
232	18	18	20	20	20	20	20	20	20	20	18	18
240	20	20	20	20	20	20	20	20	20	20	20	20
244	20	20	20	20	20	22	22	20	20	20	20	20
248	20	20	20	20	22	22	22	22	20	20	20	20
252	20	20	20	22	22	22	22	22	22	20	20	20
256	20	20	22	22	22	22	22	22	22	22	20	20
264	22	22	22	22	22	22	22	22	22	22	22	22
268	22	22	22	22	22	24	24	22	22	22	22	22
272	22	22	22	22	24	24	24	24	22	22	22	22
276	22	22	22	24	24	24	24	24	24	22	22	22
280	22	22	24	24	24	24	24	24	24	24	22	22
288	24	24	24	24	24	24	24	24	24	24	24	24
292	24	24	24	24	24	26	26	24	24	24	24	24
296	24	24	24	24	26	26	26	26	24	24	24	24
300	24	24	24	26	26	26	26	26	26	24	24	24
304	24	24	26	26	26	26	26	26	26	26	24	24
312	26	26	26	26	26	26	26	26	26	26	26	26
316	26	26	26	26	26	28	28	26	26	26	26	26
320	26	26	26	26	28	28	28	28	26	26	26	26
324	26	26	26	28	28	28	28	28	28	26	26	26
328	26	26	28	28	28	28	28	28	28	28	26	26
336	28	28	28	28	28	28	28	28	28	28	28	28
340	28	28	28	28	28	30	30	28	28	28	28	28
344	28	28	28	28	30	30	30	30	28	28	28	28
348	28	28	28	30	30	30	30	30	30	28	28	28
352	28	28	30	30	30	30	30	30	30	30	28	28
360	30	30	30	30	30	30	30	30	30	30	30	30

Appendix 2. Miscellaneous water-level measurements on the Ohio River between Cincinnati and Meldahl Dam obtained during 2004–06 bathymetry surveys.

[NAVD 88, North American Vertical Datum of 1988; Michael Griffin, USGS Kentucky Water Science Center, obtained the miscellaneous water-level measurements listed in this appendix. Robert Mason, Jr. and staff from the USGS Office of Surface Water, revised and quality assured these data in 2008]

Date and time (Eastern Standard)	River mile	Site reference	Water-surface elevation (NAVD 88)	Site description
10/5/04 13:00	471.0	Cincinnati water-level gaging station	454.94	Ohio River at Cincinnati, Ohio (03255000)
10/5/04 13:40	462.5	1005	455.30	Ohio River at the boat ramp at California, Ohio
10/5/04 13:00	436.0	Meldahl Dam	457.37	Ohio River downstream from Meldahl Dam
10/5/04 19:00	471.0	Cincinnati water-level gaging station	455.10	Ohio River at Cincinnati, Ohio (03255000)
10/5/04 19:00	462.5	1005	455.41	Ohio River at the boat ramp at California, Ohio
10/5/04 12:00	436.0	Meldahl Dam	457.35	Ohio River downstream from Meldahl Dam
10/6/04 09:00	471.0	Cincinnati water-level gaging station	455.18	Ohio River at Cincinnati, Ohio (03255000)
10/6/04 09:00	462.5	1005	455.38	Ohio River at the boat ramp at California, Ohio
10/6/04 09:00	436.0	Meldahl Dam	456.87	Ohio River downstream from Meldahl Dam
10/6/04 18:00	471.0	Cincinnati water-level gaging station	454.68	Ohio River at Cincinnati, Ohio (03255000)
10/6/04 18:30	462.5	1005	454.82	Ohio River at the boat ramp at California, Ohio
10/6/04 18:30	436.0	Meldahl Dam	456.34	Ohio River downstream from Meldahl Dam
10/7/04 09:00	471.0	Cincinnati water-level gaging station	455.08	Ohio River at Cincinnati, Ohio (03255000)
10/7/04 09:00	462.5	1005	455.37	Ohio River at the boat ramp at California, Ohio
10/7/04 09:20	436.0	Meldahl Dam	457.64	Ohio River downstream from Meldahl Dam
10/7/04 19:00	471.0	Cincinnati water-level gaging station	455.48	Ohio River at Cincinnati, Ohio (03255000)
10/7/04 19:00	462.5	1005	455.81	Ohio River at the boat ramp at California, Ohio
10/7/04 19:00	436.0	Meldahl Dam	457.89	Ohio River downstream from Meldahl Dam
10/27/05 08:30	471.0	Cincinnati water-level gaging station	456.07	Ohio River at Cincinnati, Ohio (03255000)
10/27/05 08:30	449.4	1006	458.03	Ohio River at Skippers Boat Ramp near New Richmond, Ohio
10/27/05 08:45	446.9	1007	458.51	Ohio River at Bubblers Restaurant near Clermontville, Ohio
10/27/05 09:40	442.6	1008	459.06	Ohio River at boat ramp at Moscow, Ohio
10/27/05 09:15	438.7	1009	459.25	Ohio River at Neville, Ohio
10/27/05 08:30	436.0	Meldahl Dam	459.72	Ohio River downstream from Meldahl Dam
10/28/05 09:00	471.0	Cincinnati water-level gaging station	455.86	Ohio River at Cincinnati, Ohio (03255000)
10/28/05 09:00	449.4	1006	458.12	Ohio River at Skippers Boat Ramp near New Richmond, Ohio
10/28/05 09:30	446.9	1007	458.59	Ohio River at Bubblers Restaurant near Clermontville, Ohio
10/28/05 09:00	442.6	1008	459.14	Ohio River at boat ramp at Moscow, Ohio
10/28/05 09:00	436.0	1009	459.72	Ohio River at Neville, Ohio
11/3/05 10:00	471.0	Cincinnati water-level gaging station	454.84	Ohio River at Cincinnati, Ohio (03255000)
11/3/05 09:40	449.4	1006	455.54	Ohio River at Skippers Boat Ramp near New Richmond, Ohio

Appendix 2. Miscellaneous water-level measurements on the Ohio River between Cincinnati and Meldahl Dam obtained during 2004–06 bathymetry surveys. —Continued

[NAVD 88, North American Vertical Datum of 1988; Michael Griffin, USGS Kentucky Water Science Center, obtained the miscellaneous water-level measurements listed in this appendix. Robert Mason, Jr. and staff from the USGS Office of Surface Water, revised and quality assured these data in 2008]

Date and time (Eastern Standard)	River mile	Site reference	Water-surface elevation (NAVD 88)	Site description
11/3/05 09:30	446.9	1007	455.77	Ohio River at Bubblers Restaurant near Clermontville, Ohio
11/3/05 09:05	442.6	1008	456.02	Ohio River at boat ramp at Moscow, Ohio
11/3/05 09:00	438.7	1009	456.00	Ohio River at Neville, Ohio
11/3/05 11:20	436.0	Meldahl Dam	456.32	Ohio River downstream from Meldahl Dam
11/4/05 09:15	471.0	Cincinnati water-level gaging station	455.14	Ohio River at Cincinnati, Ohio (03255000)
11/4/05 07:50	449.4	1006	455.96	Ohio River at Skippers Boat Ramp near New Richmond, Ohio
11/4/05 08:10	446.9	1007	456.15	Ohio River at Bubblers Restaurant near Clermontville, Ohio
11/4/05 08:30	442.6	1008	456.41	Ohio River at boat ramp at Moscow, Ohio
11/4/05 08:50	438.7	1009	456.36	Ohio River at Neville, Ohio
11/4/05 09:15	436.0	Meldahl Dam	456.92	Ohio River downstream from Meldahl Dam
3/21/06 19:50	471.0	Cincinnati water-level gaging station	457.29	Ohio River at Cincinnati, Ohio (03255000)
3/21/06 19:00	462.5	1005	458.35	Ohio River at the boat ramp at California, Ohio
3/22/06 14:45	471.0	Cincinnati water-level gaging station	456.58	Ohio River at Cincinnati, Ohio (03255000)
3/22/06 14:15	462.5	1005	457.46	Ohio River at the boat ramp at California, Ohio
3/22/06 22:15	471.0	Cincinnati water-level gaging station	455.38	Ohio River at Cincinnati, Ohio (03255000)
3/22/06 23:30	462.5	1005	457.65	Ohio River at the boat ramp at California, Ohio
3/23/06 14:30	471.0	Cincinnati water-level gaging station	456.42	Ohio River at Cincinnati, Ohio (03255000)
3/23/06 14:30	462.5	1005	457.20	Ohio River at the boat ramp at California, Ohio
3/23/06 21:15	471.0	Cincinnati water-level gaging station	456.41	Ohio River at Cincinnati, Ohio (03255000)
3/23/06 21:10	462.5	1005	457.20	Ohio River at the boat ramp at California, Ohio